Extraction of Nanocrystalline Cellulose from Biomass and its Dissolution in Pyridinium-based Ionic Liquid for Antioxidant and Antimicrobial Applications

QUAID-I-AZAM UNIVERSITY

ISLAMABAD

A dissertation submitted to the Department of Chemistry, Quaid-i-Azam University, Islamabad, in the partial fulfillments of the requirements for the degree of

Master of Philosophy

in

Physical Chemistry

by

Arooj Fatima

Department of Chemistry

Quaid-i-Azam University, Islamabad

2023

This is to certify that this dissertation entitled " **Extraction of Nanocrystlline Cellulose from Biomass and its Dissolution in Pyridinium-based Ionic Liquid for Antioxidant and Antimicrobial Applications**" submitted by *Ms. Arooj Fatima,* is accepted in its present form by the Department of Chemistry, Quaid-i-Azam University, Islamabad, as satisfying the dissertation requirements for the degree of *Master of Philosophy in Physical Chemistry.*

External Examiner:

Prof. Dr. Mrs. Rumana Qureshi
House No. 12, St. No.1, Block E
Soan Gardens, Zone V,
Islamabad.

Supervisor:

Dr. Faroha Liaqat
Department of Chemistry
Quaid-i-Azam University
Islamabad

Head of Section:

Prof. Dr. Hazrat Hussain
Department of Chemistry
Quaid-i-Azam University
Islamabad.

Chairman:

Prof. Dr. Aamer Saeed Bhatti (TI)
Department of Chemistry
Quaid-i-Azam University
Islamabad

Read! In the Name of Thy Lord, Who has created (all that exists), He has created man from a clot (a piece of thick coagulated blood) Read! And your Lord is most Gorgeous, who has taught (the writing) by the pen. He has taught man that which he knew not."

(Quran 96: 1-5)

Dedication

My profound gratitude to

My Father

Who is my pride and honor who taught me to believe in Allah, trust in hard work and he has always a constant source of inspiration for me.

&

My Mother

Who is a pleasure of my life and my best friend, thanks for her infinite love, prayers, support and encouragement.

My supportive siblings

Who support and guide me and are source of happiness in my life.

Acknowledgements

Abstract

Pakistan being a populated and agricultural country has a problem of massive organic waste production and disposal. Due to the large amounts of organic waste, environmental issues are becoming pressing. These concerns have increased interest in the environmental-friendly synthesis of chemicals and value-added goods from biomass waste. Owing to distinctive qualities such as high surface area, customizable surface chemistry, outstanding mechanical strength, biodegradability, and renewable nature, nanocellulose (NC) has recently received a lot of attention. However, its applications are restricted due to its poor solubility. This work produces a green solvent for dissolution of NC extracted from eucalyptus bark. Nanocellulose (NC) was extracted from hardwood of *Eucalyptus camaldulensis* by a new extraction method and confirmed by XRD, FTIR, and SEM analysis. XRD confirmed nanocellulose as nanocellulose type I with 71% degree of crystallinity. Zeta sizer provided that particle size of nanocellulose is 172 nm and zeta potential analysis showed the presence of bonded OH groups on the surface of nanocellulose. A newly derivatized ter-butyl Pyridinium chloride ionic liquid [C_4Py] [Cl](PyIL) was synthesized for NC dissolution and was characterized by NMR, FTIR, and UV analysis. The highest value for the refractive index, density and viscosity of PyIL evaluated at 20°C is 1.5312, 1.69 gcm^{-3}, and 10.04 Pa. s respectively. In vitro antibacterial activity of ionic liquid (IL) and cellulose dissolve ionic liquid (CIL) was investigated by an agar well diffusion assay against pathogenic bacteria (Escherichia *coli, Staphylococcus Aureus, Klebsiella pneumoniae,* and *Bacillus subtilis*), that causes various diseases, to scrutinize the in vitro antibacterial activity of the IL and CIL. 1,1-diphenyl-2-picrylhydrazyl (DPPH) radical-scavenging effect and FRAP assay were used to scrutinize the antioxidative activities of nanocellulose (NC), ter-butyl pyridinium chloride (PyIL), and cellulose dissolved ionic liquid. The best activity was shown by CIL giving 59% radical scavenging at IC_{50} of 24.43 μL against DPPH and giving 560 μL/mL ascorbic acid equivalent per mg of sample. The interaction of NC with PyIL was investigated at DFT/B3LYP/6-31G (d, p) level using Gaussian 09 program. Frontier molecular orbital analysis and global reactivity parameters were computed for determination of stability and reactivity of NC and PyIL before and after interaction. In the light of experimental and theoretical results, it was determined that reactivity, antimicrobial and antioxidant properties of NC increase upon dissolution in PyIL. Thus, in this study nanocellulose (NC) is not only extracted efficiently from hardwood of Eucalyptus by novel method, but the synthesis of green solvent, tertiary butyl pyridinium chloride ionic liquid (PyIL), for their dissolution made them more applicable for various applications specially in medicine.

Table of Contents

Chapter 1

Introduction

Chapter 2

Experimental and Instrumentation

Chapter 3

Results and Discussion

List of Figures

List of Tables

Abbreviations

AA	Ascorbic Acid
AAE	Ascorbic Acid Equivalent
AGU	Anhydrous glucose unit
BCNCs	Bacterial cellulose nanocrystals
BNC	Bacterial nanocellulose
CMFs	Cellulose microfibrils
CNCs	Cellulose nanocrystals
CNFs	Cellulose nanofibers
DFT	Density Functional theory
DMSO	Dimethyl sulfoxide
DMF	Dimethylformamide
DPPH	2,2-diphenyl-1-picrylhydrazyl
FTIR	Fourier Transform Infrared Spectroscopy
FMOs	Frontier Molecular Orbitals
FRAP	Ferric reducing antioxidant power
HCNC	Hairy cellulose nanocrystalloid
HOMO	Highest Occupied Molecular Orbital
HPH	High pressure homogenization
IL	Ionic liquid
LB	Lignocellulosic biomass
LUMO	Lowest Unoccupied Molecular Orbital
MCC	Microcrystalline cellulose
MEP	Molecular electrostatic potential
MSW	Municipal Solid Waste
MHA	Mueller Hinton agar
NC	Nanocellulose
NMR	Nuclear magnetic resonance
PyIL	Tertiary butyl pyridinium chloride ionic liquid
PDI	Polydispersity index
SEM	Scanning electron microscopy

| TRP | Total reducing power |
| XRD | X-ray diffraction |

Chapter 1

Introduction

1.1 Biomass and its Types

The term "biomass" refers to non-fossilized biological matter present on Earth. For example, food crops (starch-rich) and remains (such as rice and maize husks), aquatic plants (such as algae), woody plants (such as eucalyptus), garbage, and animal waste. As a renewable resource, biomass has been utilized to produce fuels, power, as well as for agricultural and industrial purposes. Accordingly, biomass meets 35% of the energy needs of developing nations and roughly 10% of the global energy demand.[1]

The term "feedstocks" refers to renewable biomass sources that can be utilized either directly (fuel) or as a raw material for another type of energy product. As examples of biomass feedstocks, include dedicated energy crops, crop wastes, forest wastes, purpose-grown grasses, woody energy crops, algae, industrial wastes, sorted municipal solid waste (MSW), urban wood waste, and food waste.[2] Other biomass feedstocks include municipal waste and wet waste.

- **Dedicated energy crops** are non-food crops classified into two general categories: herbaceous and woody.[2] For example, switchgrass, miscanthus, bamboo, sweet sorghum, etc.
- **Agricultural crop residues** include the stalks and leaves. Examples include corn stover wheat straw, oat straw, barley straw, sorghum stubble, and rice straw.
- **Forest biomass feedstocks** include dead, diseased, poorly formed, and other unmerchantable trees known as forest residue and whole tree-biomass.[2]
- **Aquatic plant and algal feedstock:** These include Eichhornia crassipes, Lemna minor, Arundo donax etc. Algal feedstock includes microalgae, macroalgae (seaweed) and cyanobacteria (blue-green algae).[2]
- **Wood processing residues** include unused sawdust, bark, branches, and leaves/needles produced as a result of wood processing for wood products, paper and pulp.[2]
- **Sorted municipal solid waste** (MSW) resources comprise a variety of commercial and household trash, including yard waste, paper, cardboard, plastics, rubber, textiles and food waste.

- **Wet waste feedstocks** include manure slurries from concentrated livestock operations, organic wastes from industrial operations, commercial, institutional, and residential food wastes, organic-rich biosolids (i.e., treated sewage sludge from municipal wastewater), industrial organic wastes, and biogas (the gaseous byproduct of organic matter decomposition in the absence of oxygen) obtained from any of the aforementioned feedstock streams. [2]

Waste management (WM) is one of the major causes of environmental pollution in Pakistan. Inappropriate management of solid waste causes hazards to residents.[3] Pakistan being a populated and agricultural country have massive organic waste production. The direct recycling method, however, has limitations when contaminants such heavy metals and organics (volatile organic compounds and polycyclic aromatic hydrocarbons) are present in considerable concentrations in waste or residues and when the removal, stabilization, or destruction of the pollutant results in emissions. Biomass valorization attracted attention as a result of the depletion of natural resources, rising greenhouse gas emissions, and for sustainable development in terms of securely utilizing waste and biomass.[4]

Biomass valorization is the method of adding value to various plants and residues, such as food crops (starch-rich) and residues (such as rice and maize husks), aquatic plants (such as algae), woody plants (such as eucalyptus), municipal garbage, and animal waste. [5] It yields biomaterials by economically efficient and eco-safe strategies and also have commercial operation capability because of the availibity of variety of biomass raw material.[6] In future, higher human density will result in greater chemical (and energy) consumption as well as fewer food supplies. In that scenario biomass is expected to provide nearly 38% of world's fuel needs and 17% of energy supply. Given this development, lignocellulosic plants are chosen for biomass conversion to value added products because they contain many components for the creation of plastics, medications, and other compounds for a variety of applications. [7]

1.2 Lignocellulosic Biomass and its Structural Composition

Lignocellulosic biomass (LB), which is the most abundant source of the most potential feedstock and efficient carbon source for the environmentally friendly synthesis of biochemicals, and biofuels, contains a variety of naturally occurring plant-based organic components.[8] Due to its exceptional environmentally favorable features, lignocellulosic biomass is a natural source of fibers that can replace petroleum-based products. Agricultural wastes and forest leftovers for example, offer a substantial potential for reusing as fuel or a

feedstock for the production of high-value commodities without putting pressure on human and animal food chains.[9]

Wood based and aquatic plant biomass have been shown to be useful in creation of high-value products and bioenergy. However, these biomasses contain lignocellulose, which presents a barrier in conversion processes.[10] Three major components of lignocellulosic biomass are;[11]

- Lignin (an aromatic polymer)

- Hemi-cellulose (a polymer of xylose, mannose and arabinose etc.)

- Cellulose (a polymer of glucose)
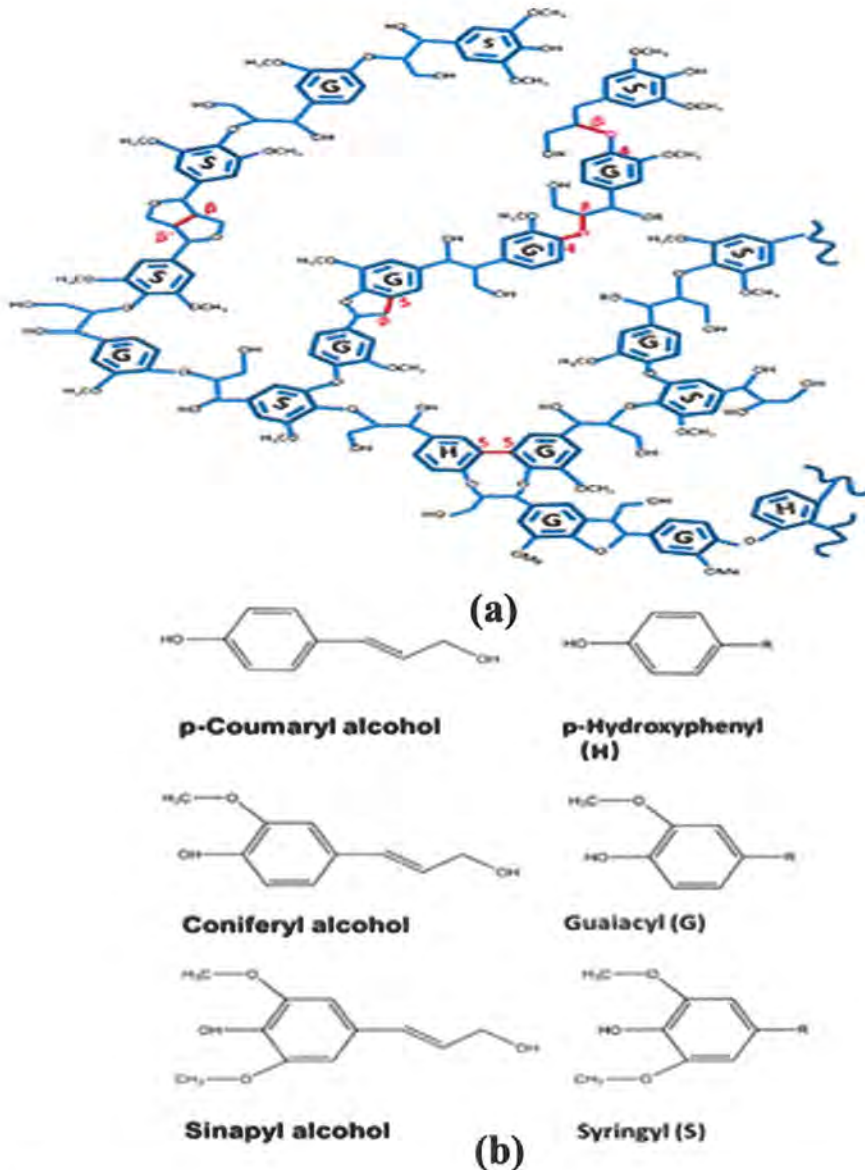
Figure 1.1: Chemical structure of (a) lignin and (b) its monolignols.[13]

Lignin is a naturally occurring macromolecule that contains a cross-linked polyphenol. The side chains of the intricate polymer structure contain a number of terminal aldehyde groups, phenolic hydroxyl groups, and methoxy groups. The three monolignols that are frequently present in lignin are p-coumaryl alcohol, coniferyl alcohol, and sinapyl alcohol.[12] **Figure 1.1** depicts chemical structure of lignin and its monolignols. [13]
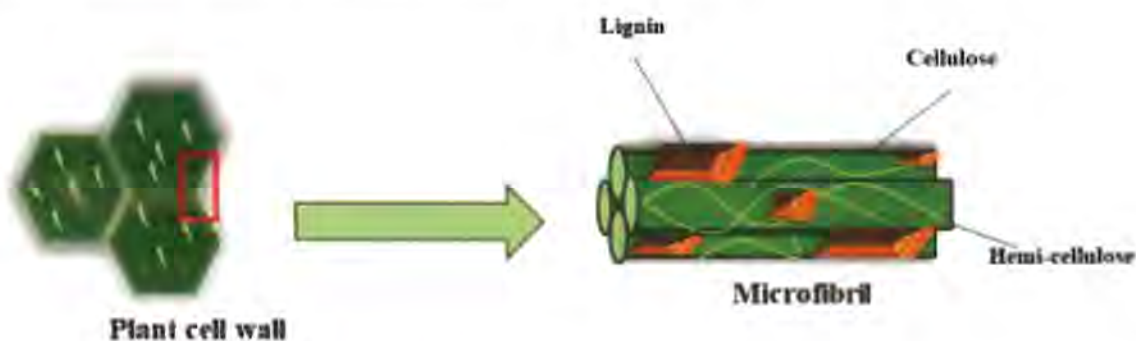
Figure1.2: Major components of lignocellulosic biomass (LB).[15]

The amount of lignin in dry lignocellulosic biomass ranges from 10 to 25 percent by weight.[14] **Figure 1.2** illustrates how lignin serves as a sealant in plant cell walls to keep cellulose and hemicellulose together.[15] Lignin gives plant cell walls their stiffness, compressive strength, resistance to decay, and water impermeability through the binding function it performs.[16] Recent research focuses mostly on depolymerizing lignin and isolating it from the lignocellulosic biomass in order to produce biofuels and compounds from natural resources. Additionally, lignin-based carbon materials which are attractively developed—are used for catalysis, energy storage, and pollutant removal.[17]
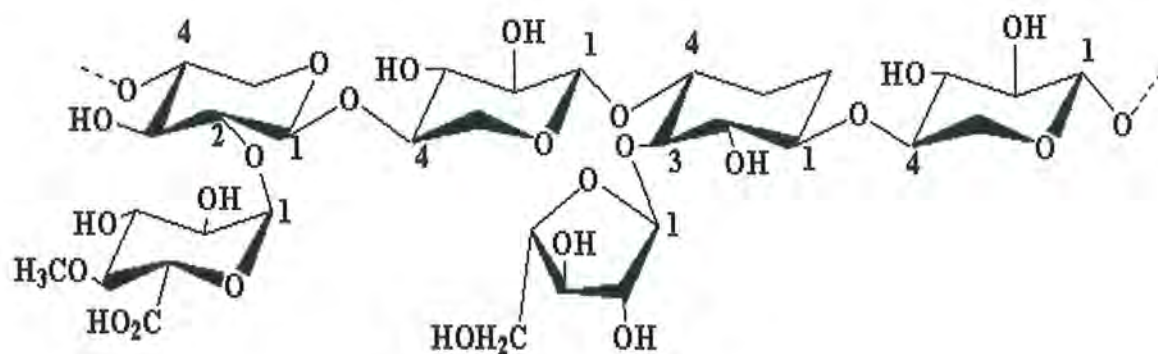
Figure 1.3: Structure of hemicellulose.[20]

Hemicellulose is second major constituent of LB and is polymer based on sugars. Glucose and a number of other water-soluble sugars created during photosynthesis make up hemicelluloses. [18] Hemicelluloses have a lower degree of polymerization because their

molecules are shorter than those of cellulose. The heteropolymer known as hemicellulose is made up of pentoses and hexoses as well as other types of monomers in short, linear, and branching chains.[19] **Figure 1.3** shows a xylopyranose backbone, with side branches of glucuronic acid ($1 \rightarrow 2$) and arabino furanose ($1 \rightarrow 3$), makes up the structure of hemicellulose (xylans).[20]

Hemicellulose in lignocellulosic biomass, accounts for 20–35% of the total.[14] Glucomannans and xylans are the two most prevalent forms of hemicellulose. While glucomannans are usually found in softwood, xylans are frequently found in hardwood.[21-22] Through hydrogen bonds and Van der Waal interactions, hemicellulose is linked to the cellulose fibrils. In addition, lignin and hemicellulose cross-link in structure of lignocellulosic biomass.[21] Incorporating hemicellulose alongside lignin and cellulose generates an additional strength to the plant cell wall.[22] In mild conditions, hemicellulose's oligomers or monomers can be hydrolyzed by an acid, an alkali, or an enzyme to yield valuable chemicals that can be used in the food, cosmetic, mining, and other sectors.[23]
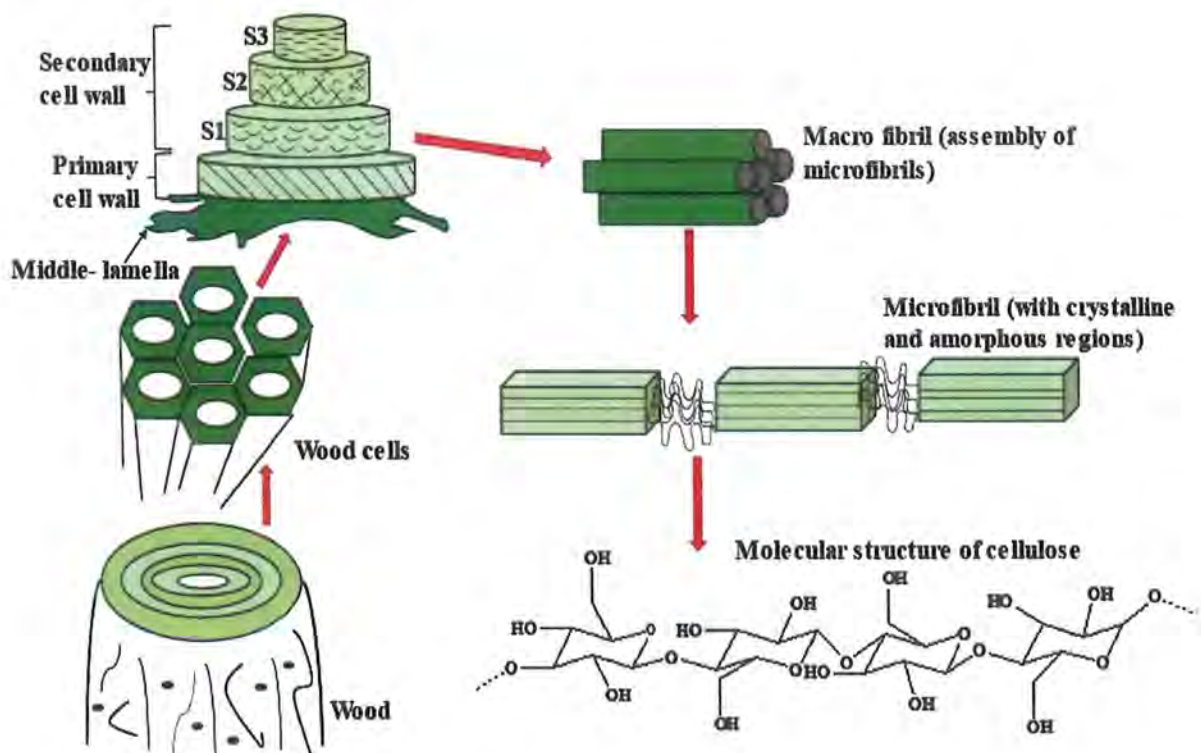
Figure 1.4: Macroscopic to microscopic structure of cellulose in wood.[26]

Cellulose makes up about 35-50 % of lignocellulosic biomass as the principal component.[14] **Pectin** is another non-common component present in lignocellulosic biomass. Despite being present in small amounts in cell walls, pectin has been found to affect the establishment of

secondary walls. Pectin provides porosity and accelerates intake, while cellulose increases water uptake and hydrophilicity. [24-25] Macroscopic to microscopic structure of cellulose with its crystalline and amorphous regions in woody biomass is illustrated in **Figure 1.4**.[26]

1.3 Cellulose

Cellulose was discovered by Anselme Payen, a French agricultural scientist in 1833. Payen removed various tissues from plant cell wall, leaving behind a substance with the chemical formula $C_6H_{10}O_5$. The residue was found to be a significant constituent of the plant cell wall and a molecular isomer of starch, but it had different characteristics from starch. Diastase enzyme had no effect on the residue unlike starch, although acid hydrolysis produced glucose. Iodine causes starch to become blue, but Payen's newly discovered carbohydrate did not.[27] In 1839, it was named as cellulose.[28]

Hermann Staudinger claimed that long chains of repeating monomers were covalently bonded in cellulose and other natural polymers when he first coined the word "macromolecule" in the 1920s.[29] It wasn't until the late 1920s that methylation studies revealed that the 2, 3, and 6 positioned carbons in cellulose were occupied by hydroxyl groups as sown in **Figure 1.5**. These results revealed that the 1 and 4 carbon positions in cellulose served as links connecting the glucose. [30] The ultimate evidence that cellulose was a linear macromolecule was provided in 1932 when methylated end groups were recovered from the hydrolysis byproducts of methylated cellulose.[31]

A linear glucose homopolymer having a (1-4) glycosidic structure and the D configuration connections were revealed to be the fundamental component of cellulose as shown in **Figure 1.5**. It was discovered that glucose units were connected by their hydroxyl groups at carbon 1 and carbon 4 through dehydration, which demonstrates that the β (1-4) glycosidic link holds the units of the cellulose molecular chain together.[30]

Anhydrous Glucose Units (AGUs), the smallest monomers in the polymer chain, repeat as cellobiose units. The cellulose chain has an AGU with three hydroxyl groups.[31] Through the hydrogen bonding, these OH-groups are in charge of the cellulose's chemical and physical behavior in addition to its supramolecular structure.[32] The two ends of cellulose chain are chemically different from one another. At one end, anomeric carbon (carbonyl carbon in open structure of glucose) atoms of the D-glucopyranose unit are linked together in a glycosidic linkage, but at other end anomeric carbon is free. The hemiacetal function (RHC(OH)OR) equilibrium results in production of a small amount of aldehyde, which confers reducing

properties at free end of the chain, making cellulose chemically polar .[30] However, the OH group at C4 end of cellulose chain is alcoholic hydroxyl, making it non-reducing.[33]
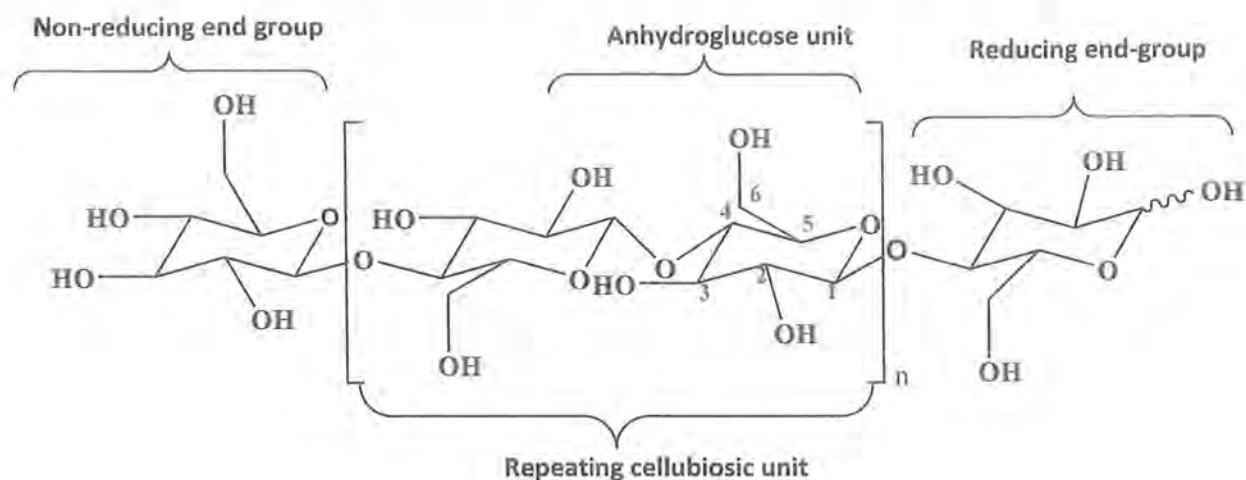
Figure 1.5: Molecular structure of cellulose depicting the repeating anhydrous glucose unit (AGU) and β (1-4) glycosidic bond.

The origin of cellulose has a significant impact on its molecular weight.[32] Degree of polymerization (DP) of cellulose (which is a measure of the size of the chain molecule) is frequently employed to describe its linearity. Estimated plant cellulose polymerization degrees range from 15300 for capsules to 305 for rayon fibres in technical cellulose products.[34] In order to maintain cohesion between cellulose molecules, a long intra- and intermolecular hydrogen bonding network is the basis of organization from a anhydro glucopyranose unit, or AGU, to the micro and the macro fibrils.[33] It is thought that the assembling of the linear polymer molecules into sheet like structure is made possible by intermolecular hydrogen bonding, whilst intramolecular hydrogen bonds are thought to provide chain stiffness.[35]In cellulose lower order amorphous areas and high order crystalline areas coexist, making it a semi-crystalline polymer, as shown in **Figure 1.4** .[26,36] The cellulose is commonly found to be crystalline between 40% and 60% depending upon the source and pretreatment technique of a cellulose.[37]

1.3.1 Interactions in Cellulose

Because of the complexity of the biopolymeric network, its partially crystalline structure, and the numerous non-covalent interactions between molecules, chemical processing of cellulose is relatively difficult. Ordinary aqueous and organic solvents do not cause cellulose to melt or make it soluble due to hydrogen bonding network in it.[38]

Different crystalline structures of cellulose are classified based on hydrogen bonding patterns present within. The C-6 hydroxyl group's rotational shape plays vital role in the

hydrogen bonding network. Different allomorphs of cellulose are produced as a result of the vast orientation range of the hydrogen bonding networks in cellulose and glucose molecules. The four different types of cellulose allomorphs are generally referred to as cellulose types I, II, III, and IV.[39]

- **Cellulose type I** is common allomorph of cellulose, also called native cellulose, which contains the parallel packing of a hydrogen-bonded network. [40]

- **Cellulose type II** forms when cellulose type I undergoes chemical regeneration by swelling in an acidic or alkaline solution or by simply dissolving in a solvent. Mercerization is the process by which cellulose I is treated with the right amount of alkali to produce cellulose II as well. These chemical regenerations result in the formation of different antiparallel hydrogen-bond network packing configurations in cellulose type II. [41]

- **Cellulose type III** forms on thermal treatment of Cellulose type I and type II after treatment with ammonia.

- While **cellulose type IV** is created by heating cellulose III to 260 degrees Celsius in glycerol as shown in **Figure 1.6**.[42]
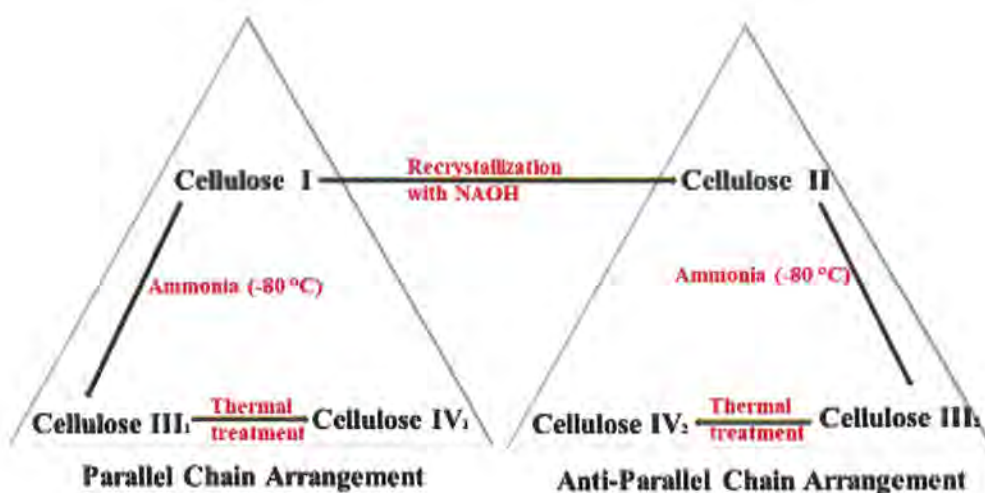
Figure 1.6: Interconversion of different allomorphs of cellulose.[42]

The elaborative hydrogen bonding network in cellulose type I is shown in **Figure 1.7**. Native cellulose contains intramolecular hydrogen bonds between C-3 hydroxyl and O-5 oxygen as well as C-6 hydroxyl and O-2 oxygen. Stabilization through hydrogen bonding is made easier by the shape of β (1-4) glycosidic linkage and the configuration of the hydroxyl groups nearby. This explains why cellulose is a stiff polymer and prevents the AGU from freely rotating.[40] A hydrogen bond between two molecules of cellulose is created by the main C-6 hydroxyl and the O-2 oxygen on a parallel cellulose chain.[43] All types based on their nature of hydrogen network have different chemical properties and shapes.[44]
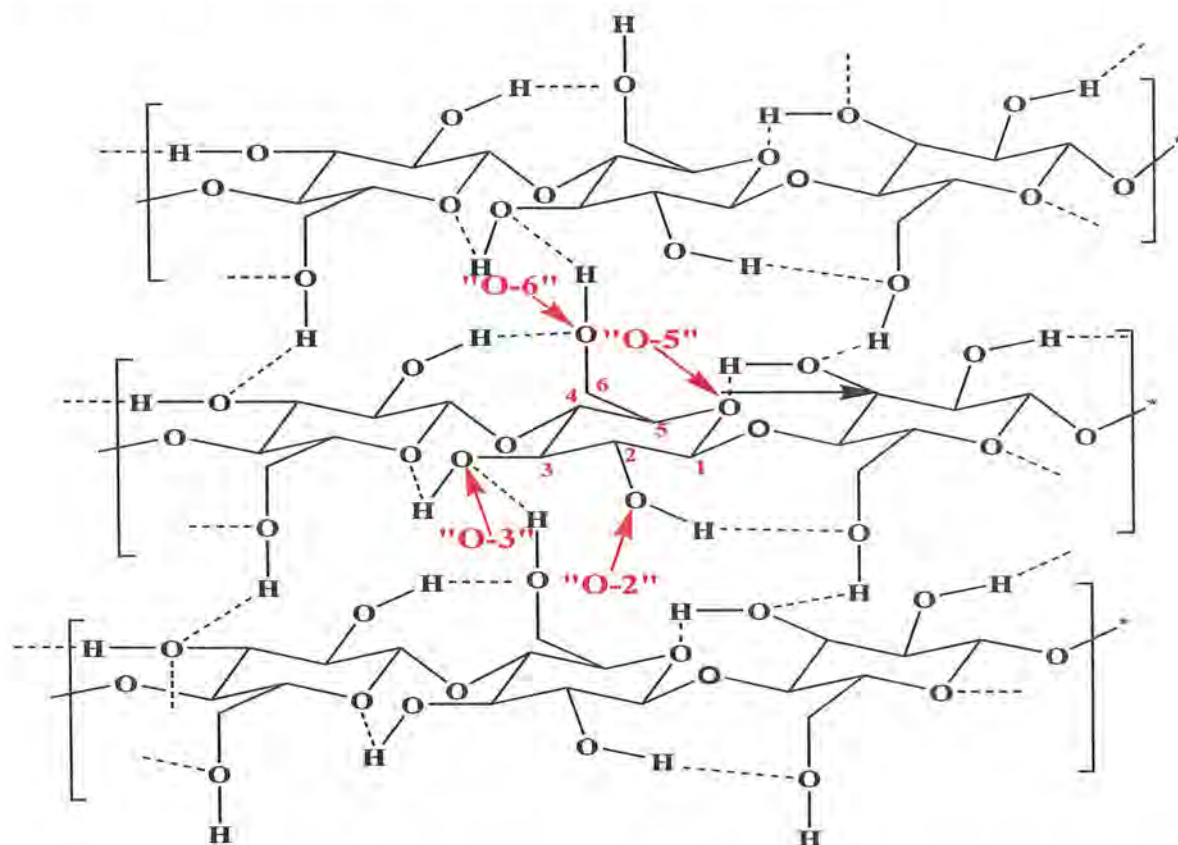
Figure 1.7: Molecular model of cellulose type I exhibiting the parallel chain conformation

1.4 Nanocellulose (NC) and its Sources

A cellulose material is considered to be nanocellulose (NC) if at least one of its dimensions is between 1 and 100 nanometers in size. Typical lignocellulosic biomass contains cellulose fibers that range in size from 3mm to100 mm in diameter and 1mm to 4 mm in length.[45] [45] Nanocellulose is becoming a more desirable research topic than cellulose due to advancements in the rapidly developing science of nanotechnology. The fundamental benefit of nanocellulose is that it can be produced uniformly, with improved physicochemical, mechanical, and crystallinity properties, by simply shrinking cellulose fibres.[46]

Generally, nanocellulose extracted from cellulose is derived from sources including tunicates, microorganisms, soft wood, agricultural waste, and hardwood, etc.[47] All sources of cellulose have the same chemical make-up, however depending on the hydrogen bonds that exist within, the structure of the material may differ slightly.[48] The diameter and crystallinity of the cellulose obtained from plant species are approximately 13–22 μm and 44–65%, respectively.[49] Whereas bacterial cellulose is the term for cellulose produced by bacteria. These are naturally occurring nanoscale fibrils with a crystallinity (degree of structural order) of about 90% and a diameter of between 10 and 100 nm.[50]

Nanocellulose has numerous sources, including grasses (bamboo, bagasse, etc.), algae, bacteria, bit fibres (jute, kenaf, flax, hemp, ramie, coir, etc.), fungi, wood (softwood and hardwood), seed fibres (coir, cotton, etc.), aquatic animals (tunicates), and the invertebrates.[47] Wood is the utmost popular source of cellulose, which also contains lignin, hemicellulose, and a relatively small number of inorganic salts and extracts.[51]

Recent research focuses on the manufacture of cellulose nanofiber (CNF) and cellulose nanocrystal (CNC) from grasses, water plants, wood pulp, and annual plants. These materials are significant potential sources of cellulose that have the necessary characteristics to produce nanocellulose.[8] Investigators have proposed employing agricultural crops (bunches, wheat, pineapple, rice, and sugarcane) and crops (sisal, hemp, kenaf, and flax) together to extract NC. In addition to these smaller sources, cellulose can also be taken from fungi, bacteria, algae, and marine creatures such as tunicates.[52]

1.5 Types of Nanocellulose

Extraction of nanocellulose (NC) from organic waste is the best way of waste treatment due to its energy sustainability and high-value added products can be obtained.[46] Three main kinds of nanocellulose are typically mentioned when discussing cellulose nanostructured materials as shown in **Figure 1.8**.[53]

- Cellulose nanofibers (CNFs)

- Cellulose nanocrystals (CNCs)

- Bacterial nanocellulose (BNC)

Although all forms of cellulose share a similar chemical makeup, variations in source types and extraction techniques result in variations in morphology, particle size, crystallinity, and other features.[54]

Cellulose Nanofibers (CNFs) are also known as nanofibrillated cellulose, cellulose nanofibril, or nanofibrillar cellulose. They have a long, flexible structure and are made of entangled nanocellulose that may be removed mechanically from cellulose fibrils.[55] CNFs have fibril shapes having diameter 1nm to 100 nm and length 500–2000 nm.[56] By chemical make-up, they are entirely composed of cellulose and have both crystalline and amorphous sections. They are often extracted from wood pulp via TEMPO (2,2,6,6-tetramethylpiperidin-1-oxyl)-mediated oxidation method.[57-58]

Cellulose nanocrystals (CNCs), often referred to as nanocrystalline cellulose or cellulose nano-whiskers, are typically recovered from cellulose fibrils by acid hydrolysis. [39] These have a 2–20 nm diameter and a length of 100–500 nm, resembling a small rod or a whisker. Additionally, CNCs have a chemical makeup that is 100% cellulose, with the highest crystallinity found in these locations (between 54 and 88%).[56] Acid hydrolyzes and dissolves the amorphous components, leaving the crystalline components intact.[45] High crystallinity and a short-rod-like form are both characteristics of nanocrystalline cellulose. Nanofibrillated cellulose has a higher aspect ratio (length to diameter), a larger surface area, and a greater number of hydroxyl groups for surface modification than nanocrystalline cellulose.[59]
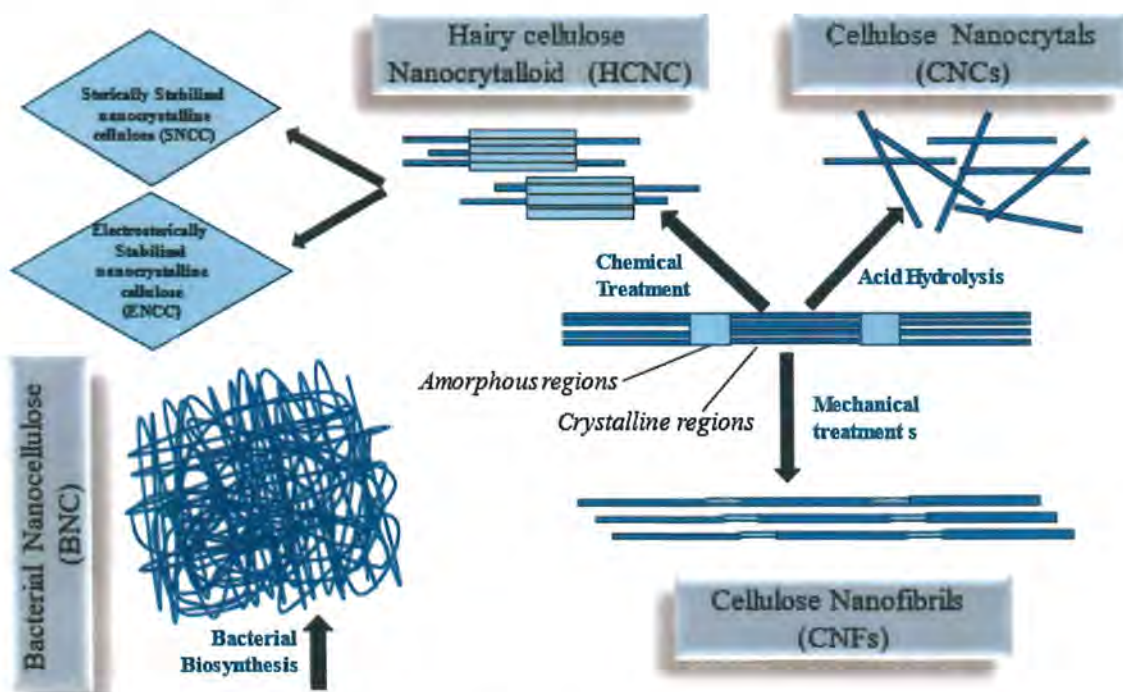
Figure 1.8 Types of nanocellulose.[53]

Bacterial nanocellulose is shaped like a ribbon and ranges in size from 20 to 100 nm, with a length of several micrometres.[15] The extracellular byproduct of bacterial fermentation produced by numerous species of the genera Rhizobium, Agrobacterium, Gluconacetobacter, and Sarcina is bacterial nanocellulose.[46] The fundamental benefit of bacterial nanocellulose is that, unlike cellulose from plant sources, it is not connected to other undesirable polymers.[53] The source, processing conditions during isolation, and any pre- or post-treatments affect the kind of nanocellulose, its size, shape, and other features.[47]

Van de Ven and associates have recently reported on **hairy cellulose nanocrystalloid (HCNC)**.[60] Chemical treatment was used to extract HCNC from cellulose chains rather than acid hydrolysis and the mechanical extraction. As a result, the crystalline areas are maintained while the amorphous parts are solubilized, much like when nanocrystalline cellulose was extracted using traditional techniques. It is important to remember that HCNC has some cellulose chains that can split and protrude from the crystal's two ends.[61] Because of this, similar to nanocrystalline cellulose, HCNC is highly crystallin and generally possesses rod-like shapes. However, it also includes elements that are both crystalline and amorphous, like nanofibrillated cellulose. Based on its protruded tails, which are impacted by diverse chemical processes, HCNC has a variety of derivatives.[62]

One typical HCNC derivative is **sterically stabilized nanocrystalline cellulose (SNCC)**. It can be made by heating treatment after a chemical reaction with periodate (IO_4). Periodate ions' negative charges have the ability to rupture glucose molecules bonds. It can also change hydroxyl groups to aldehydes in the interim. This is the amorphous parts of cellulose chains can be penetrated. While creating and cleaving dialdehyde chains at the ends, leaving crystalline areas intact. Dialdehyde chains have a high degree of reactivity, making it possible to functionalize SNCC with various chemical groups with no charge.[60]

Electrosterically stabilized nanocrystalline cellulose (ENCC) is another form of HCNC. It can be extracted from cellulose chains by periodate/chlorite oxidation reaction. By using a periodate/chlorite oxidation reaction, it can be removed from the chains of cellulose. The result is that the dicarboxylated chains extract and protrude the rod-shaped crystalline portions. In comparison to regular nanocrystalline cellulose, ENCC can be more heavily charged with dicarboxylated chains, which increases colloidal stability.[47] **Table 1.1** shows the comparison of different properties of types of nanocellulose.

Table 1.1: Comparison of three major types of nanocellulose

Properties	Cellulose nanofibers (CNFs)	Cellulose nanocrystals (CNCs)	Bacterial nanocellulose (BNC)
Common Sources	Wood, cotton, cassava peel, banana	Wood, cotton, bacterial cellulose	Rhizobium, Agrobacterium, Gluconacetobacter and Sarcina. [63-64]
Morphology	Rope like	Needle like	Ribbon like.[55,65]
Size	5–60 nm diameter and length in many microns	5 nm diameter and 20–100 nm length	20–100 nm diameter and length in many micrometers. [15,47,55]
Crystallinity	59–64%	54–88%	84–89%.[66-67]
Aspect Ratio (l/d)	30–300	11	~50. [68-69]
Young's modulus in longitudinal direction	180 GPa	150 GPa	78 GPa. [70-71]

1.6 Synthesis of Nanocellulose from Lignocellulosic Biomass

A variety of lignocellulosic biomass treatment techniques, such as conventional treatment and enzymatic treatment, can be used to produce nanocellulose from cellulose fibres. A two-step procedure is used to extract nanocellulose and these two steps involved are;

❖ Pretreatment of lignocellulosic biomass.

❖ Extraction of nanocellulose from micro-cellulose
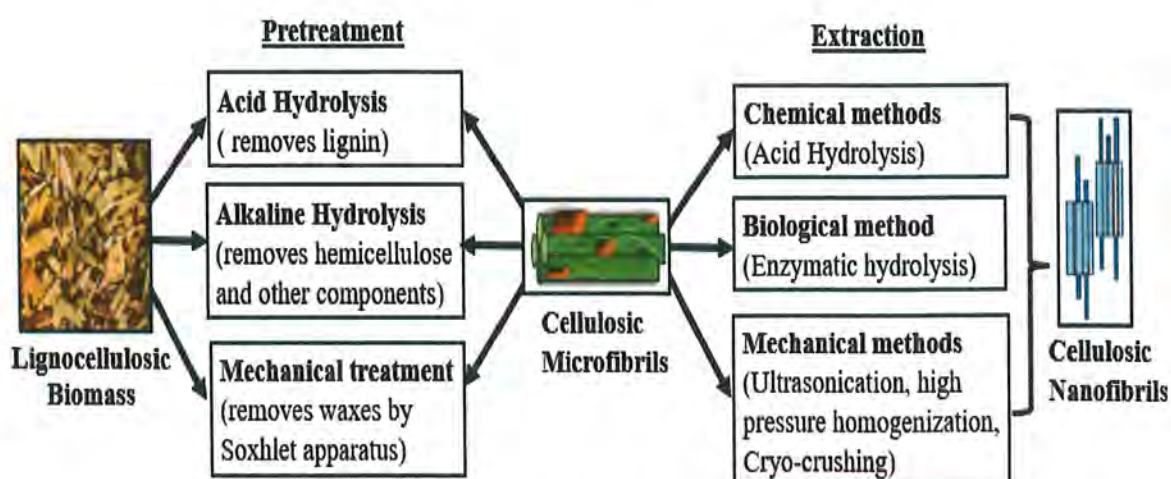
Figure 1.9: Synthetic pathway for extraction of nanocellulose from lignocellulosic biomass.

The pretreatment of native cellulose biomass is carried out in the first phase, producing treated cellulose fibres. The pretreated cellulose fibres are transformed into nanocellulose utilizing a variety of processes in the second stage using methods such as electrospinning, high-pressure homogenization, micro fluidization, micro grinding, and steam explosion. After extraction the nanocellulose can be functional for various applications by surface modification.[72] Development of nanocellulose from lignocellulosic biomass is depicted in **Figure 1.9**.

1.6.1 Pretreatment of Lignocellulosic Biomass

Lignocellulosic biomass contains a lot of cellulose as well as other substances like lignin and hemicellulose, waxes, and pectin. Pretreatment procedures are required to improve the quality of micro-cellulose fibrils by removing ashes, waxes, and undesirable polymers (such as lignin and hemicelluloses).[73] Additionally, the pretreatment procedure enhanced fibrillation and the transformation of cellulose fibre into nanofibrils. The traditional procedures for biomass pretreatment are;[63]

➢ Acid chlorite treatment

➢ Alkaline treatment

➢ Mechanical treatment

The Acid-chlorite treatment/bleaching procedure is also referred to as delignification process. It is commonly employed in the paper industry.[63] The bulk of lignin and other components can be extracted by combining distilled water, sodium chlorite, and acetic acid with lignocellulosic biomass and stirring at 70-80 °C for 4-12 hours.[65] To adjust pH value, acetic acid and sodium chlorite are periodically added to the mixer, or once per hour. The mixture is then left to swirl for an additional night before using distilled water to wash them until the pH is neutral. The resulting solid products, known as *holocellulose* because they primarily include cellulose and hemicellulose in the fibres, are collected and oven dried at 50 °C. Holocellulose comprises of white colour fibre, demonstrating the removal of lignin and other contaminants.[74]

Alkaline treatment involves adding alkaline to remove the residual lignin and the amorphous polymer of hemicellulose. The most used alkali for alkaline treatment is sodium hydroxide (4–20 wt %), and holocellulose is always combined with it for 1–5 hours. After being rinsed with distilled water until the pH is neutral, the completed solid is then dried in an

oven at 50 °C. Other non-cellulosic elements are eliminated from the resulting fibre products after this treatment.[75]

Mechanical processes such as grinding, steam explosion, cryocrusting, microfluidation, homogenization, ultrasound, etc. yield cellulose microfibrils (CMFs. Pure cellulose is directly acid hydrolyzed to recover cellulose microcrystals (CMCs).[42]

1.6.2   Extraction of Nanocellulose

From cellulosic materials, nanocellulose can be extracted utilizing a number of techniques. The varied extraction methods lead to a variety in the types and characteristics of the generated nanocellulose.[76] Major extraction techniques used are;

- Acid Hydrolysis
- Mechanical Techniques
- High pressure Homogenization (HPH)
- Green chemical extraction technique

Acid hydrolysis is primary step involved for extracting nanocellulose from cellulosic products. Since cellulose chains have both ordered and disordered regions, the ordered regions sustain acid hydrolysis while the disordered regions are swiftly dissolved away by the acid.[74] The esterification of the hydroxyl group by the sulphate ions in sulfuric acid allows it to not only securely isolate nanocrystalline cellulose but also stabilize it. The three main controlling factors that affect the properties of the created nanocellulose are reaction time, temperature, and acid concentration.[76] The biggest drawback of acid hydrolysis is the acid wastewater created during the washing process to balance the pH of the nanocellulose solution. Washing with ice water and centrifugation are typically used to neutralize acidified fibres. Utilizing an alkali i.e., NaOH to neutralize the pH is another approach for cleaning the finished fibres.[77] **Mechanical techniques** like cryocrushing, twin screw extrusion, ball milling, etc. are typically used for extraction of nanocellulose fibres (CNFs) from treated cellulose.[78]

High pressure homogenization (HPH) is another approach that is particularly effective for developing CNCs both in laboratory and on industrial scale. In this process, a very high pressure is used to enter the cellulosic suspension into a small nozzle, and then the pressure suddenly drops, creating a tremendous shear stress that results in the formation of nanoscale fibres.[78]

Recently, **greener extraction techniques** are being used to extract nanomaterials by involving the use of deep eutectic solvents, ionic liquids, and ammonium persulfate oxidation.[72] By offering more affordable ways to attach different biopolymers onto CNCs, these environmentally friendly techniques substitute hazardous chemicals and solvents.[42] **Table 1.2** provides a list of the primary extraction techniques used to produce the various forms of nanocellulose.

Table 1.2: Typical sources, pretreatment methods, extraction methods and types of nanocellulose.

Type of nanocellulose	Typical source	Pre-treatments	Extraction methods
Cellulose nanofibers (CNFs)	Wood and other lignocellulosic fiber sources	Mechanical process	Ball milling, cryo-crushing, Twin screw extrusion, High intensity ultra-sonication, Super mass collision
Bacterial Nanocellulose (BNC)	Bacterial cultures	Microbial fermentation, Chemical pretreatments (e.g., alkali treatment)	Microbial fermentation, chemical extraction
Bacterial Cellulose Nanocrystals (BCNCs)	Bacterial cellulose, Microbial cultures	Acid hydrolysis, Enzymatic hydrolysis	Acid hydrolysis, enzymatic hydrolysis
Cellulose nanocrystals (CNCs)	Agricultural residues, wood pulp, paper industry sludge	Pressure induced methods	Steam explosion High pressure homogenization Micro-fluidization Aqueous counter collision Subcritical water method
Cellulose nanocrystals (CNCs) Cellulose nanofibers (CNFs)	Cotton linters, sugarcane bagasse, agro-biomass	Enzyme assisted	Static culture Stirred culture
Cellulose nanofibers (CNFs) Cellulose nanocrystals (CNCs)	Wood pulp Agricultural residues Bamboo, grasses	Surface modifications	TEMPO oxidation Deep eutectic solvents Ammonium persulphate oxidation
Cellulose nanocrystals (CNCs)	Pulps (softwood and hardwood)	Green strategies	Using phosphor-tungstic acid Ionic liquids as solvents

1.7 Applications of Nanocellulose

Nanocellulose (NC) is appealing to be used in various applications due to its exceptional mechanical qualities, strength, light weight, low manufacturing costs, and durability.[63] Three categories can be used to catalogue the anticipated markets for nanocellulose:

- High-end applications (like printed electronics, batteries, and value-added paper products)
- Mid-range applications (such as structural materials and food)
- Low-end applications; pulp and paper that are common (like normal paper goods that are lighter and tougher).

One of the distinctive qualities of NC is its hygroscopic nature and chemical inactivity. A few industries where nanocellulose is used are medicines, packaging, cosmetics, electronics, food, automobiles, optical materials, aerospace, and building are some examples. The usage of freeze-dried nanocellulose hydrogels in daily-use items like sanitary pads, diapers, tampons, bandages, and diapers is increasing. NC can be employed in biotechnological and medicinal applications as elastic cryo-structured gels.[76] However, nanocellulose has several applications as a highly scattering substrate for corrosion inhibitors, electronic parts, ultra-white coatings, speaker membranes, capacitors, high-flow membranes, and tobacco filter addition, etc.[79] **Table 1.3** lists the primary application area and their function in these areas.

Table 1.3: Potential applications of nanocellulose.

Area of application	Properties	Key applications
Food packaging	Flexible, rigid, improved barrier	Packaging films.[79-80]
Biomedical	Nontoxic, excellent biocompatibility and biodegradability	Scaffolds, water absorbent pads, antimicrobial films and tampons, sanitary napkins or wound dressing.[81-83]
Cosmetics	Durability, compatibility, good elasticity	Composite coating agent for nails, hair, or eyelashes.[83]

Electronics	High dielectric, excellent mechanical and biocompatible	Sensor, electronic displays and windows.[83-85]
Optical materials	Crystalline, flexibility, biocompatible	Electronic transistor, sensors.[86]
Automobile	Good electrical, thermal, magnetic, physio-chemical properties	Lightweight and high strength components such as bumpers, side panels and dashboards.[87]
Construction	Increase fracture toughness, cheaper, low density, high strength	Blocks, sensors to monitor stress levels in bridge.[88]
Aerospace	High strength, light weight	Windows.[89]
Textiles	Easy care, low impurity, good mechanical strength, biocompatible	Antimicrobial medical field, paste printing.[90]
Paper Industry	Easy availability, eco-friendly, renewability	Grease-proof paper.[90-91]
Water purification	Bioresorbable, low cost, nontoxic	Filtration.[92]

1.7.1 Antimicrobial Activity of Nanocellulose

Antibiotic materials have some drawbacks, including the fact that they are pricy, poisonous, and unfriendly to the environment.[93] Because of the exceptional physical features, unique surface chemistry, and good biological qualities, NC has attracted attention for use in antibacterial applications. The sole disadvantage of this well researched natural polymer for biomedical applications is that it lacks antibacterial characteristics due to its compact hydrogen bonded structure.[93] However, through surface modification with biocidal chemicals, nanocellulose-based antimicrobial materials can be created that are effective against wound infection. Meanwhile, several methods involving the chemistry of the hydroxyl function, such as oxidation, esterification, and etherification, can be used to carry out surface functionalization.[94] Other cellulose conjugation agents that have been found to have antimicrobial characteristics include metal/metal oxide nanoparticles, chitosan, and silanes.[95] Treatment of nanocellulose with ionic liquids also makes them bioactive, as ionic liquids are

bioactive moieties. In addition, due to their antibacterial and antiviral activities, quaternary ILs containing 4-vinylpyridine, imidazolium, and pyridinium are the most popular biocidal agents. They are thought to be environmentally beneficial and low toxicity. [96]

Ionic liquids are now the most popular research tool for dissolving nanocellulose; they also appear to have antibacterial properties. The antimicrobial potential of various ionic liquid types was investigated by Florio, et al.[97] using conventional microbiological techniques, and they testified that the chosen ILs displayed low hemolytic and potent antimicrobial activity, as well as effective inhibition of biofilm formation, especially against *S. aureus*, suggesting their potential use as anti-biofilm agents. Additionally, cellulose dissolved in ionic liquid has effective antibacterial action as a result of ionic liquids functionalizing the cellulose.

1.8   Nanocellulose Dissolution

Cellulose is water insoluble and a few popular organic solvents at ambient conditions, which restricts its applicability. This is caused by the crystal structure's high degree of organization, the abundance of Van Der Waals forces, and the solid's robust inter- and intramolecular hydrogen bonds.[38] In order to dissolve cellulose, numerous traditional solvents have been studied, including Dimethyl sulfoxide/tetrabutylammonium fluoride (DMSO/TBAF), N, N-dimethylacetamide/lithium chloride (DMAc/LiCl), N-methylmorpholine-N-oxide (NMMO), and aqueous NaOH/urea solutions.[98] These solvents do, however, have some drawbacks, including instability, high toxicity and pollution levels, and difficulties in recovery.[99]

Ionic liquids (ILs), a novel class of solvents that adhere to the twelve green chemistry principles and are a possible replacement for traditional solvents, have been developed as a consequence of numerous studies.[100] ILs are thought to be one of the best solvents for dissolving carbohydrate polymers because they have loosely binding anions that can strongly interact with the polar functional (-OH, -NH$_2$) groups of polysaccharides and cause them to solubilize.[101]

1.8.1 Ionic Liquids (ILs) for Nanocellulose Dissolution

An organic salt known as an ionic liquid (IL) is made completely of ions, often a sizable organic cation and an organic or inorganic anion. ILs have drawn a lot of interest due to their distinctive characteristics as negligible vapor pressure, thermal stability, low melting point (around 100 °C), recyclable nature, mechanical stability, and non-flammability.[102] Swatloski

et al. identified 1-butyl-3-methylimidazolium chloride [C4MIM][Cl] as a potent cellulose-dissolving solvent.[103]

Depending on the cations, cellulose dissolves in different ionic liquids; imidazolium, pyridinium, morpholinium, and phosphonium has been the subject of several researches.[104-106] Another current research area is the dissolution of cellulose with diverse degrees of polymerization in different ILs with cellulose levels ranging from 5 to 20 wt% and regeneration by the addition of water or protic organic solvents. The capacity of IL to dissolve cellulose depends on its degree of polymerization. [107]

In a number of different ionic solutions, cellulose can sometimes be easily dissolved. The ionic liquid 1-Ethyl-3-methylimidazolium acetate [C2MIM][Ac] may dissolve 21.1% of cellulose (microcrystalline cellulose MCC with DP of 229) after 24 hours at 80 °C, according to research by Brehm et al.[108] However, Li et al. reported that after 7 hours of dissolution, only 16% of cellulose (cotton fibre with DP of 510) could be dissolved by the same ionic liquid ([C2MIM][Ac]) at 90 °C.[109] Furthermore, when temperature and dissolution time increased, regenerated cellulose's level of polymerization reduced. For instance, 1-butyl-3-methylimidazolium chloride [C4MIM][Cl] may dissolve 13% of cellulose by weight at a temperature of 90 °C. However, the amount of polymerized regenerated cellulose decreased from 510 to 240%.[110]

Nanocellulose dissolves in an ionic liquid due to the competitive formation of electron donor-electron acceptor complexes with nanocellulose, which leads in the breakage of intermolecular hydrogen bonds, as shown in **Figure 1.10**. Additional characteristics of the optimum ILs for cellulose dissolving include low viscosity, low toxicity, and ease of recycling. The anion's basicity makes it more important in dissolution, which leads to a large capacity for accepting hydrogen bonds.[107] While the impact of cations is less evident, they are nonetheless essential for the dissolution of cellulose due to their protonic acidity and functional groups. Imidazolium and pyridinium cations dissolve cellulose more efficiently than other cations in ILs because of the acidic protons on their heterocyclic rings.[104] The cations of the ILs may lessen cellulose's solubility through strong interactions with anions or the steric hindrance impact of high size groups in their alkyl chains. At this point, a large amount of cellulose can dissolve with little degradation because of hydrogen bonding interactions between cellulosic material and ionic liquid. [111]
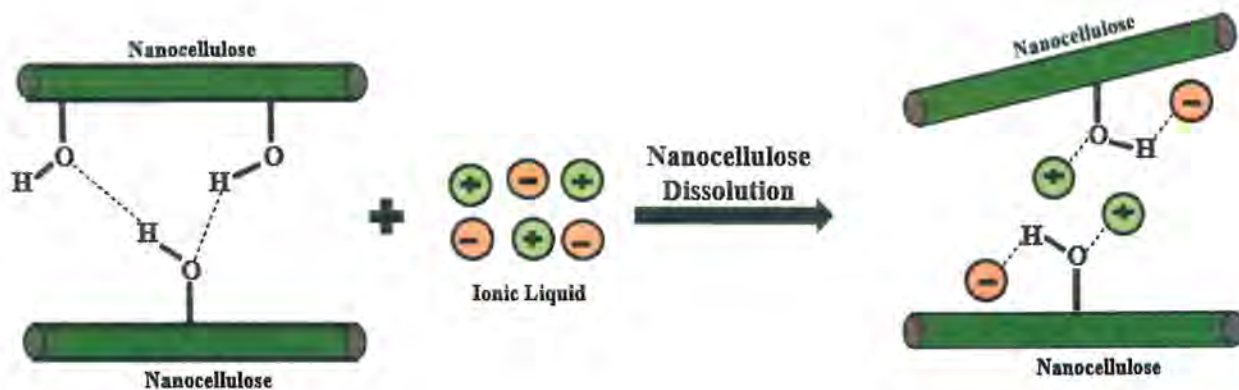
Figure 1.10: Dissolution of nanocellulose in ionic liquid.

The purpose of this study is to develop Eucalyptus wood wastes into potentially profitable sources of biopolymers with high value-added process as extraction of nanocellulose by novel procedure. Eucalyptus is genus of evergreen, tall, magnificent trees used for various domestic applications especially for making furniture, shades, paneling, millworks, and support beams yielding significant amount of wood residues. The production of cellulose nanostructure is a great alternative when taking into account the significance of developing sustainable materials for reducing environmental impacts as well as ensuring adequate disposal of eucalyptus wood residues. NC have previously been extracted from different species of Eucalyptus by various techniques.[112-114] As mentioned above that variety of ILs have been reported to be used as solvent for cellulose dissolution but among this imidazolium and pyridinium based ILs are reported to have better nanocellulose dissolution.[115] But among imidazolium and pyridinium based ionic liquids, latter is reported to have better nanocellulose dissolution.[116] Thus, a new derivative of butyl-pyridinium chloride ionic liquid was synthesized for dissolution of NC; thus, making NC more viable for wide range of applications.

1.9 Literature Survey

Raju, Vishnu, et al. reported extraction of nanocellulose by steam explosion process from pulp of two hardwood species, namely *Casuarina equisetifolia* L. and *Eucalyptus tereticornis* Sm. The group used TEM and AFM techniques giving average diameter 28.690 nm for casuarina and 27.801 nm for eucalyptus. derived nanocellulose, FTIR peaks providing confirmation of successful lignin removal and nanocellulose synthesis, EDAX confirmation of elemental purity, the (101), (002), and (040) crystal plane peaks identified by XRD confirmed the crystalline structure of cellulose and the conversion of cellulose I to cellulose II., and TGA provided high thermal stability of synthesized nanocellulose manifesting its thermal degradation at 375 °C.[117]

Tozluoglu, Ayhan, et al. fabricated cellulose nanofibers (CNFs) and cellulose microfibers (CMFs) from kraft pulp and $NaBH_4$-modified kraft pulp obtained from *Eucalyptus camaldulensis* and characterized them by HPLC, FTIR, DSC and ^{13}C-NMR. SEM revealed micron-wide fibres and fine nanofibrils for CMFs and CNFs while their viscoelastic properties were explained by rheometry respectively. NMR of CNFs and CMFs obtained from $NaBH_4$-modified kraft pulp is reported to show minor shifts. The CMF and CNF made from kraft pulp displayed superior thermal stability and crystallinity values. The CNF film made from kraft pulp was found to have a maximum storage modulus value of 9.71 GPa.[118]

Hassan, Rabia, et al. developed three series of ionic liquids using the cations 1-methyl-3-butyl imidazolium, butyl pyridinium, and diethyldibutylammonium and the anions bromide, methane sulfonate, bis(trifluoromethanesulfonic)imide, dichloroacetate, tetrafluoroborate, and hydrogen. The structures of the ILs produced in the lab were verified using spectroscopic techniques. They used agar well diffusion method to investigate the bactericidal activity of these ILs, and they came to the conclusion that because of their antibacterial properties, ILs are a possible alternative to the present antibiotics and antiseptics.[119]

D. Ashokan and K. Rajathi synthesized five ionic liquids based on pyridinium and used spectroscopic methods like FTIR, NMR, and mass spectroscopy to analyze them. The synthesized compounds had anti-inflammatory, anti-fungal, antibacterial, anticoagulant, and anticancer properties that were also investigated to analyze how the substituents affect the biological activities of ionic liquids.[120]

Ben, Haoxi, et al. reported the synthesis of pyridinium based ionic liquid (1-Allyl-3-Butylpyridinium Chloride) and this pyridine-based ionic liquid has been studied for the dissolving of cellulose, hemicellulose, and lignin as well as two entire biomasses, switchgrass and poplar, at a low temperature of -50°C, giving researchers a chance to investigate the original structures of the biomass components. Five different hydroxyl groups in biomass were quantitatively characterized using a variety of biomass model compounds (glucose, cellotriose, and cello hexose), artificial mixtures of biomass components (cellulose, hemicellulose, and lignin), and computational simulation for the assignments using density functional theory calculations.[121]

Taheri et al. formed an acidic ionic liquid, 1-(carboxymethyl) pyridinium chloride. The artificial ionic liquid, which was used as a solvent, has the untapped potential to dissolve cellulose, chitosan, and chitin. Upto 11 weight percent of cellulose can be dissolved by

synthetic ionic liquid, and up to 40 weight percent of water is the ideal water quantity for effective dissolution.[122]

Saher, Saliha, et al. reported fabrication of three ionic liquids: 1-butylpyridinium chloride [C$_4$Py][Cl] (A1), 1-butyl-3-methylpyridinium chloride [C$_4$C1Py][Cl] (A2), and 1-octyl pyridinium chloride [C$_8$Py][Cl] (A3). The produced ionic liquids were tested for their ability to dissolve cellulose, and [C$_4$C1Py][Cl] was found to be the most effective solvent, dissolving it up to 28% at 110 °C. Based on the catalytic conversion of cellulose to TRS, the modification in cellulose following IL pretreatment was used to facilitate metal salts.[123]

Alrefaee, S. H., reported DFT based computational study of thirty ionic liquids based on imidazolium and pyridinium to demonstrate anticorrosive potential. The results demonstrated that ionic liquids function like an efficient anticorrosive material, and that their ability to suppress corrosion is dependent, respectively, on the nature of alkyl groups and halide ions. It has also been proposed to use pyridinium- and imidazolium-based ionic liquids to exhibit adsorption behavior and suppress corrosion.[124]

1.10 Plan and Objectives of the Study

- The goal of this research is to extract nanocellulose (NC) from hardwood of *Eucalyptus camaldulensis* by novel method involving mechanical treatment with Soxhlet apparatus.

- Characterization of structural properties of extracted nanocellulose by XRD, FTIR, SEM, and Zeta potential analysis.

- Synthesis of newly derivatized tertiary-butyl pyridinium chloride ionic liquid (PyIL) and its characterization by NMR, FTIR, and UV analysis.

- Determination of thermophysical properties of PyIL through refractometry and viscometry.

- Dissolution of nanocellulose in ionic liquid (PyIL) and its confirmation by UV, FTIR and XRD.

- Investigation of anti-bacterial activity of ionic liquid and nanocellulose dissolved ionic liquid (CIL) by agar well diffusion method.

- Identification of antioxidant properties of NC, PyIL, and CIL via DPPH assay and FRAP assay.

- Density functional theory (DFT) based computational study for the interaction of nanocellulose and ionic liquid will be investigated by Gaussian 09 software. Frontier

molecular orbitals analysis and global reactivity indices will be computed to determine the stability and reactivity of compounds. Mulliken charge distribution and Molecular electrostatic potential analysis will be performed to confirm the electrophilic and nucleophilic regions in PyIL, NC and CIL before and after interaction.

Chapter 2

Experimental and Instrumentation

2.1 Materials

Analytical grade chemical reagents were utilized directly in the experiment without further purification. Benzene (C_6H_6, 99.5%), Acetic acid (CH_3COOH, 99.8%), Sodium acetate ($C_2H_3NaO_2$, 99%), Sodium hydroxide (NaOH, 97.5%), Hydrochloric acid (HCl, 37%), Pyridine (C_5H_5N, 98%), Ter-butyl chloride (C_4H_9Cl, 97%), Ethyl acetate ($C_4H_8O_2$, 99.7%), DMF (C_3H_7NO, 99.8%) were purchased from Sigma-Aldrich. Ethanol (C_2H_5OH, (99.8%), Methanol (CH_3OH, 99.5%) and Sodium hypochlorite (NaOCl, 12.5%) were purchased from BDH. In order to prepare various solutions and for other uses, both distilled water and deionized water (DI water) were used.

2.2 Extraction of nanocellulose from *Eucalyptus camadulensis* Wood

Extraction of nanocellulose (NC) is carried out from the hardwood of *Eucalyptus camaldulensis* following method with a slight modification, as stated in literature.[126-127] Firstly, the wood of eucalyptus was grinded to reduced wood fibres. Then the reduced wood was washed with deionized water (5 g of ground raw wood and 100 mL of deionized water) in an Erlenmeyer flask and stirred at 70 °C for 1 hour. The resulting mixture was filtered and rinsed with deionized water numerous times. The acquired washed fibres were then treated mechanically for dewaxing in Soxhlet apparatus.[128] To remove the cuticular wax, 3.5g of wood fibres wrapped in filter paper was placed in thimble. It was refluxed in benzene and ethanol solution (2:1) for 6 hours at 80°C. Ground bark was dewaxed and then allowed to air dry for 12 hours.

The resultant washed raw fibres were treated with an alkaline solution containing a 6-weight percent NaOH solution at 80°C for two hours while being mechanically stirred at 450 rpm. Three times the treatment was done. Fibres were filtered and thoroughly cleaned with distilled water after each treatment to get rid of any remaining alkali and solution pH was neutral. This treatment of sample is carried out to remove and leach out hemicellulose, residual starch, and pectin.[75] A subsequent acid hydrolysis treatment was carried out for delignification and bleaching of fibers.

Figure 2.1: Extraction of nanocellulose (NC) from hardwood of *Eucalyptus camaldulensis*

The solution used in this treatment consisted of equal parts acetate buffer (of pH 5.5), aqueous hypochlorite (1.7 % in water), and distilled water. The bleaching procedure was carried out four times at a temperature of 80°C for four hours while being mechanically stirred at 350 rpm. The fibres were filtered and cleaned with distilled water following each treatment. These three steps yielded pure cellulose microfibers. Nanocellulose was extracted from cellulose macrofibres by sulfuric acid hydrolysis.[78] Using 64 weight percent sulfuric acid (56.4 mL of acid in 55.4 mL of ice-cold water), acid hydrolysis was carried out at 55 °C for around 30 minutes while being mechanically stirred. Ice cubes were used to dilute the suspension to stop the reaction and centrifuged successively at 12000 rpm at 15°C for 20 minutes. The nanocellulose suspension was then sonicated (using a Branson sonifier model 450) for 30 minutes in an ice bath. After that, a 12-hour air drying period was used to eliminate any remaining water from the sonicated suspension. **Figure 2.1** shows the scheme for extraction of nanocellulose from *Eucalyptus camaldulensis.*

2.3 Synthesis of Tertiary Butyl Pyridinium Chloride Ionic Liquid (PyIL)

The previously established process was followed in the synthesis of the ionic liquid used in the current study.[129] Tertiary butyl pyridinium chloride ionic liquid. By directly reacting pyridine and ter-butyl chloride in ethyl acetate, [C4Py][Cl] was formed. The purification was

carried out utilizing the earlier technique with slight modifications.[119] The assembly containing 5 mL of pyridine in 25 mL ethyl acetate was stirred at 60 °C. Following this 10ml of haloalkane (ter-butyl chloride) was added dropwise to the above solution with the help of syringe.

Figure 2.2: Synthetic scheme of tertiary butyl pyridinium chloride ionic liquid (PyIL)

Then, the mixture was refluxed and stirred for 72 hours to obtain the maximum yield of product. After 72 hours, a rotating evaporator was put to use to evaporate the solvent, and the reactants were decanted. The product was subsequently dried for 12 hours around 50 °C in a vacuum oven. A brown greasy liquid with a 94% yield served as the final product.

Table 2.1. Solubility of ionic liquid in different solvents.

Solvent	Solubility	Naked eye appearance
Deionized water	Soluble	Less viscous light brown liquid
Methanol	Soluble	Less viscous light brown liquid
Ethanol	Soluble	Less viscous light brown liquid
DMSO	Soluble	Less viscous brown liquid
Methanol + H_2O	Soluble	Faded brown liquid
Ethanol + H_2O	Soluble	Faded brown liquid
DMF	Soluble	Less viscous brown liquid
Toluene	Insoluble	Layered brown liquid
Ethyl Acetate	Insoluble	Layered brown liquid

Synthetic route for the synthesis of ionic liquid is shown in **Figure 2.2**. The solubility of synthesized PyIL was checked in various solvents as shown in **Table 2.1** and PyIL was found to be soluble in water, ethanol, methanol, DMSO and DMF. Ionic liquid (PyIL) is soluble in wide range of solvents showing their good solvation capability.

2.4 Dissolution of Nanocellulose in Ionic Liquid

Because of inter- and intramolecular hydrogen bonding between the polymeric chains, nanocellulose (NC) has a well-defined crystalline and amorphous structure. NC is insoluble in the majority of frequently used solvents owing to a strong intramolecular van der Waal (mostly H-bonding) force of attraction.[130] In a typical cellulose dissolution experiment, 10mg of nanocellulose was added to a 20 mL vial which contained 2 mL of solvent and co-solvent at 80 °C. Several typical solvents that have been used to dissolve nanocellulose are; water (at pH 5 and 10), NaOH, NaOH/Urea, methanol, ethanol, acetone, methanol with H_2O as co-solvent and ter-buytl pyridinium chloride ionic liquid. Nanocellulose showed solubility in water, methanol, ethanol, acetone, methanol/H_2O, NaOH and NaOH/H_2O mixtures after sonicating the samples for 12 hours in ultrasonicator.

Heating the mixture of ionic liquid and nano lignocellulose in a sealed flask allowed to measure the pyridinium ionic liquid's capacity to dissolve cellulose. Because moisture greatly slows down the dissolution,[131] prior to dissolution, nanocellulose was dried for 6–8 hours in an oven at 70–80 °C. A solution was formed after adding a tiny quantity (10 mg) of nanocellulose to PyIL and stirring the mixture for 12 hours around 80 °C. Continuous monitoring was done of the dissolving process. The point of ultimate dissolution is defined as the stage where a solution of extreme viscosity formed and no additional cellulose dissolution was seen. In addition, water can also act as co-solvent with prepared ionic liquid and cellulose dissolution in binary solvent system was observed. **Table: 2.2** gives the solubility of nanocellulose in different solvents.

Table 2.2. Solubility of nanocellulose in different solvents.

Solvent	Solubility	Naked eye appearance
Deionized water	Insoluble	No change
Acidified H_2O	Slightly soluble	Partial milkiness
Alkaline H_2O	Partially soluble	Milky solution
Methanol	Partially soluble	Milky solution
Ethanol	Slightly soluble	Partial milkiness

Acetone	Insoluble	No change
Methanol+ H_2O	Slightly soluble	Partial milkiness
Ethanol + H_2O	Very slight solubility	Partial milkiness
Acetone + H_2O	Insoluble	No change
IL	Slightly soluble	Brown viscous solution
IL + H_2O	Partially soluble	Less viscous brown solution

Water content for dissolution of nanocellulose was optimized in prepared PyIL/H_2O mixtures (2 mL) of different composition.[122] The mixture was sonicated to obtained homogeneous mixtures. **Table 2.3** illustrated specifications of different compositions of PyIL/H_2O mixtures. To explore the capability of the prepared solvents to dissolve cellulose, different mixtures of nanocellulose in PyIL/ H_2O solvent system were prepared and heated to 80 °C for 12h. After mixing given amounts of cellulose (10 mg), in IL and water solvent system, the resultant mixture was vigorously stirred for different time intervals. The first examinations showed that solvents M1 to M3 showed no solubility for cellulose. For solvent M4 and M5, slight cellulose dissolution was observed. On the other hand, M6 could partially dissolve cellulose, thus affirming that presence of too much water impairs the dissolution process.

Table 2.3. Dissolution of nanocellulose in different compositions of PyIL /H_2O mixtures.

Mixture ID	Components		Solubility
	IL(v/v%)	Water(v/v%)	
M1	50	50	Insoluble
M2	60	40	Insoluble
M3	70	30	Insoluble
M4	80	20	Slightly soluble
M5	90	10	Most soluble
M6	100	0	More soluble

Ionic liquid (PyIL) showed best dissolution at 9:1 IL/water mixture (M5) because of synergistic solvation (water and PyIL in specific ratio create a biphasic system). IL disrupts H-bonding in nanocellulose and water enhances dissolution process by facilitating PyIL diffusion in cellulose chains. But too much water impairs dissolution. When water content increases, water molecules

compete with IL for interaction with cellulose. As water is not efficient in disrupting hydrogen bonding network in cellulose so leads to reduced dissolution as seen in case of M1, M2, and M3.

2.5 Characterization Techniques

A number of techniques were used for explaining the electrical, structural, and mechanical characteristics of synthesized nanocellulose, Ionic liquid, and cellulose dissolved Ionic liquid, which are briefly explained below.

2.5.1 Nuclear Magnetic Resonance (NMR) Spectroscopy

The purity and structure of synthesized ionic liquid was determined using nuclear magnetic resonance (NMR) spectroscopy. The basic principle behind NMR is that when subjected to an external magnetic field, some nuclei exist in particular nuclear spin states. In the presence of external magnetic field nuclei align themselves either in the direction of magnetic field or against the field. When the spin returns to ground state level, the emitted radiofrequency signal gives NMR of concerned nucleus. Chemical shift (δ) is the resonance frequency of a nucleus relative to a standard in magnetic field and is expressed in parts per millions(ppm). Trimethyl silane (TMS) is the most common reference compound in NMR with $\delta = 0$ ppm.

$$\delta_{sample} = \left(\frac{v_{sample} - v_{ref.}}{v_{ref}} \right) \times 100 \qquad (2.1)$$

For NMR, the sample was diluted in 0.9 cm^3 of deuterated chloroform solvent (CDCl$_3$) using its approximate amount of (50 to 100) μL. The JEOL JNM-ECA400 Bruker Advance (300 Hz) spectrometer was put to use to record the ^{1}H and ^{13}C NMR spectra at room temperature. As an internal benchmark, the ^{1}H and ^{13}C chemical changes are presented in parts per million (ppm) compared to TMS. The terms "singlet," "doublet," "triplet," and "quadruplet" are all abbreviations for multiples.

2.5.2 X-ray Diffraction (XRD)

For the purpose of analyzing crystal structure, lattice parameters, and crystallite size of nanomaterials, X-ray diffraction (XRD) is a well-known non-destructive technique. Instrument employed for X-rays diffraction is X-ray diffractometer. The source of electromagnetic radiations in an X-ray diffractometer are high energy X-rays (~100 keV) with a wavelength of about 0.1 Å. X-ray diffractometer works on the basic principle of the monochromatic X-rays interfering constructively with the material under observation. This

phenomenon is governed by Bragg's Law which states that when any material is bombarded with X-rays at a certain incident angle, these electromagnetic radiations are reflected by the crystal lattice planes. Some interfere destructively and cancel each other out while others interfere constructively when the travel path is an integral multiple of wavelength of X-rays.[133] These reinforced diffracted X-rays produce a characteristic X-ray pattern that is provides information about the phase, crystallite size, structure and crystallinity of a material. If the spectrum exhibits sharp intense peaks, the material is crystalline in nature while for amorphous materials, broad regions are generally observed.

Each plane in atoms is a representative member of a parallel set of equally spaced planes, and each lattice point must lie on one of the planes, as shown in the interaction of X-rays with planes of atoms in three-dimensional lattices that display translational symmetry of structure. The planes are characterized by Miler indices (h, k, l where h, k, l takes values of positive or negative integers or zero). The distance between successive planes is known as d-spacing/ inter-atomic spacing (d_{hkl}), constructive interference follows Bragg's equation given as;

$$2d \sin \theta = n\lambda \qquad\qquad (2.2)$$

where

n = reflection order

λ = wavelength of X-rays

d = the distance between atomic planes in a crystal

2θ = the angle of diffraction of X-rays

The 2θ values in the XRD spectrum, which are indicative of the particular phase of the sample being used, specify the peak positions. Using Philips X'pert Pro diffractometer of Cu Kα wavelength (1.54 A), an X-ray diffraction pattern was obtained. With an increment of 0.02, all samples were scanned over the range of 20 ° to 80°.

2.5.3 Fourier Transformation Infrared (FTIR) Spectroscopy

FTIR is a type of spectroscopy which studies interaction between a material and incoming IR radiations due to changing dipole moment of the molecules. FTIR refers to the study of the vibrations of molecule due to the electromagnetic radiations (EMRs) in the 400-4000 cm^{-1} range that absorb infrared radiation.[134] Each functional group present in a compound has distinctive vibrational energy bands, which are useful for identifying a compound based on

their vibrations in the functional group region. In addition, FTIR is an excellent technique for particle analysis and identification of unknown samples depending on the vibrations in the fingerprint region.

The dipole moment of the compound must change as a result of the vibrations for the molecule to be IR active that occur when infrared radiations are absorbed. The operating principle of FTIR spectroscopy follows the passage of IR light passes through a sample, that triggers the vibration of molecular bonds by absorption of light. Some light is reflected while some part of it is transmitted through the sample and falls on detector thereby producing an IR spectrum. In an IR spectrum, % transmittance is plotted vs. wavenumber (cm^{-1}) typically in the range of 400-4000 cm^{-1}. The entire FTIR spectrum is comprised of two regions; the region between 4000-1000 cm^{-1} is called as functional group region while the region between 1000-400 cm^{-1} is finger print region. The vibrations typically include symmetric or anti-symmetric stretching vibrations, symmetric or anti-symmetric bending vibrations, out of plane and in plane deformation vibrations.[135]

Attenuated total reference (ATR) is a primary sampling accessory of FTIR spectrophotometer. In FTIR equipped with ATR, when light reflects off of the crystals such as diamond, zinc selenide or germanium, it undergoes total internal reflection with only small amount absorbed by the sample. An ATR-FTIR has enhanced surface sensitivity, requires easy sample preparation for liquids and solid samples, and is time efficient.[136] FTIR analysis of synthesized materials was performed on ATR PRO ONE (JASCO) FTIR-6600typeA spectrometer in frequency range of 500 cm^{-1} to 4000cm^{-1}.

2.5.4 Ultraviolet-Visible (UV-vis) Spectroscopy

UV-visible spectroscopy is employed to study the solvating properties of synthesized ionic liquid and effect of nanocellulose dissolution on λ_{max} of ionic liquid. The study of how electromagnetic radiations (EMRs) in the UV-vis region interact with matter is the subject of UV-vis spectroscopy. The absorption in UV-vis of light source is attributed mainly to the electronic transitions. Absorption of light by electrons in the matter causes excitation of these electrons to the higher energy levels.[137] Energy gaps between orbitals select the radiation types that electrons will absorb to reach higher levels. Low energy gap requires less energy for photoexcitation. Absorption in UV-vis region is helpful for quantitative and qualitative analysis of material as the absorption wavelength is characteristic of the absorbing material. This technique is widely used for studying the behavior of a molecule in different solvents. Change in λ_{max} and sometimes intensity of absorbing material with the changing polarity of solvent is

referred as solvatochromic effect. Ionic liquids are good solvents for spectroscopic studies, particularly in the ultraviolet-visible (UV-vis) range due to their strong solvating capabilities and high spectral transparency. They may be used with organic or inorganic solvents to "solvate" the ionic liquid's constituent ions, which reduces ion aggregation and results in higher conductivity and lower viscosity.[138] In current research, UV-1700 UV-vis spectrophotometer (Shimadzu) was used for studying solvatochromic effect of ionic liquid in water, methanol, ethanol, DMF and DMSO and for studying the change in λ_{max} of ionic liquid upon nanocellulose dissolution in it.

2.5.5 Scanning Electron Microscopy (SEM)

Analysis of the morphology and size of nanomaterials using scanning electron microscopy is common. SEM gives the magnified image of sample by using electron beam instead of light. In SEM, a focused beam of electrons scans the sample surface and electrons are back scattered or secondary electrons are emitted. This technique provides high resolution image of sample on the nm scale and upwards.

An electron gun acting as cathode is used to produce electron on application of high voltage. This electron beam is accelerated by a strong electric field. As a result, the electron beam is pointed at the condenser lenses where it is focused on a spot that is up to 5 nm in size. This focused beam is permitted to travel through the coils utilized for deflection. Following the beam's deflection along the x and y axes by means of these coils, the sample surface is scanned. The principal electrons are those that strike the sample. After interacting with the sample, the primary electrons produce secondary electrons.[139] SEM was carried out using a scanning electron microscope (Nova NanoSEM 450) to get knowledge of surface structure of nanocellulose.

2.5.6 Zeta Potential and Particle Size Analyzer

Investigating colloidal systems involves either the zeta potential or the electrophoretic mobility (μ). The zeta potential, which can be used to investigate electrical interactions between colloidal particles, is created when charged particles are present on the surfaces of suspended particles in solution.[140] Zeta potential is the potential difference between electrical double layer of electrophoretic mobile particle and layer of dispersant. Zeta potential is calculated using a variety of electrochemical processes, including electrophoresis, sedimentation, and electroosmosis.[141] In the electrophoresis method, the dispersion of nanomaterials is subjected to an electric field that enables them to move at a speed determined by zeta potential.[140] In Zeta

sizer, the velocity of Brownian motion of particles is converted to size of particles. Laser interferometry is used to measure this velocity. The electrophoretic mobility is computed using the calculated velocity, and the zeta potential is estimated using this information.

In this work, by calculating the zeta potential value of nanocellulose, its electrostatic stabilization was calculated. The surface charge and size distribution of nano lignocellulose fibres were determined with Malvern-Zetasizer Nano-ZS ZEN3600, in range of 0.1-1000 nm at 25 °C. Disposable zeta cells were utilized to measure zeta potential and average zeta size and concentration of nanocellulose processed was 150 μM in methanol as solvent. Following equilibration, measurements were taken three times using cuvettes containing 1 mL of material.

2.6 Anti-Bacterial Studies

The minimum inhibitory concentration (MIC) approach was chosen as the test for antibacterial activity of nanocellulose crystals (CNCs), ionic liquid (PyIL), and nanocellulose dissolved ionic liquid (CIL) against 4 bacteria, namely, *Escherichia coli* (*E. coli*), *Staphylococcus aures* (*S. aures*), *Bacillus subtills* (*B. subtills*), and *Klebsiella pneumoniae* (*K. pneumoniae*). The inhibition zone was calculated with Mueller-Hinton (MHA) agar by well diffusion method.[119] The sterilized Petri dishes were kept at 4 to 8 °C in tight polyethylene bags. Mueller-Hinton agar (38 g/L) was suspended in distilled water and autoclaved for 20 minutes at 121 °C and 15 psi pressure to create the Mueller-Hinton agar media.[120] The plates were seeded with inoculum (bacterial culture in MHA) using sterile cotton brushes. In sterilized 90 mm Petri dishes, nutrient agar was distributed. Additionally, the sterile borer was used to drill wells into the agar plates. The materials for analysis — ionic liquid, nanocellulose dissolved in ionic liquid, and nanocellulose — were poured into wells. After that, agar dishes were kept at 37 °C for 24 hours to encourage microbial growth. Antimicrobial drugs diffused into the surrounding agar, inhibiting growth near the reservoir or source and creating zones or clearances where (for sensitive organisms) microbiological growth is impeded. By measuring the width of the inhibitory zone, each sample was evaluated. Using a vernier caliper, the inhibition zone was measured. The extent of the antibacterial action is determined by the zone's size.

2.7 Antioxidant activity Studies

Antioxidant activity was checked via 2,2-diphenyl-1-picrylhydrazyl (DPPH) assay and Ferric reducing antioxidant power (FRAP)/Total reducing power (TRP) Assay. DPPH was utilized as the free radical source to measure the antioxidant activity of Ionic liquid (PyIL),

nanocellulose (NC) and nanocellulose dissolved ionic liquid (CIL). In this method, the 50% inhibitory concentration (IC_{50}) can be determined and reported by detecting the lowered absorbance capacity of the DPPH free radical with a maximum absorbance of 517 nm "IC_{50}" denotes to least amount of scavenger needed to reduce DPPH absorption to 50%. The colour of DPPH would shift from purple to yellow after it acquired an electron from the antioxidant molecule due to reduction of DPPH. The method outlined by Brand-Williams et al. was applied to investigate activity of DPPH in scavenging radicals with slight modifications.[142] Using the stable free radical 2, 2-diphenyl 1-picrylhydrazyl (DPPH), the compounds were briefly tested for antioxidant activity. 10 aliquots of the sample were combined with 190 μL aliquots of the DPPH solution (9.6 mg/100 mL methanol). The absorbance at 517 nm was measured using a microplate reader after 30 minutes of incubation at 37°C in the dark. The positive and negative controls were ascorbic acid and DMSO, respectively. The results are shown as mean values standard deviations for all measurements that were carried out in triplicate. In this assay, positive control is used to check the accuracy of commercial DPPH and negative control is used as solvent for antioxidant. The DPPH antioxidant activity was calculated using **equation 2.4**

$$\% \text{ DPPH activity} = \frac{A_{DPPH} - A_{sample}}{A_{DPPH}} \times 100 \qquad (2.4)$$

According to a modified version of Oyaizu's method, the ferric reducing antioxidant power (FRAP) assay, also known as potassium ferricyanide colorimetric assay, was used to calculate the reducing power of various substances.[143] Potassium ferricyanide (1 % w/v in DI water) and a buffered phosphate solution (0.2 M, pH 6.6) were added to an aliquot of 100 μL of sample, which was then incubated at 50 °C for 20 minutes in a bath of water that resulted in yellow colored complex formation between sample and potassium ferricyande. After adding 200 μL of trichloroacetic acid (TCA) (10 % w/v in distilled water) to antioxidant, mixture was centrifuged at 3000 rpm at 25 °C for period of ten minutes. TCA decreases the pH of reaction mixture and this decreased pH ceases formation of complex between antioxidant and potassium ferricyanide. Following that, 50 mL of $FeCl_3$ (0.1% w/v in distilled water) was added to the 150 mL of supernatant on a 96-well plate. The absorbance was then read at 630 nm as this wavelength corresponds to the ferrous ion formed after reduction of ferric ion. Higher absorbance corresponds to greater reducing power. The assays were performed three times, and the outcomes are shown as mean values ± standard deviations. An effective control was ascorbic acid (1 mg/mL DMSO). Ascorbic acid equivalent (AAE) per mg of sample (g AAE/mg) is a unit used to measure a sample's reducing power.

2.8 Density Functional Theory (DFT)

Gaussian 09 is a software package that performs relativistic calculations based on DFT. Initially, it was developed by John Pople and his coworkers. Atoms and molecular calculations can be performed on both solution and gaseous phase. The software uses Slater Type Orbitals (STOs) as basis functions to correctly predict the structural-electronic calculations. Gaussian comprises of database with verified basis set files varying from the single-zeta basis set to quadruple – zeta basis sets with different polarization and diffused functions. Different calculations can be performed on this package such as;

- Geometry optimization
- Single point calculations
- Frontier molecular orbital analysis
- Computation of excited state is possible using time-dependent density functional theory
- Molecular electrostatic potential surface determination
- Point charges can be introduced in calculations

The most well-known hybrid density functional theory model, B3LYP, incorporates local exchange, Hartree-Fock exchange, gradient exchange correction, local correlation, and gradient correlation correction. Computational studies were carried out by B3LYP/6-31G+ (d, p) using DFT.

Chapter 3

Results and Discussion

3.1 Nuclear Magnetic Resonance (NMR) Analysis

The ^{1}H-NMR and ^{13}C-NMR spectra of the tertiary butyl pyridinium chloride ionic liquid was obtained on Bruker Advance III (300 MHz) NMR Spectrometer.

3.1.1 ^{1}H-NMR and ^{13}C-NMR Analysis of Ionic Liquid

Figure 3.1 shows the ^{1}H-NMR spectra of tertiary butyl pyridinium chloride ionic liquid (PyIL) recorded at an applied radiofrequency of 300 MHz. The peak showing singlet at 1.02 ppm as shown in **Figure 3.2** corresponds to the methyl groups attached to the pyridinium ring.
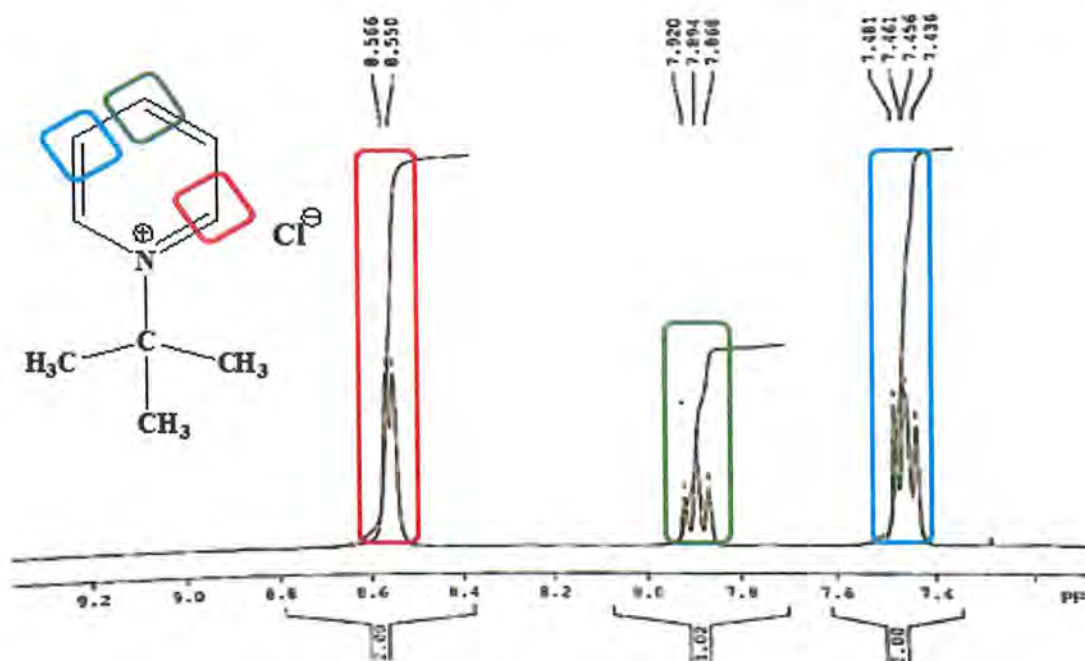
Figure 3.1: ^{1}H-NMR of PyIL in CDCL$_3$

The hydrogens attached to the ortho carbon of pyridinium ring showed doublet at 8.55 ppm and 8.56 ppm. The hydrogens attached to meta carbon of pyridinium ring showed a doublet of doublet at 7.43, 7.45, 7.46 and 7.48 ppm. The hydrogens attached to the para carbon showed a triplet at 7.86, 7.89 and 7.92 ppm. **Figure 3.2** shows that other two peaks located around 1.8 ppm and 11.0 ppm shows presence of solvent which was not evaporated completely. The observed chemical shifts are as under;

H^1 NMR (300 MHz, CDCL$_3$) δ, ppm: 8.55-8.56(d, 2H), 7.43-7.48(dd, 2H), 7.86-7.92(t, 1H), 1.02 (1H) and solvent peak at 1.817 and 11.016.
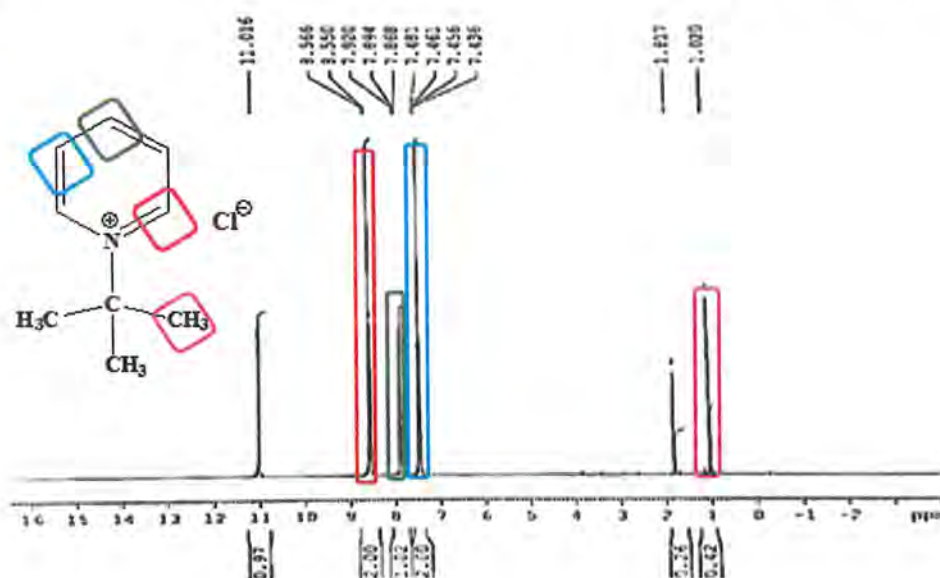
Figure 3.2: ^{1}H-NMR of PyIL in CDCl$_3$

In ^{13}C-NMR spectra of Ionic liquid represented in **Figure 3.3**; four different peaks appear due to the presence of four different carbon nuclei. The singlet peak with an upfield shift located at 31.05 ppm corresponds the four equivalent methyl carbons of the alkyl group attached to the pyridinium ring. Another singlet at 140 ppm occurs due to ortho carbons of pyridinium cation. Meta carbon of pyridinium ring shows a peak at 125 ppm. The para carbon shows a singlet at 145 ppm. While chemical shifts around 77 ppm are due to CDCl$_3$, the solvent used. The observed chemical shifts are as under;

^{13}**C-NMR** (300 MHz, CDCL$_3$) δ, ppm: 140.87(N-CH$_2$ of aromatic system), 125.49(C-CH$_2$ of aromatic system), 145.43(C-CH$_2$-C of aromatic system), 31.05(three equivalent CH$_3$ of Ter-butyl group attached to nitrogen) and CDCl$_3$ shifts at 77.04, 77.47 and 77.89.[134]
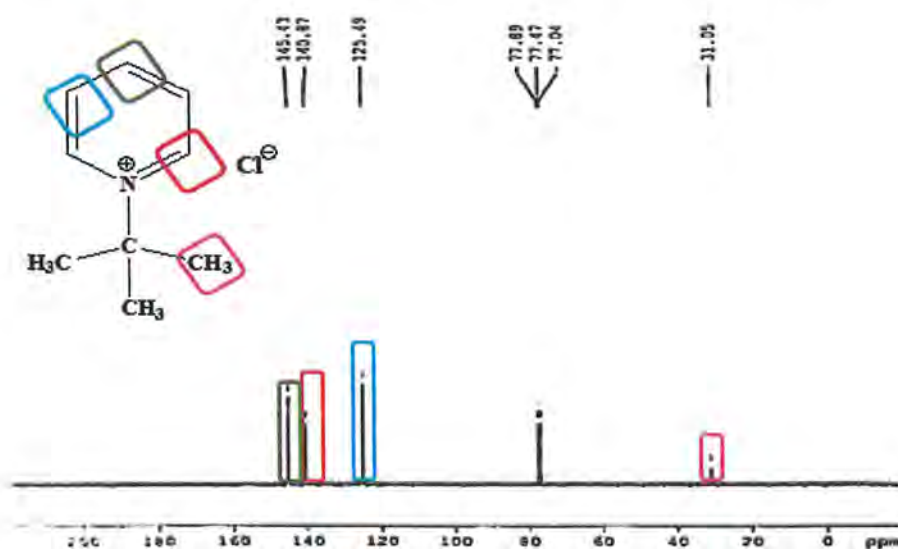
Figure 3.3: ^{13}C-NMR of PyIL

38

The NMR analysis confirms the structure and purity of the synthesized PyIL.

3.2 X-ray Diffraction (XRD) Analysis

The semi-crystalline supramolecular structure of extracted nanocellulose and the impact of PyIL on crystallinity of extracted nanocellulose upon dissolution of NC in PyIL were studied using X-ray diffraction. Since NC's molecular structure is both amorphous and crystalline in parts. The crystalline (ordered) regions of cellulose are securely bonded by H-bonding, whilst amorphous (disordered) regions of the cellulose chains lack H-bonding. Chemical interactions have an impact on the crystallinity of cellulose that is determined with the help of X-ray diffraction. [144]

XRD pattens of extracted NC and nanocellulose dissolved tertiary butyl pyridinium chloride- ionic liquid (CIL) were recorded using PANalytical X pert PRO X-ray diffractometer model (3040/60) operated at 45 kV voltage and 40 mA current having a Cu-Kα radiation source of wavelength $\lambda = 1.54°$ with a scan rate of 0.025 over a diffraction angle range from 10° to 80°. Samples were analyzed under constant and ambient conditions. The XRD pattern of extracted NC is depicted in **Figure 3.4**. NC shows different diffraction peaks in the angular range of 10° to 50° due to scattering patterns from (110), (200), and (004) planes of nanocellulose. [145] Semi-crystalline nature of NC is reflected from the data.
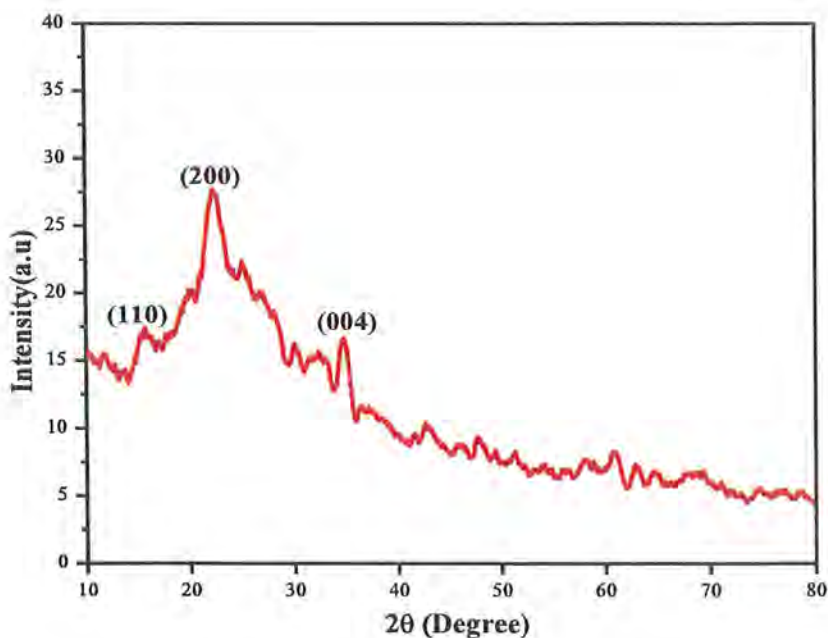
Figure 3.4: XRD of extracted nanocellulose (NC)

The sharp peaks around $2\theta = 22°$ and 35° are result of scattering from (200) and (004) diffraction planes and confirm semi-crystalline nature of extracted nanocellulose. The

relatively broader peak at $2\theta = 16°$ agreeing to the (110) planes of diffraction exhibit presence of amorphous region in extracted nanocellulose.[146-147] The elimination of amorphous constituents including hemicellulose, lignin, and less-perfect sections of cellulose led to the crystallinity of the nanocellulose and the efficient extraction of nanocellulose from lignocellulosic biomass. These characteristic peaks corresponded to the crystalline structure of cellulose I so it can be inferred that the extracted nanocellulose belong to type I cellulose.[148] The degree of crystallinity of extracted nanocellulose was found to be 71% calculated by using equation;

$$X_c = \frac{A_c}{A_a + A_c} \times 100 \qquad (3.1)$$

Where X_c is the degree of crystallinity, A_c is the area under the crystalline peaks and A_a is the area under amorphous peak.

Figure 3.5 illustrates the diffractograms of the nanocellulose dissolved ionic liquid (CIL). Structural studies show that dissolution of nanocellulose in pyridinium ionic liquid cause changes in its crystalline characteristics as reported previously.[149]
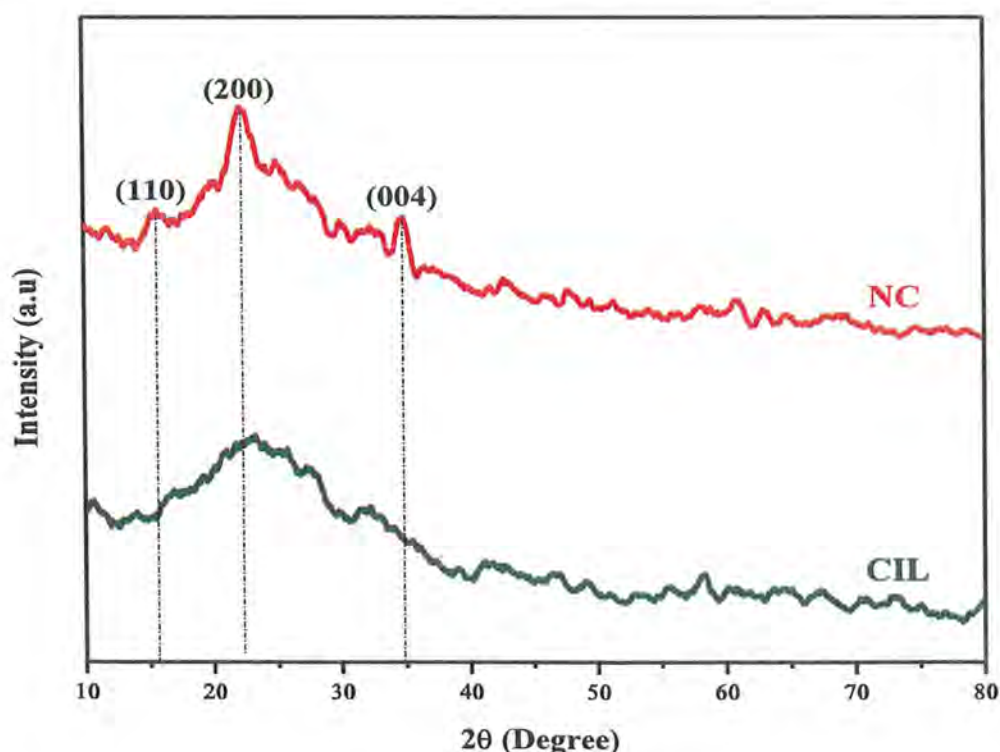
Figure 3.5: Comparison of XRD of NC and nanocellulose dissolved ionic liquid (CIL)

The dissolution of NC in PyIL caused the vanishing of the peak at (110) lattice planes, due to a removal of amorphous domain. But the broadness of peak at $2\theta= 22°$ and $35°$ corresponding

to the planes (200) and (400) showed a decrease in the crystallinity of nanocellulose (NC) of on dissolution in tertiary butyl pyridinium chloride ionic liquid (PyIL). Hence, tertiary butyl pyridinium chloride ionic liquid caused change in the crystallinity of nanocellulose by attacking the OH groups on surface of nanocellulose for its dissolution feasible in ionic liquid providing a solution to the problem of dissolution of nanocellulose making it more efficient and useful biopolymer.

3.3 FTIR Analysis

FTIR analysis of the synthesized pyridinium based ionic liquid (PyIL), extracted nanocellulose (NC) and nanocellulose dissolved ionic liquid (CIL) was performed on ATR PRO ONE (JASCO) spectrometer in the frequency range of 500 to 4000 cm^{-1} and the resulting spectra are depicted in **Figure 3.6 - Figure 3.8.** The FTIR spectrum of synthesized IL (brown in colour) had several peaks, some of which were designated as the following at max cm^{-1} as shown in the **Figure 3.6.**
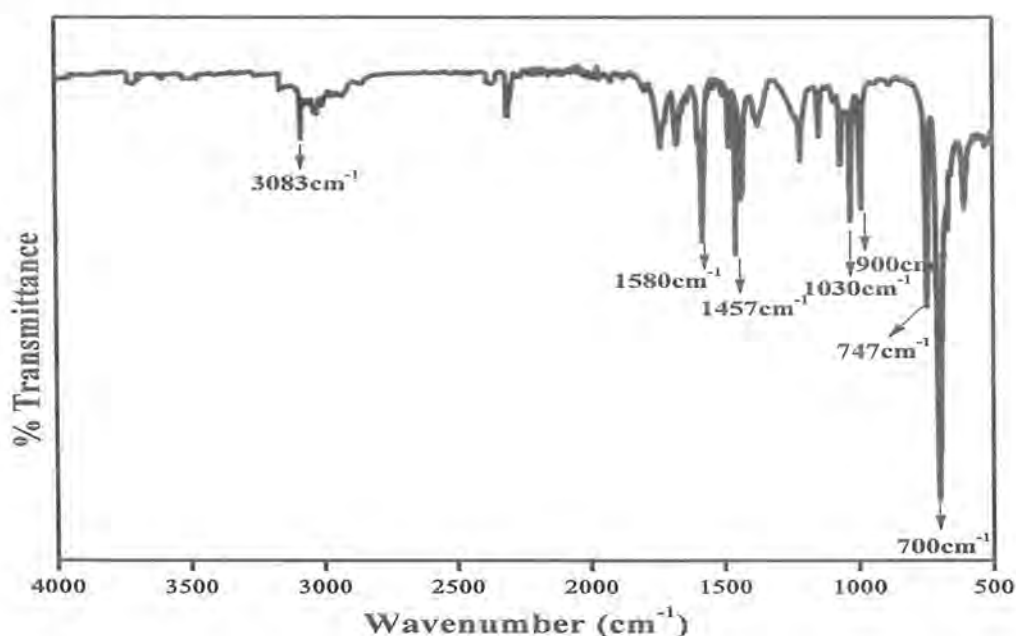
Figure 3.6: FTIR of PyIL

The peak located at 3083 cm^{-1} is due to (double bonded) C-H bond stretching of aromatic system of pyridinium. The peak appearing at 1580 cm^{-1} is owing to C-C multiple bonds stretch of pyridinium ring. The spectral peak centered at 1457 cm^{-1} is due to medium to strong absorption of aromatic pyridine ring. [134] The peaks at 990 and 1030 cm^{-1} are induced due to C-N stretching vibrations of alkyl-pyridinium ring. The peaks at 700 and 747 cm^{-1} are due to aromatic out of plane C-H bending of five adjacent hydrogen atoms respectively. [150] The FTIR spectra of nanocellulose a shown in **Figure 3.7** and features a broad band for hydrogen bonded

O-H group stretch at 3300-3400 cm^{-1},[151] and C-H bond stretching at 2850-3000 cm^{-1}. The peak appeared at 1652 cm^{-1}, correlating with the water-nanocellulose interaction chemical group and β glycosidic bands at 1000-1300 cm^{-1}. The peak at 640 cm^{-1} appears due to out of plane C-C bond stretching.[134]
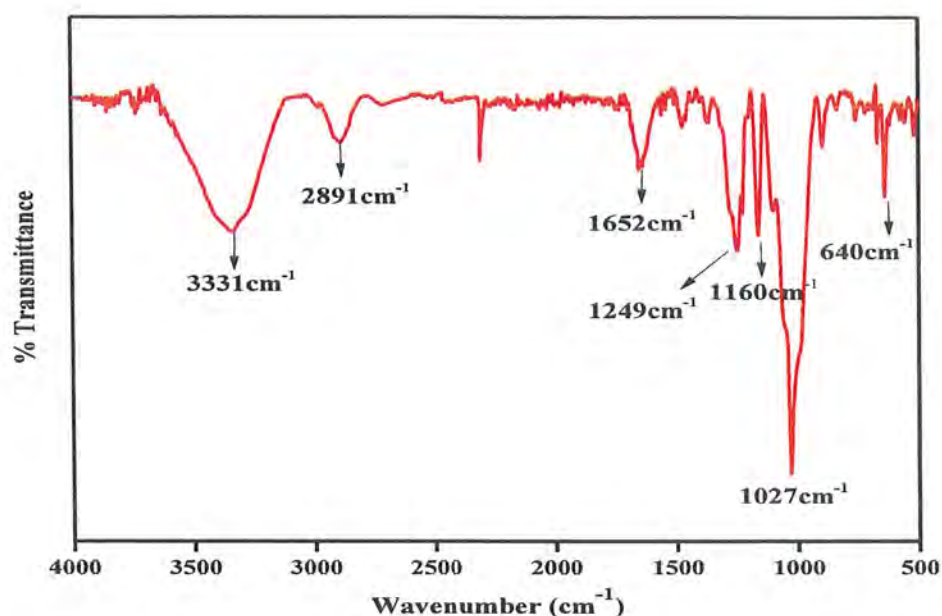
Figure 3.7: FTIR of nanocellulose (NC)
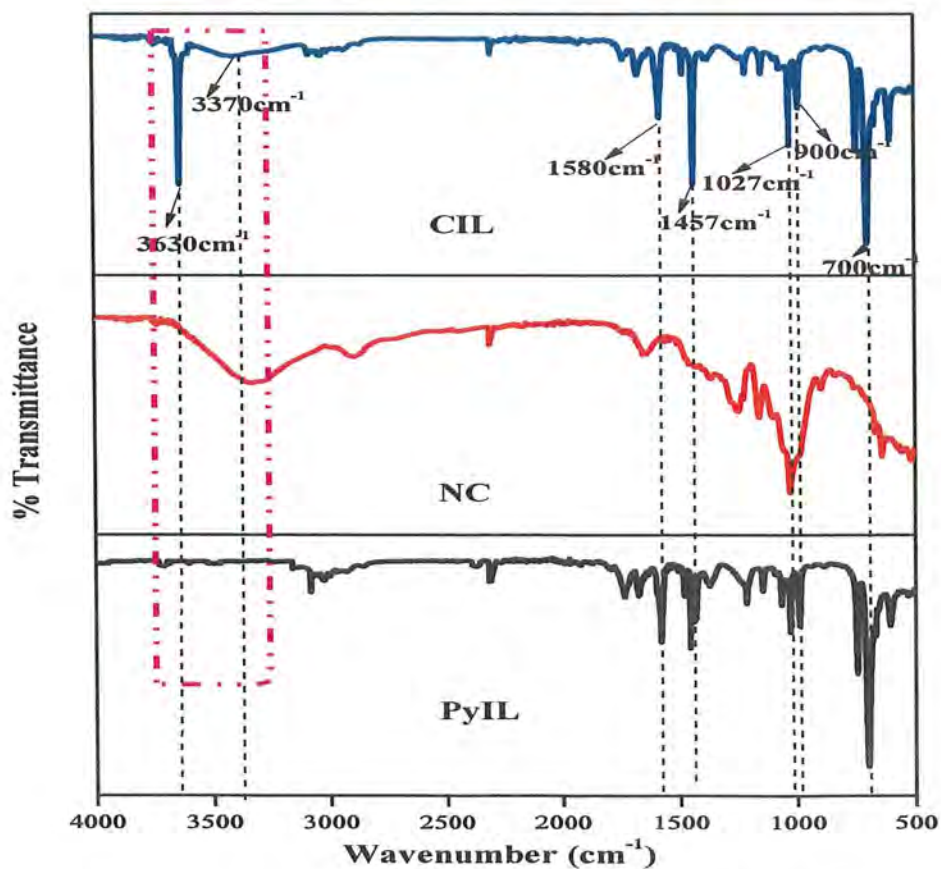
Figure 3.8: FT-IR of nanocellulose dissolved ionic liquid (CIL)

The FTIR spectra of nanocellulose dissolved ionic liquid as in **Figure 3.8** showed a sharp peak due to free O-H group at 3600-3650 cm^{-1} and a broad peak due to hydrogen bonded O-H group at 3300-3400 cm^{-1}. The peak at 1675 cm^{-1} appears due to aromatic C=C bond absorption in nanocellulose dissolved ionic liquid (CIL) with lower intensity. The peak at 1581 cm^{-1} featured C-C multiple bonds stretching of aromatic ring of ionic liquid. The sharp peak at 1437 cm^{-1} appeared due absorption of aromatic pyridine ring in ionic liquid. The peak at 1027 cm^{-1} defined a β glycosidic bond in nanocellulose. The peaks 990 cm^{-1} illustrated C-N stretching of ionic liquid. The peaks 747 cm^{-1} and 700 cm^{-1} characterized C-H bending of aromatic system of ionic liquid.[134, 152]

The appearance of peak at 3630 cm^{-1} that corresponds to free OH bonds on surface of NC and a slight shift in band for bonded OH groups to 3370 cm^{-1} shows the successful dissolution of NC in PyIL. Also, the appearance of peak at 1027 cm^{-1} that agrees to β glycosidic bond in nanocellulose showed that PyIL has not interacted with β glycosidic bond of nanocellulose and the internal structure of NC is intact instead PyIL has just interacted with the bonded surface OH groups of nanocellulose yielding free OH groups. Hence posing a solution to NC dissolution and making its dissolution feasible in PyIL and presenting PyIL, a good solvent for dissolution of nanocellulose to be used for applications.

3.4 UV- Visible Spectral Analysis

To study the optical properties of synthesized ter-butyl pyridinium chloride ionic liquid (PyIL) in terms of absorption; UV Visible spectral analysis was performed in different solvents to study its solvatochromic effect. Solvatochromic effect refers to the shift in the position along with the intensity of absorption maxima caused by change in the medium's polarity. Solvatochromism is of three types positive and negative.[153] In negative solvatochromism, λ$_{max}$ exhibits a red shift with decrease in solvent polarity and opposite behavior is observed in positive solvatochromism.

The absorption maxima of ionic liquid were measured in various solvents including; water, ethanol and methanol (a protic solvents) as well as dimethylformamide (DMF), dimethyl sulfoxide (DMSO) (polar aprotic solvents) as shown in **Figure 3.9**. The absorption spectra of PyIL shows intense absorption maxima in the range of 220–300 nm due to the π– π* transition in all solvents. A bathochromic shift was observed for PyIL when going from polar protic solvents to polar aprotic solvents, in a way that H$_2$O < MeOH < EtOH < DMSO < DMF. The synthesized ionic liquid tertiary-butyl pyridinium chloride showed slight red-shift of 2 nm in polar aprotic solvent with decreasing solvent polarity as absorption maxima in DMSO is 287

nm and 289 nm in DMF. However, there is a red shift of 12 nm observed for the polar protic solvents with decreasing polarity as EtOH (λ_{max} = 269 nm) < MeOH (λ_{max} = 257 nm) and a pronounced blue shift was observed for protic solvent as H_2O (λ_{max} = 230 nm).
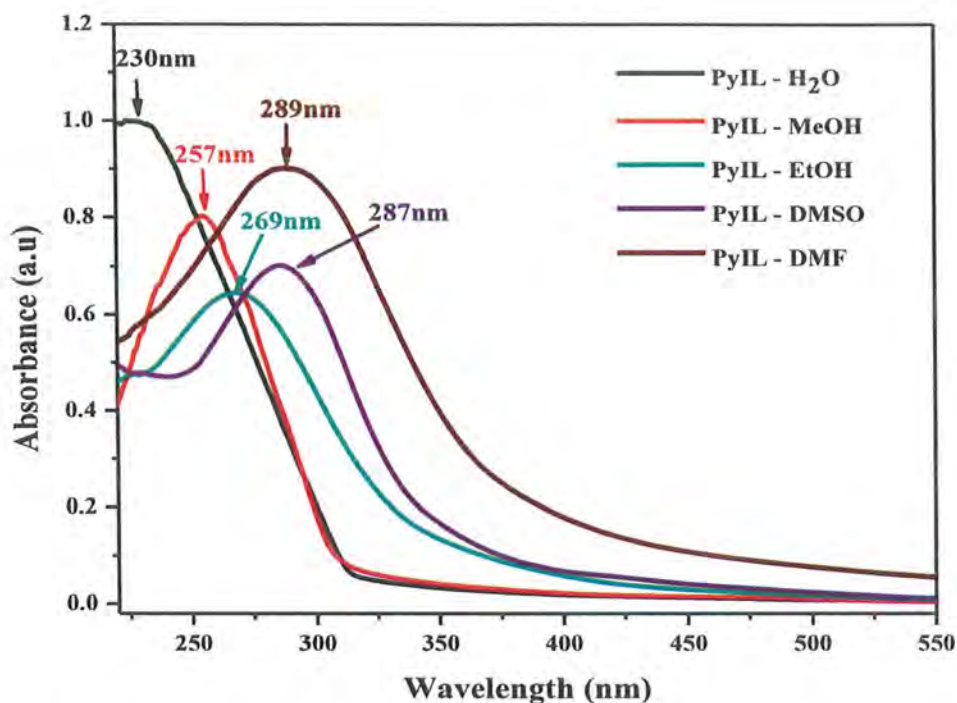
Figure 3.9: Solvatochromic effect of PyIL in range of solvents

Table 3.1: Absorption maxima of ionic liquid (PyIL) in different solvents with different polarity index

Sample	λ_{max} (nm)	Polarity Index of Solvents Used
PyIL + H₂O	230	1.00
PyIL + Methanol	257	0.80
PyIL + Ethanol	269	0.70
PyIL + DMSO	287	0.40
PyIL + DMF	289	0.38

However, polar aprotic solvents (DMF, DMSO) showed higher absorption maxima than polar protic solvents (MeOH, EtOH) and protic solvent (H_2O). **Table 3.1** shows that PyIL an increase in their λ_{max} with decreasing polarity index of different solvents and the increase in λ_{max} with decreasing polarity of solvents is called to be negative solvatochromism. Hence PyIL

showed bathochromic shift in λ_{max} with decrease in solvent polarity thus exhibiting negative solvatochromic effect.[154-155]
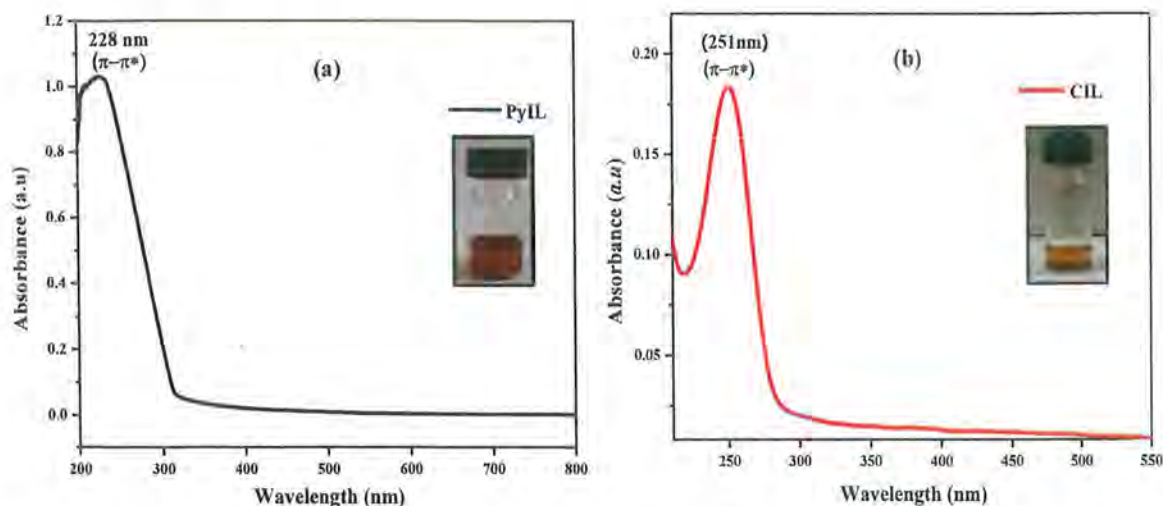
Figure 3.10. UV-vis plot of (a) PyIL and (b) PyIL + Nanocellulose (CIL)

UV visible spectra of PyIL and nanocellulose dissolved IL are recorded in Figure **3.10** which shows the PyIL has λ_{max} of 228 nm while nanocellulose dissolved ionic liquid (CIL) exhibits λ_{max} at 251 nm. The absorption maxima for nanocellulose dissolved ionic liquid shows a red shift of 23 nm as compared to absorption maxima of ionic liquid/H_2O mixture. This red shift is attributed to the dissolution of nanocellulose in ionic liquid as a result of hydrogen bonding O-H moieties on nanocellulose surface and ionic liquid. Hence, nanocellulose dissolution in ionic liquid causes this red shift, due to the stabilization by H-bonding interations.[156]

3.5 Scanning electron microscopy (SEM) Analysis

In order to reveal the surface topography and morphology of extracted nanocellulose, scanning electron microscopy was performed on Nova NanoSEM 450 field emission electron microscope. The SEM micrograph was examined to study superficial structure of extracted nanocellulose at a magnification of 10 μm. **Figure 3.11** depicts the SEM images of nanocellulose (NC) extracted from the hardwood of *Eucalyptus camaldulensis*.

SEM micrographs confirmed the fibre-shaped cellulose nanofibers as are reported previously.[157] The smooth surface of NC is ascribed to the absence of fibres as hemicellulose, lignin, and waxes. [158-159] The narrow and reticular structure of NC manifests that is pure curtailed cellulose as manifested by the SEM. The alkaline treatment and delignification process did not entirely destroy the cellulose structure and the amorphous regions within it, according to the SEM.

Figure 3.11: SEM micrograph of extracted NC taken at magnification 10 μm.

Thus, SEM micrograph of NC affirms its successful extraction from hardwood of *Eucalyptus camaldulensis* and its rod-shaped morphology affirms that the synthesized NC is cellulose nanofibers (CNFs). Size of nanofibers evaluated via image is approximately 3.6 μm in length.

3.6 Thermophysical Properties of PyIL

$$y = -0.01483x + 2.00778$$
$$R^2 = 0.98436$$

Equation	y = a + b*x		
Weight	No Weighting		
Residual Sum of Squares	0.00458		
Pearson's r	-0.99313		
Adj. R-Square	0.98436		
		Value	Standard Error
B	Intercept	2.00778	0.02776
B	Slope	-0.01483	6.60487E-4
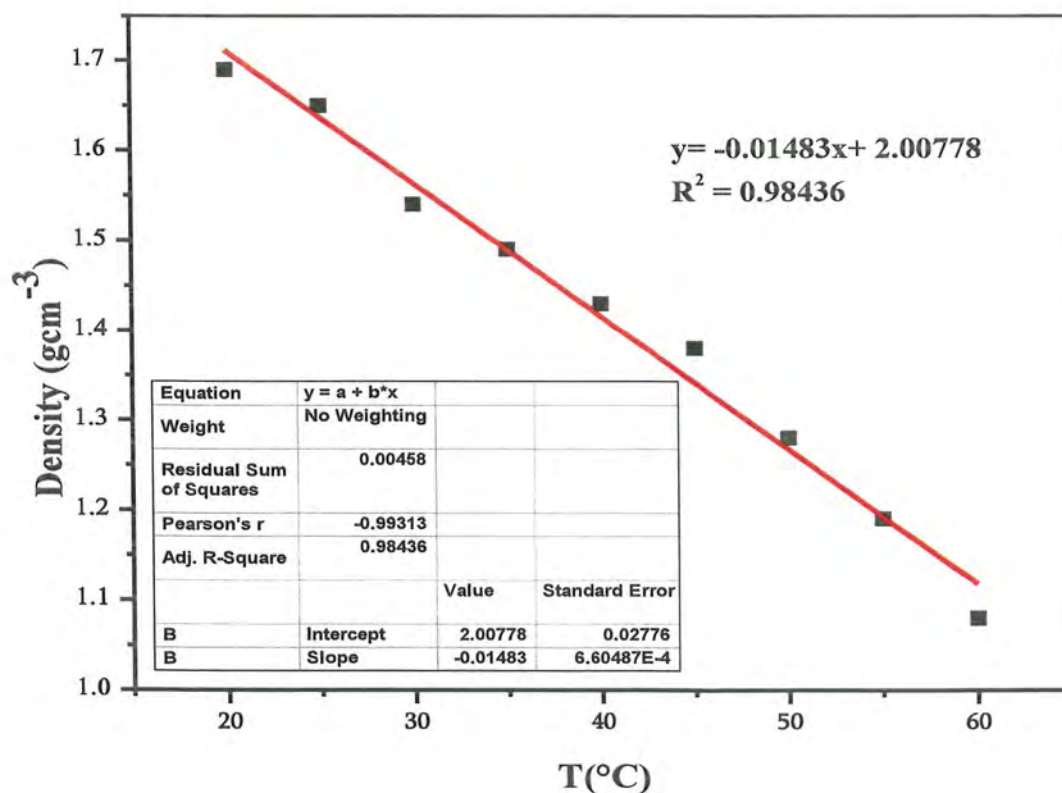
Figure 3.12: Density of PyIL with change in temperature

The thermophysical properties of synthesized ter-butyl pyridinium chloride ionic liquid were studied to evaluate the effect of temperature on the three physical properties of PyIL as viscosity, density, and refractive index of the IL. The results are shown in **Figures 3.12 - 3.14**. Using a rotationally automated Anton Paar Stabinger Viscometer SVM3000, the viscosity and density of the ionic liquids were measured simultaneously at temperatures ranging from (20 °C to 60 °C). ATAGO RX-5000 Alpha digital refractometer was used to determine refractive index values. Following the calibration of the viscometer and refractometer, Millipore quality water was used as well as the supplier's standard calibration fluid.[160 - 161]

The plot shows $y=-1.67333E-4x + 1.53$ and $R^2 = 0.99534$.

Equation	y = a + b*x	
Weight	No Weightin	
Residual Sum of Squares	1.71889E-7	
Pearson's r	-0.99796	
Adj. R-Square	0.99534	
		Value	Standard Err
B	Intercept	1.53476	1.70062E-4
B	Slope	-1.67333E-	4.04603E-6
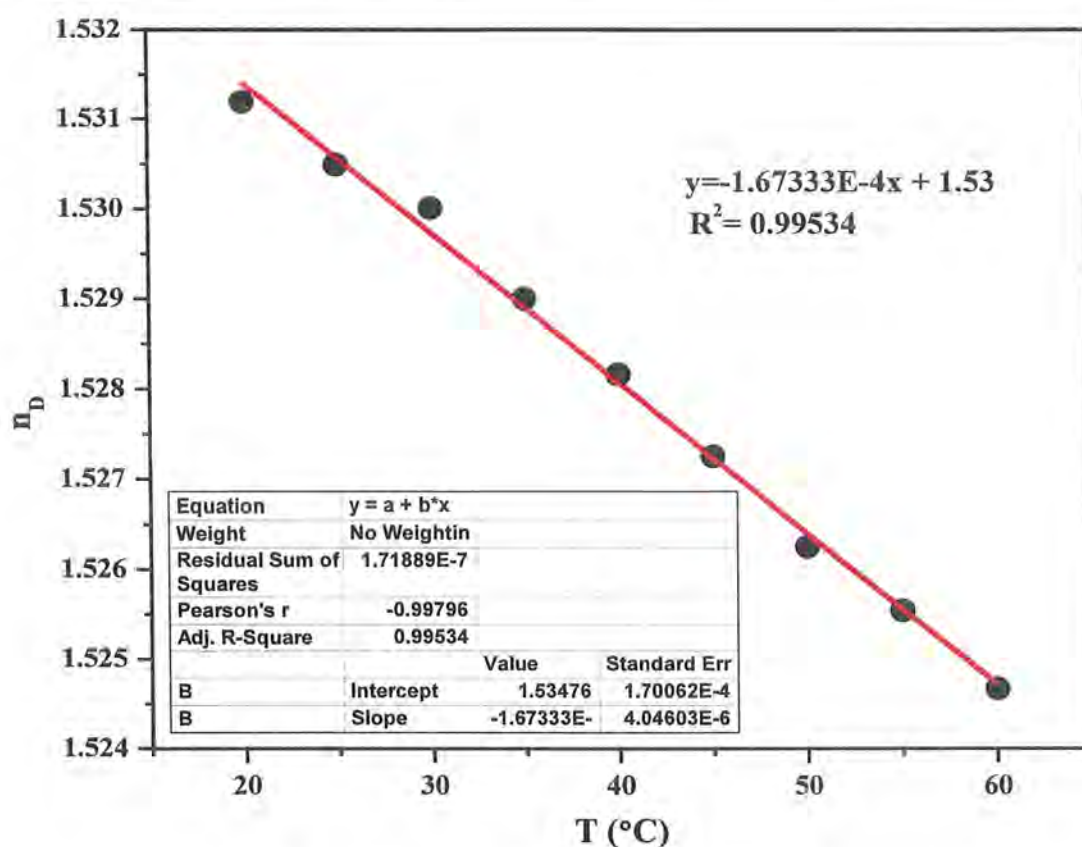
Figure 3.13: Refractive Index of PyIL with increasing temperature

The experimental values of density, viscosity, and refractive index for PyIL are presented in **Figures 3.12, 3.13, and 3.14** for the studied temperature range. Density (ρ), dynamic viscosity ($\eta_{dynamic}$) and refractive index (n_D) of PyIL decreases linearly with temperature and are in good accord with those reported by Yunus, N. *et al.*[162] All the three properties were found to follow the 1st order straight line equation as given below;

$$\rho = -0.0148T + 2.0078 \qquad (3.2)$$

$$n_D = -1.673E\text{-}4T + 1.58 \qquad (3.3)$$

$$\eta_D = -0.2615T + 15.47 \qquad\qquad (3.4)$$
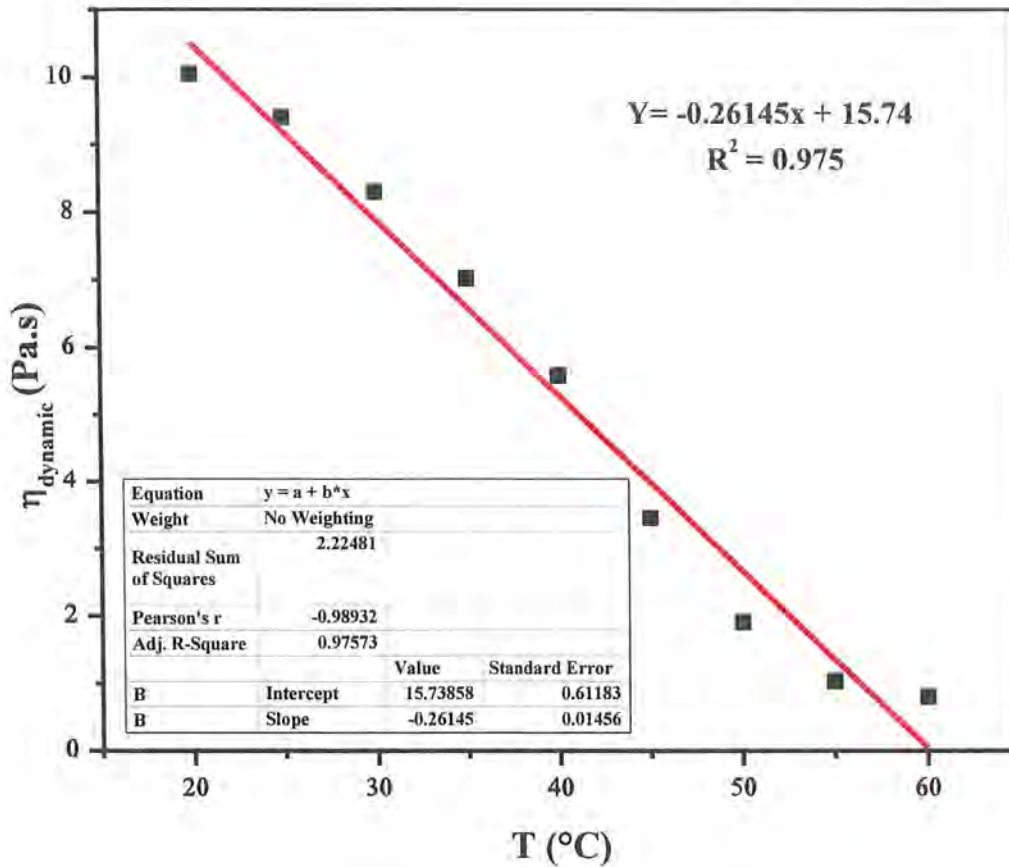
Figure 3.14: Viscosity of PyIL with increasing temperature

The highest value for the refractive index, density and viscosity of PyIL is evaluated at 20 °C with 1.5312, 1.69 gcm^{-3}, and 10.04 Pa. s respectively values.

3.7 Zeta Potential and Particle Size Analysis

The zeta size analysis is performed to determine the particle size distribution of NC and heterogeneity of size distribution of nanocellulose as shown in **Figure 3.15.** The zeta potential (δ) is measured to evaluate the electrostatic stability of the NC and is measure of charges present on the surface of nanocellulose.

The results are given in **Figure 3.16.** Values of zeta potential less than ±15.0 mV represent the tendency of NC to agglomerate and formation of an unstable colloidal suspension. However, the values greater than ±30.0 mV means that the samples show electrostatic charges and can form stable colloidal suspension.[163] **Figure 3.15** also provides the average value of poly dispersity index (PDI) to be 0.117. The level of non-uniformity in polymeric particles is measured using PDI. It is commonly accepted that if PDI is greater than 0.7, the corresponding

sample is recognized to have a broad size distribution, whereas values less than 0.5 indicate the formation of a monodisperse sample with a limited size distribution.[164] The average size of nanocellulose was found to be 172 nm.
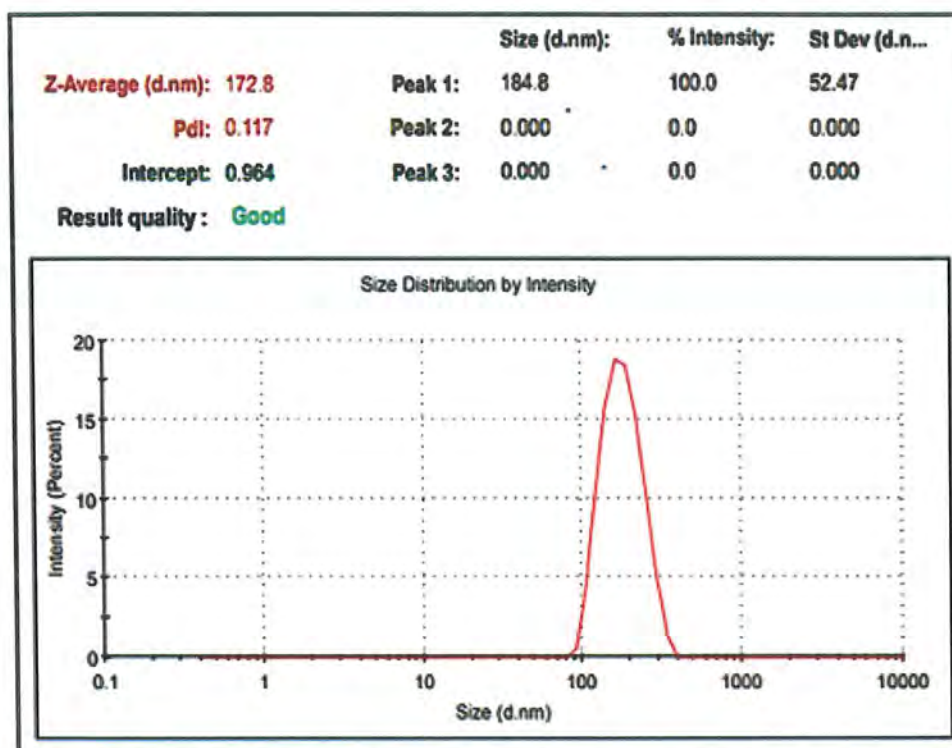
Figure 3.15: Zeta sizer of NC presenting the average size and PDI of NC.
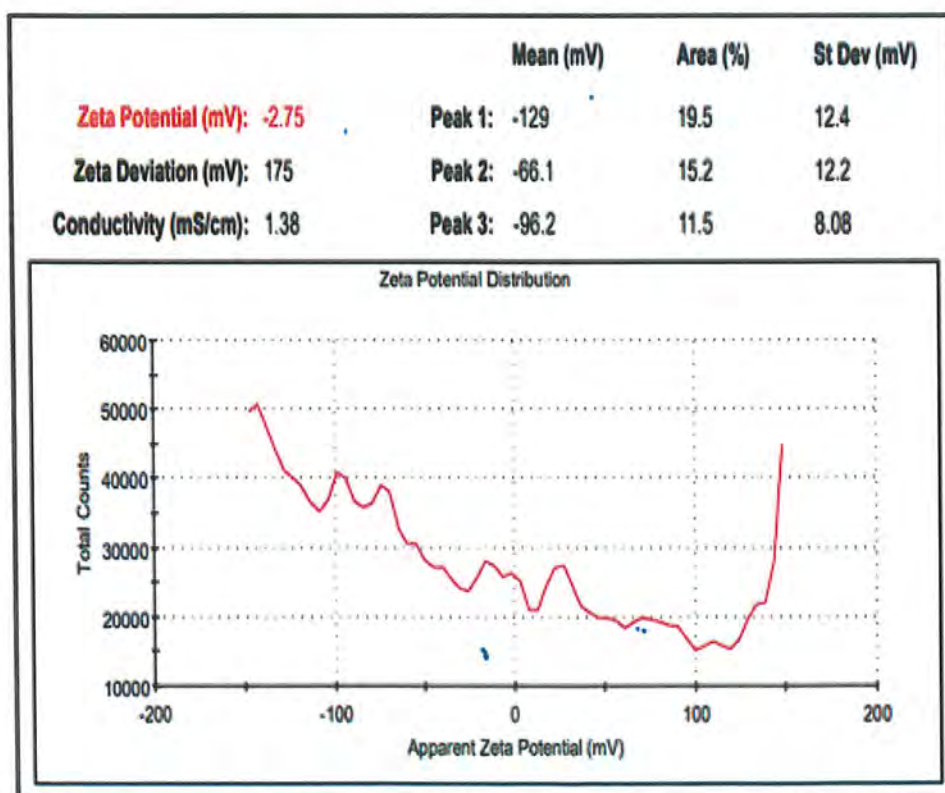
Figure 3.16: Zeta potential analysis of NC

The zeta potential (δ) indicates colloidal stability of the NC and its value is found to be -2.75 mV as shown in the **Figure 3.16** with a conductivity of 1.38 mS/cm. Results of particle size and zeta potential of NC in this study in comparison to literature are shown in **Table 3.2**.

Table 3.2: Zeta potential and particle size of particles in this study, measured by Malvern equipment, in comparison to literature.

	Zeta Potential (mV)	Particle Size (nm)	Ref.
Wood NC	-2.75	172.8	**This study**
Coir CNC	-10.8	90	Mehanny, Sherif, et al.[163]
Husk CNC	-35	212	Yang, Xue, et al.[165]
Linter CNC	-45	179	Cruz, Mab, Ribeiro da, et al.[166]

The zeta size analysis shows that the size of extracted NC is 172 nm. Zeta potential value of NC shows electrostatic instability, i.e., a tendency of aggregation and flocculation due to the low presence of free hydroxyl groups. Also, the gravitational forces act and tend to flocculate nanocellulose. Due to this less electrostatic stability of NC in methanol solvent minor conductivity is observed indicating that there are very few charged groups on surface of NC. This electrostatic instability of NC in methanol confirmed the fact that PyIL can be a better solvent for the dissolution of NC.

3.8 Transmission electron microscopy (TEM) Analysis

Transmission electron microscopy (TEM) has played a significant role in the characterization of cellulosic materials, especially the so-called "nanocelluloses" (nanofibers and nanocrystals), from visualizing nanoscale morphologies to identifying crystal structures.
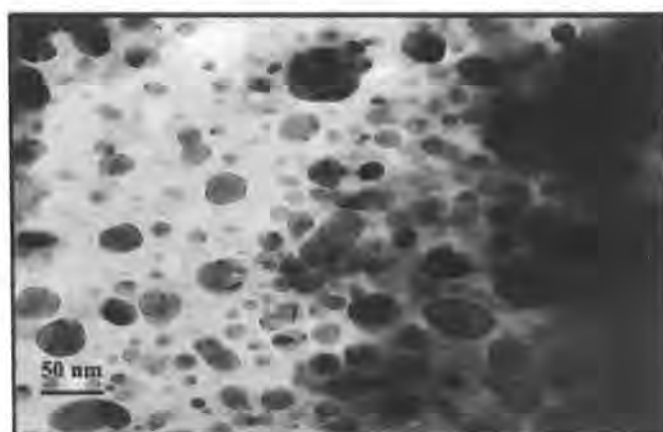
Figure 3.17: TEM micrograph of extracted NC in PyIL taken at magnification 50 nm

TEM micrographs of nanocellulose were obtained by JEM-1011 TEM instrument operating at 80 kV. **Figure 3.17** depicts the TEM micrograph of NC dissolved ionic liquid (CIL). TEM was taken of nanocellulose dissolved in IL, which has broken the long cellulose fibers into short rods and this has assisted in the dissolution of NC. The imaging revealed the spherical or short rod-like morphology of nanocellulose with an average particle size of 18nm.

3.9 Antibacterial Studies

The study of antibacterial activity of pyridinium-based IL (PyIL) and nanocellulose dissolved ionic liquid (CIL) provides an understanding for the advancement of ILs in biomedical applications.[119] Antibacterial activity of PyIL and CIL is investigated by Well diffusion method using Muller Hinton Agar against four infectious pathogenic bacteria (*Escherichia coli, Staphylococcus aures, Klebsiella pneumoniae,* and *Bacillus subtills*).[167]
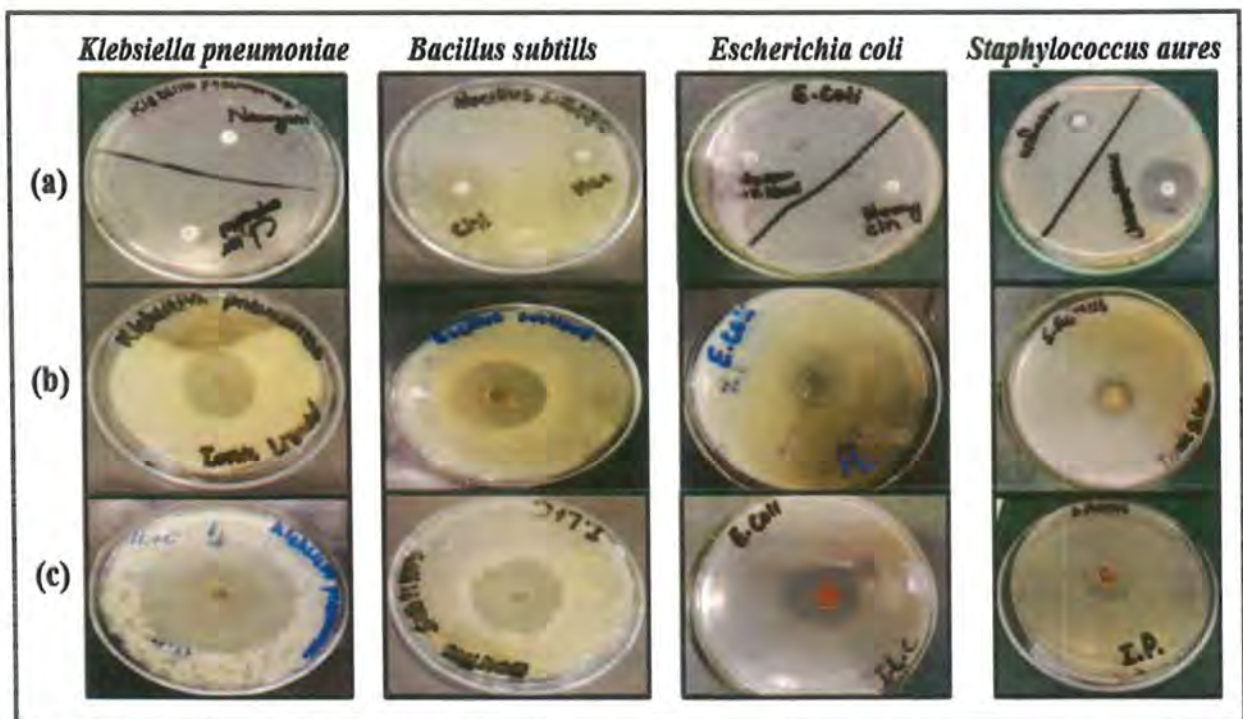
Figure 3.18: Visuals of antibacterial activity of (a) controls, (b) ionic liquid (PyIL), and nanocellulose dissolved ionic liquid (CIL)

Among these four bacterial strains, two are gram positive (*Staphylococcus aures* and *Bacillus subtills*) and two are gram negative (*Escherichia coli* and *Klebsiella pneumoniae*). Chloramphenicol (CHL) and Neomycin (NEO) are used as control drugs for investigating the biocidal effect of PyIL and CIL. **Figure 3.18** shows the visuals for the antibacterial activity of PyIL, CIL and control drugs. These visuals manifests that the antibacterial activity of

nanocellulose dissolved ionic liquid (CIL) was higher compared to PyIL against all four bacterial strains.

Table 3.3: Inhibition zones of Ionic Liquid (IL), nanocellulose dissolved Ionic Liquid (CIL) and controls.

Bacterial strain	Strain Type	Agar-well (zone of inhibition) (mm)			
		PyIL	CIL	Control Drugs	
				Chloramphenicol (CHL)	Neomycin (NEO)
S. Aureus	+ve	18	26	28	11
K. Pneumoniae	-ve	19	41	0	0
E. Coli	-ve	22	29	0	0
Bacillus subtills	+ve	32	36	24	16
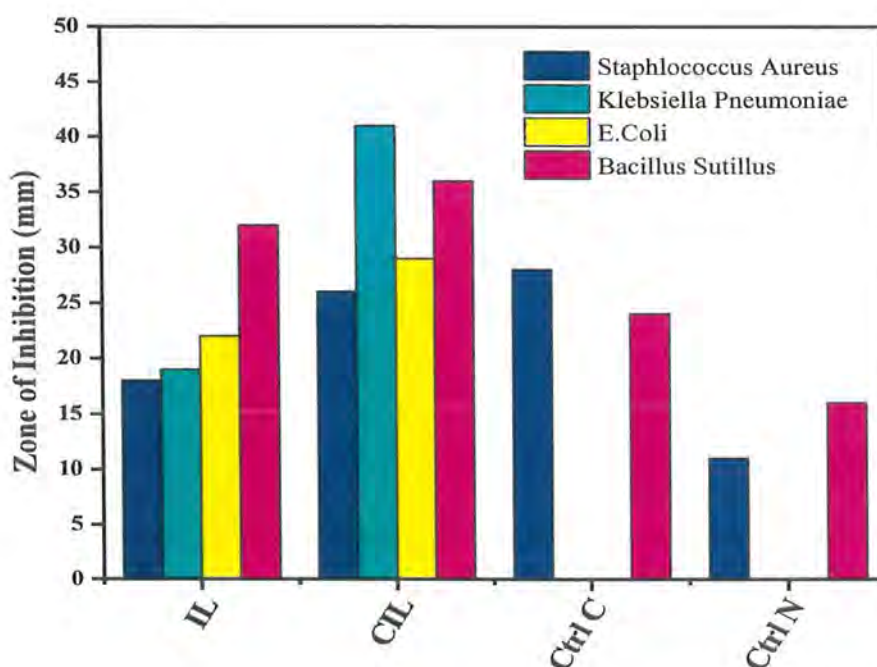
Figure 3.19: Bar graph indicating antibacterial activity of ionic liquid (PyIL), nanocellulose dissolved ionic liquid (CIL) and controls

The zone of inhibitions for controls (CHL and NEO), PyIL and CIL are also calculated and shown in **Table 3.3**. The PyIL showed the best bacterial growth inhibition against *Bacillus subtills* and least against *S. aureus* while CIL showed best bactericidal action against *K. Pneumoniae*. The results are also shown in the bar graph in **Figure 3.19**. Bactericidal action of PyIL and CIL is due to interaction of their hydrophobic alkyl groups that interact with bacterial

cell membrane causing the membrane disruption and ultimately bacterial cell death. Due to difference in cell membrane composition of bacterial strains and hydrophobicity of PyIL and CIL they have shown different best antibacterial activity. However, CIL is found to have better bactericidal effect as compared to PyIL making it a more efficient candidate in biomedicine as compared to PyIL.

3.10 Antioxidant Studies

The antioxidant properties of synthesized PyIL, extracted nanocellulose (NC), and CIL are investigated for their use in medical field i.e., due to their capacity to shield the body from oxidative damage, they can reduce the risk of disease and promote health. The antioxidant activity of PyIL, NC, and CIL is known to arise from the electron transfer (ET) to the oxidants.[168] It was investigated by two chemical assays; 2,2-Diphenyl-1-picrylhydrazyl (DPPH) radical scavenging assay and Ferric reducing antioxidant power (FRAP)/total reducing power (TRP) assay.

3.10.1 2,2-Diphenyl-1-Picrylhydrazyl (DPPH) Radical Scavenging Assay

The antioxidant activity of the substances PyIL, NC, and CIL was examined using 2,2-diphenyl-1-picrylhydrazyl (DPPH) as free radical source. In this method, the 50% inhibitory concentration (IC_{50}) is measured and reported.[169] The inhibitory concentration (IC_{50}) is the concentration of antioxidant that lowers the absorption value in λ_{max} of DPPH to half.[170] DPPH has λ_{max} of 517 nm and the colour of DPPH changes from purple to yellow after interaction with antioxidant as shown in **Figure 3.20**.

Figure 3.20: Visuals for DPPH radical scavenging by PyIL, NC, and CIL

When the antioxidant reduces DPPH, there is a reduction in its λ_{max}, which is directly proportional to the quantity of the antioxidant chemical used. For this purpose, different samples of compounds NC, PyIL and CIL with 190 µL of DPPH solution (9.6 mg/100 mL methanol) was put into the 96-well plate with four different concentrations (6.25, 12.5, 25, and 50 g/mL). The absorbance (A) of these samples was measured at the wavelength of 517 nm via

PowerWave XS2 plate reader. The results are shown in **Figure 3.21**. The Ascorbic acid (AA) was used as a positive control in the experiments. After the extrapolation of the trend-line equation (**Fig. 3.21**), The calculated IC_{50} values of each chemical were determined. The data is reported in **Table 3.4**.

The lower the IC_{50} value and the higher the % DPPH scavenging, the more active antioxidant the compound is.[170] The values of % DPPH scavenging for the samples shows that among PyIL, NC and CIL samples; PyIL is a good antioxidant with an IC_{50} value of 31.7 µL. Th antioxidant activity of NC is evident by its % scavenging value of about 33%. However, its antioxidant activity was enhanced upon its dissolution in PyIL, and with % DPPH scavenging for CIL found to be 59% associated with IC_{50} of 24.4 µL. Hence, DPPH assay manifested CIL is considered the best antioxidant among the three investigated compound.
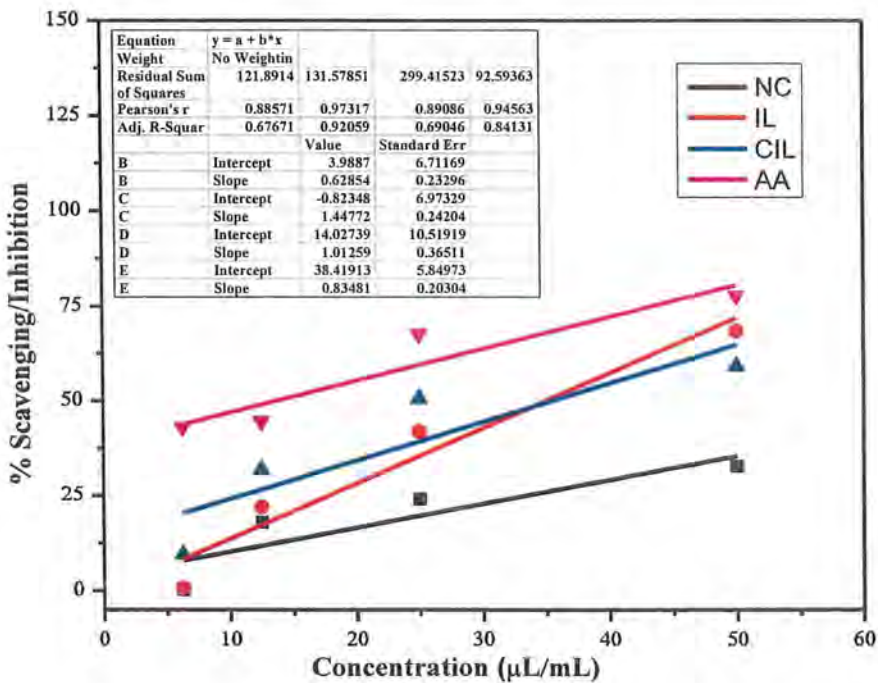
Figure 3.21: Comparison between the antioxidant activity of NC, PyIL, CIL and AA against DPPH based on their % inhibition values

Table 3.4: DPPH activity of nanocellulose (NC), ionic liquid (IL), nanocellulose dissolved ionic liquid (CIL)

Sample no.	Sample name	Scavenging (%) ± S.D. (Standard deviation)	IC_{50}
1	NC (50 µg/mL)	32.7 ± 1.10	-
2	CIL (50 µL/mL)	59.1 ± 0.53	24.43 µL

| 3 | PyIL/IL (50 µL/mL) | 68.1 ± 0.64 | 31.7 µL |
| 4 | AA (50 µg/mL) | 77.35 ± 0.43 | 12.4 µg |

3.10.2 Ferric Reducing Antioxidant Power (FRAP) Assay

Total reducing power (TRP)/Potassium ferricyanide colorimetric assay was used to determine the reducing power of compounds NC, PyIL, and CIL. The test solution's yellow colour in this assay changes to various hues of green and blue based on each sample's reducing power as shown in **Figure 3.22**. The Fe^{3+}/ferricyanide complex is reduced to the ferrous form in the presence of reducing agents, such as antioxidants.[171] Therefore, the Fe^{2+} concentration can be observed by observing the development of Perl's Prussian blue at 630 nm. Ascorbic acid was utilized as a positive control (1 mg/mL DMSO). The sample's reducing power was calculated as g of ascorbic acid equivalent per mg of sample (µg AAE/mg) as shown in the **Table 3.5.**

Figure 3.22: Visuals for Fe^{3+} reduction by PyIL, NC, and CIL in FRAP assay.

The higher the value of TRP, the higher reducing power the antioxidant has. The value of TRP for NC, PyIL and CIL shows that PyIL has the least reducing power compared to NC. However, the reducing power of NC upon dissolution in PyIL increases from 535 µg AAE/mg to 560 µg AAE/mg inferring its better antioxidant activity. The results are highlighted in **Table 3.5.**

Table 3.5: Potassium ferricyanide assay of nanocellulose (NC), ionic liquid (IL), nanocellulose dissolved ionic liquid (CIL)

Sample no	Sample Name	Total reducing power (TRP) (µg AAE/mg of sample) ± S.D.
1	NC (100 µg/ml)	535.71 ± 0.33
2	PyIL/IL (100 µl/ml)	341.06 ± 0.24
3	CIL (100 µl/ml)	560.49 ± 0.25

S.D = Standard deviation

3.11   Computational Studies

To our knowledge, no computational analysis has been done thus far to investigate how NC interacts with PyIL. Therefore, density functional theory (DFT)[172] was used to study the structure-property correlation of extracted NC with synthesized PyIL. For sake of simplicity PyIL interacted NC will be known as CIL from now onwards. Also, the electronic properties of NC, PyIL and CIL were studied using Becke's three parameter exchange functional, a Lee-Yang-Parr correlation functional (B3LYP), which is one of the most powerful functional for reproducing experimental results.[173] Using B3LYP, frontier molecular orbital analysis (FMOs), molecular electrostatic potential (MEP), global reactivity parameters, and Mulliken charges were investigated. All the calculations were performed in gaseous phase using Gaussian 09 package at default pressure and temperature of 1.00 atm and 298.15 K, respectively. The DFT method was chosen due its accuracy and reliability. Charges on all the compounds (PyIL, NC and CIL) was set to zero with singlet spin.[174]

3.11.1   Geometry Optimization

Geometry optimization is first and most important stage in determining the stable geometry with minimum energy. [175] Structures of PyIL, NC, and CIL were optimized using B3LYP functional and 6-31G+ (d, p) basis set.
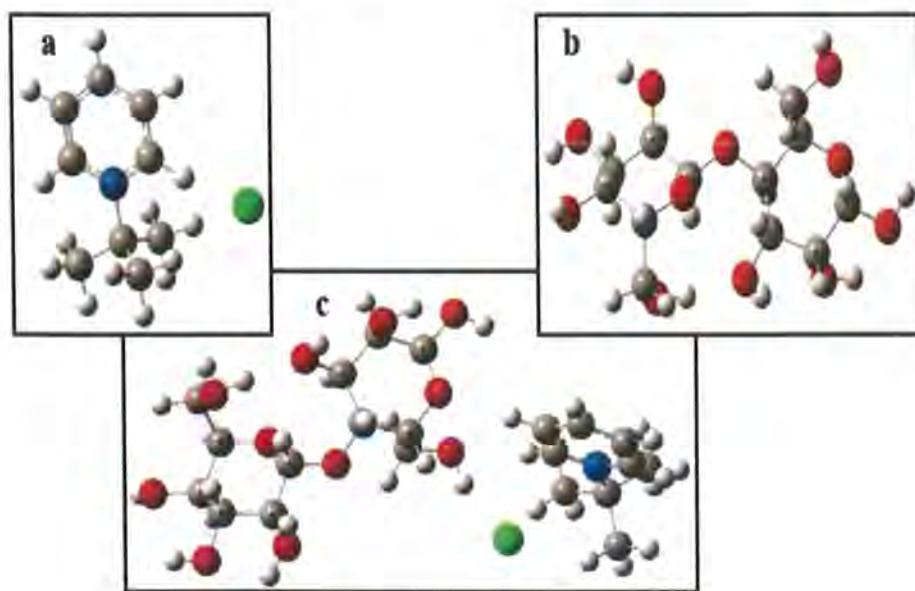

Figure 3.23: Optimized geometries of (a) PyIL, (b) NC, and (c) CIL at B3LYP/6-31G+ (d, p) using DFT

The optimized structures are displayed in **Figure 3.23**. The white colored sphere represents the hydrogen atom, grey sphere represents the carbon atom, blue color shows nitrogen atom,

red color shows the oxygen atom and green color shows the chlorine atom in the figures. The optimized structure of CIL shows the oxygen of terminal OH of NC to be co-planar with nitrogen of pyridinium ring of PyIL while the hydrogen of OH group of NC is coplanar with chlorine atom of PyIL. This coplanarity between them indicates that these moieties were mainly contributing in interaction of NC and PyIL upon dissolution of NC in PyIL.

3.11.2 Frontier Molecular Orbital (FMOs) Analysis

Frontier molecular orbital (FMOs) analysis was conducted to examine the compounds' electronic characteristics and their interactions with one another. Single point energy calculations are associated with determining the lowest potential energy configuration for a given atomic arrangement in molecules. According to the quantum mechanics, two species interact because of the overlapping of frontier molecular orbitals (HOMO and LUMO). When two species approach each other, an increase or decrease in their HOMO and LUMO energies occur because of their molecular orbital's interaction. E_{HOMO} is the ability to donate electrons. A high E_{HOMO} means that the molecule is more reactive (unstable). While E_{LUMO} is measurement of electron affinity. Energy differences between HOMO and LUMO is known as bandgap (ΔE) which is an important indicator of chemical stability. Greater the ΔE, higher the stability (less reactivity).[175]

The single point energies were calculated and FMOs were obtained as shown in **Table 3.6**. HOMO of PyIL is delocalized on chloride of tertiary butyl pyridinium chloride ionic liquid, indicating the high electron density on the chloride of PyIL, while the LUMO of PyIL is delocalized on the pyridinium ring of ionic liquid presenting the low electron density site for interaction. Similarly, the HOMO of NC is delocalized on the glucopyranose ring of cellulose unit and LUMO is delocalized on the terminal hydroxyl group indicating the available site for interaction. HOMO of CIL is delocalized on the pyridinium ring and chloride of PyIL and terminal OH group of NC indicating the interaction between PyIL and NC, while LUMO is delocalized on the PyIL because of presence of pronounced charges on this moiety. Hence, the HOMO of CIL affirmed the interaction between PyIL and NC.

The energies of HOMO, LUMO levels and band gap values are computed in **Table 3.7**[176] Molecules having small band gap value are considered soft, easily polarized, less stable and more reactive, while large value of band gap corresponds to hard molecule and less reactivity. Band gap values for the PyIL, NC and CIL show that PyIL is polar and most reactive, while NC is less polarizable and least reactive among the investigated compounds. However, the reactivity of NC increases upon interaction with PyIL.

Table 3.6. FMOs diagrams of PyIL, NC, and CIL at B3LYP/6-31G+ (d, p) using DFT method
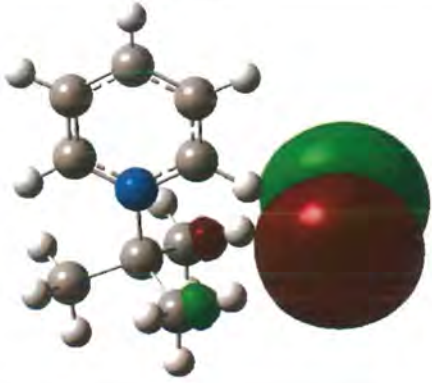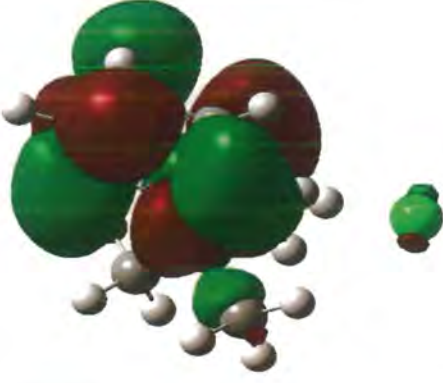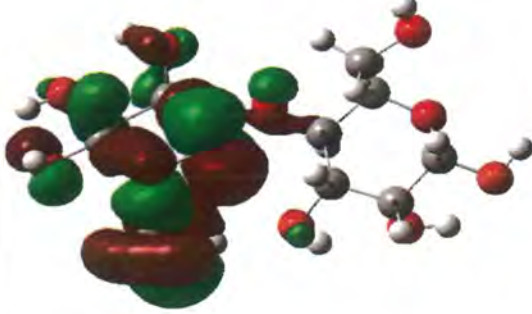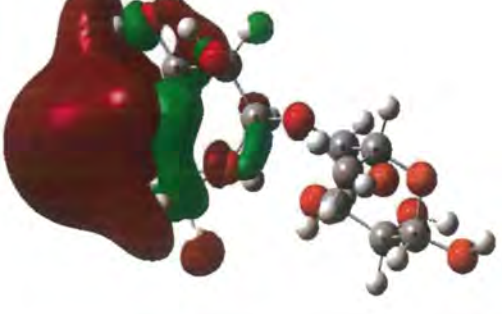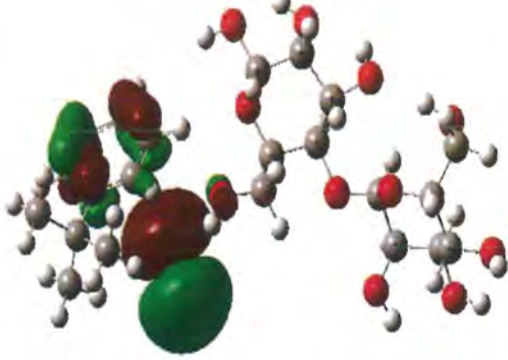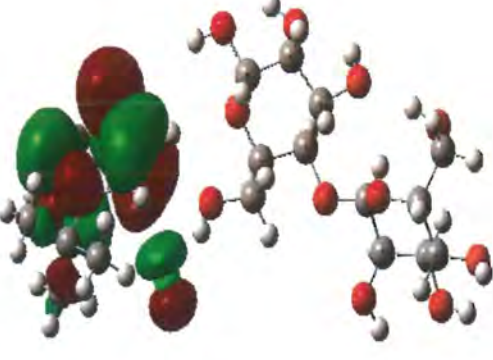
	HOMO	LUMO
PyIL		
NC		
CIL		

Table 3.7: Calculated E_{HOMO}, E_{LUMO} and band gap for investigated compounds at B3LYP/6-31G+ (d, p) using DFT method

Compound	E_{HOMO} (eV)	E_{LUMO} (eV)	E_g (eV) = E_{LUMO} - E_{HOMO}
PyIL	-4.7138	-2.6572	2.0566
NC	-6.3647	-1.3606	5.0041
CIL	-5.4259	-2.1959	3.2300

3.11.3 Global Reactivity Parameters

Interaction of PyIL with NC causes changes in the electronic properties of NC. For investigation of changes on interaction, global reactivity parameters were computed. The extended Koopman theorem is utilized for the computation of to calculate the ionization potential; measure of strength by which electron remains bounded to a molecule (I), electron affinity; ability to take electrons (A), electronegativity; ability to attract shared pairs of electrons (χ), chemical softness, measure of electron cloud polarization (σ), chemical hardness; resistance towards electron cloud polarization (η) and chemical potential; measure of energy stored in a bond (μ), electrophilicity index, measure of ability of molecule to take up electrons based on chemical potential and hardness (ω) of the compounds.[177] All these parameters give information regarding the molecule's stability and equations to calculate them can be seen in equations 3.5-3.11.

$$I = -E_{HUMO} \qquad (3.5)$$

$$A = -E_{LUMO} \qquad (3.6)$$

$$\eta = \frac{I-A}{2} \qquad (3.7)$$

$$\chi = \frac{(I+A)}{2} \qquad (3.8)$$

$$\sigma = \frac{1}{2\eta} \qquad (3.9)$$

$$\mu = -\frac{(I+A)}{2} \qquad (3.10)$$

$$\omega = \frac{\mu^2}{2\eta} \qquad (3.11)$$

Table 3.8. Ionization potential (I), electron affinity (A), electronegativity (χ), chemical softness (σ), chemical hardness (η) and chemical potential (μ), electrophilicity index (ω) of the compounds investigated at B3LYP/6-31G+ (d, p) level of theory.

Sample ID	E_{HOMO} (eV)	E_{LUMO} (eV)	ΔE (eV)	I (eV)	A (eV)	χ (eV)	σ (eV^{-1})	η (eV)	μ (eV)	ω (eV)
PyIL	-4.71	-2.66	+2.05	4.71	2.66	3.67	0.49	1.03	-3.67	6.57
NC	-6.36	-1.36	5.0	6.36	1.36	3.86	0.2	2.5	-3.86	2.98
CIL	-5.43	-2.19	3.24	5.43	2.19	4.34	0.46	1.09	-4.34	8.60

The values of calculated global reactivity parameters are given in **Table 3.8.** The ionization potential is the measure of strength by which an electron remains bound to the molecule. A high ionization potential means more difficulty to remove an electron, while a high electron affinity means greater reactivity. Thus, both ionization potential and electron affinity are criteria to determine the reactivity of a molecule.[177] Tertiary butyl pyridinium chloride (PyIL) exhibits ionization potential of 4.71eV and an electron affinity of 2.66 eV. Nanocellulose (NC) shows an ionization potential of 6.36 eV and an electron affinity of 1.36 eV. Upon Interaction of NC with PyIL the ionization potential was decreased to 5.43 eV and electron affinity was increased to 2.19 eV. This suggests that reactivity of NC increases on interaction with PyIL.

Other two important descriptors to predict the reactivity of a compound are its chemical hardness and softness. These two parameters depend upon band gap of compound. Large bandgap means compound is hard and less reactive. Small band means compound is soft and more reactive. Interaction of NC with PyIL makes extracted NC softer and more reactive in nature. Electrophilicity and chemical potential is directly related to the reactivity of compound. The electrophilicity index of PyIL, NC and CIL calculated is 6.57, 2.98, and 8.60, respectively. The chemical potential calculated for PyIL, NC and CIL are -3.67 eV, -3.86 eV, and -4.34eV. The increase in the electrophilicity index and chemical potential is attributed to increase in reactivity of investigated compounds.

3.11.4 Molecular Electrostatic Potential (MEP)

MEP is an electrostatic potential plot used to determine favorable sites for nucleophilic and electrophilic attack as well as to anticipate the distribution of electrostatic charges on distinct regions including positive, negative and neutral regions by presenting different color zones.[178] Different color appearance on the structure revealed the unequal distribution of charges. Red color regions showed the maximum negative region and depicted as electrophilic site whereas the blue regions represented the most positive region and could act as suitable site for nucleophilic site. Neutral region having zero electrostatic potential in the molecule is represented by the green hue. The decrease in the electrostatic potential is shown in the order; blue > green> yellow> orange> red.[179] By utilizing the optimized geometries of three compounds molecular electrostatic potential surfaces are shown in **Figure 3.24**.

Figure 3.24 (a) shows that the chlorine in PyIL is most electronegative region while the pyridinium ring found to have most electropositive or nucleophilic region. (b) shows that the terminal oxygen is most electronegative while other oxygen sites are also electronegative sites

but the carbons adjacent to oxygen are electropositive regions in NC. (c) shows that in CIL the β glycosidic bond of NC and chlorine of PyIL are most electronegative sites and pyridinium ring is most electropositive site in PyIL after interaction.
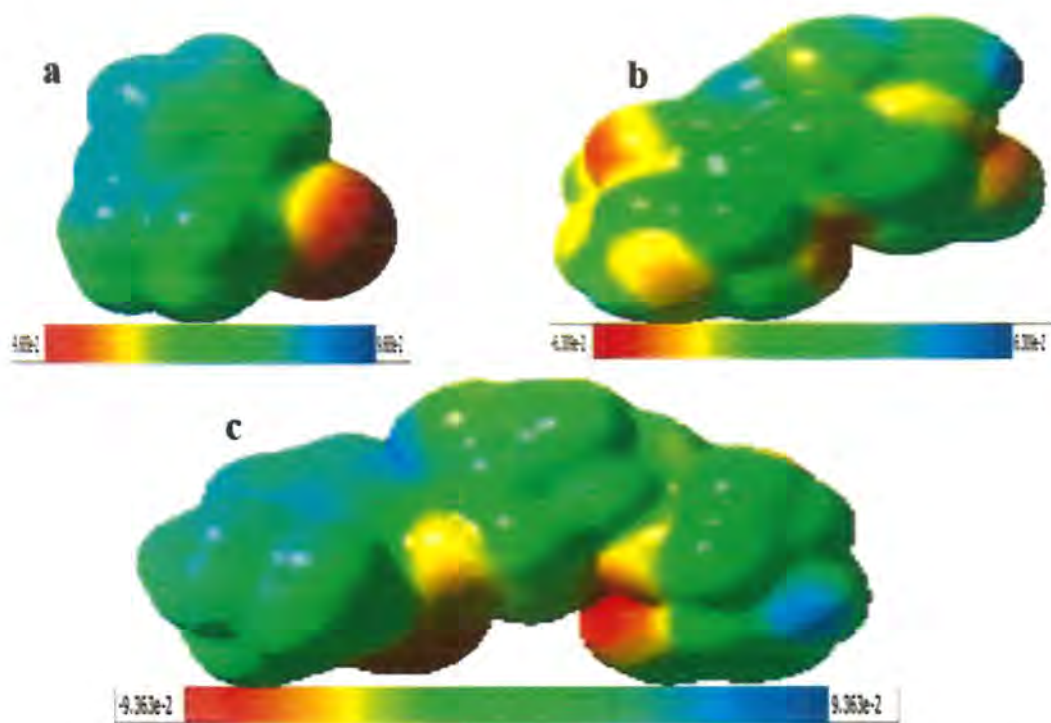
Figure 3.24: MEP surfaces of (a) PyIL, (b) NC, and (c) CIL at B3LYP/6-31G+ (d, p) at DFT level

3.11.5 Mulliken Charge Analysis

Mulliken charge analysis is directly related to vibrational characteristics and distribution of electrostatic charges present on the molecular system.[180] This analysis has a strong application in predicting the electronic charges on the structure by undergoing atomic displacement and pertaining to the molecule's chemical bonds. In present work, the carbon atom attached to the hydrogen atom has partial negative charge while the carbon atom attached to the electronegative atoms like nitrogen and oxygen carries a partial positive charge as the electronegative atoms pull the electron density towards themselves. **Figure 3.25 - 3.27** shows Mulliken Charges on (a) PyIL, NC, and CIL at B3LYP/6-31G+ (d, p) using DFT. **Figure 3.25** shows the most negative charge on the chlorine and most positive charge on the nitrogen of pyridinium ring of PyIL. **Figure 3.26** shows that the most negative charge is on the oxygen atom of terminal OH groups while the hydrogen attached to oxygen of OH groups and the carbons adjacent to the OH groups carry most positive charges.
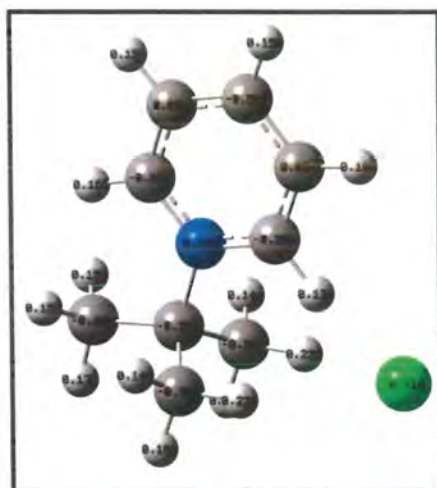
Figure 3.25: Mulliken charges on PyIL at B3LYP/6-31G+ (d, p) at DFT level.
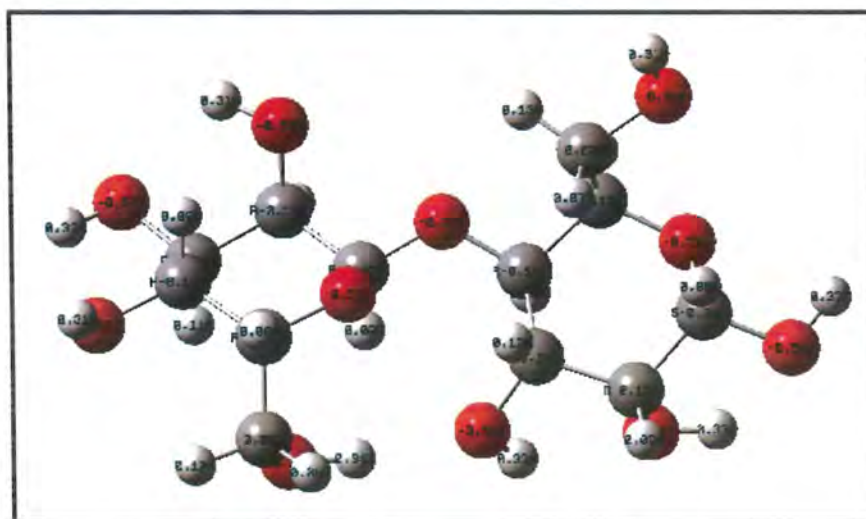
Figure 3.26: Mulliken charges on NC at B3LYP/6-31G+ (d, p) at DFT level
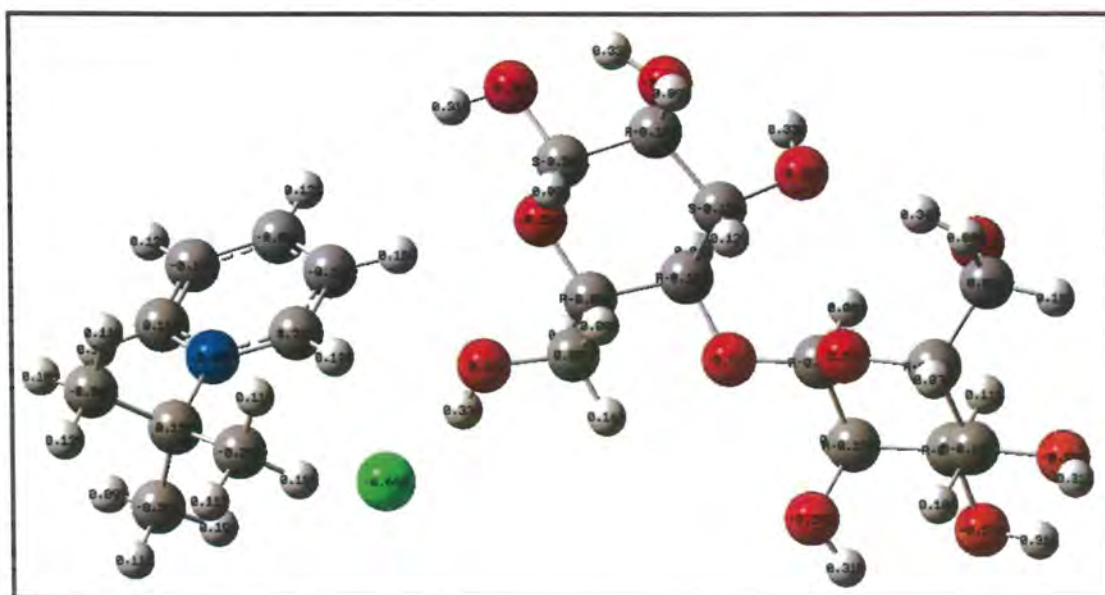
Figure 3.27: Mulliken charges on CIL at B3LYP/6-31G+ (d, p) at DFT level

Figure 3.27 showed the redistribution of charges on atoms affirming that NC and PyIL interact with each other, which in turn supports the dissolution of NC in PyIL. Although all compounds have different distribution of charges on atoms but the overall charge on all the three moieties was found to zero.

Conclusions

Nanocellulose (NC) was extracted from hardwood of *Eucalyptus camaldulensis* by newly developed extraction method and characterized by XRD, FTIR and SEM analysis. The XRD of nanocellulose (NC) affirmed its successful synthesis as Nanocellulose I having 71% degree of crystallinity. FTIR results showed the presence of three peaks for β glycosidic bonds at 1027, 1160 and 1249 cm^{-1} and a band for bonded OH groups on NC surface around 3331 cm^{-1}. SEM of NC manifested rod-shaped morphology confirming the synthesized NC with intact structure. The zeta potential value showed unstable suspension of NC in methanol due the presence of fewer free hydroxyl bonds and its restricted solubility. The zeta sizer of NC further confirmed NC as CNCs with average size 172 nm. The PDI value of 0.117 provided the uniform size distribution of NC.

A ter-butyl pyridinium chloride ionic liquid (PyIL) was synthesized for the first time and characterized by NMR, FTIR, and UV studies. NMR confirmed the structure and purity of synthesized PyIL. FTIR spectrum provided peaks at 990 and 1030 cm^{-1} of C-N stretching of alkyl-pyridinium ring while a peak at 1580 cm^{-1} corresponding to pyridinium ring. UV results showed that PyIL exhibits negative solvatochromic effect. Thermophysical properties of PyIL were investigated with increasing temperature (20 °C – 50 °C). The refractive index (n_D) with 1.5312 highest value at 20 °C was determined using refractometer. The viscosity ($\eta_{dynamic}$) and density (ρ) values obtained by viscometer with highest values of ρ = 1.69 gcm^{-3} and $\eta_{dynamic}$= 10.04 Pa. s at 20 °C respectively. Extracted nanocellulose was dissolved in various solvents and in different PyIL/water mixtures. The best nanocellulose dissolution was observed in 9:1 volume ratio of PyIL/water mixture. The dissolution of NC in PyIL was confirmed by various techniques as UV (251 nm), FTIR, and XRD. XRD analysis manifested a decrease in crystallinity of NC upon dissolution in ionic liquid while FTIR showed the presence of free hydroxyl groups on NC surface.

Antibacterial activity against four different bacterial strains was investigated and cellulose dissolved ionic liquid depicted best biocidal effects against *Klebsiella pneumoniae* with inhibition zone of 41 mm. Antioxidant studies against DPPH radical showed ionic liquid as good antioxidant with 68% radical scavenging and IC_{50} value of 31.7 µL. NC showed the least antioxidant behavior that was increased upon dissolution in PyIL with an IC_{50} of 24.4 µL. FRAP assay showed that total reducing power of NC was increased from 535 to 560 µg AAE/mg on dissolution in PyIL.

Theoretical studies were also conducted using the DFT method to investigate interaction between PyIL and CIL. The geometry optimization of PyIL, NC, and CIL was performed at B3LYP/6-31G+ (d, p) level of DFT using Gaussian 09 program. Coplanarity of O and H of OH group in NC and N^+ and Cl^- in PyIL supported the interaction between NC and PyIL. Frontier orbital analysis and global reactivity parameters confirmed PyIL as most reactive among NC, PyIL, and CIL compounds while NC is the least reactive. However, its reactivity increased on dissolution in PyIL.

Results conclude that not only CNCs were synthesized from hardwood of Eucalyptus by novel method, but a suitable solvent for them tertiary butyl pyridinium chloride (PyIL) was also synthesized to make them more useful for further applications.

References

1. Shah, S. S.; Aziz, M. A.; Usman, M.; Hakeem, A. S.; Ali, S., & Alzahrani, A. S. Biomass-based supercapacitors: Lab to Industry. *Biomass-Based Supercapacitors: Design, Fabrication and Sustainability*, 2023, 8, 435-459.

2. Vymazal, J. Removal of nutrients in various types of constructed wetlands. *Science of the Total Environment*, 2007, 380, 48-65.

3. Mahar, A.; Malik, R. N.; Qadir, A.; Ahmed, T.; Khan, Z.; & Khan, M. A. Review and analysis of current solid waste management situation in urban areas of Pakistan. *In Proceedings of the International Conference on Sustainable Solid Waste Management*, 2007, 8, 36.

4. Nzihou, A. Toward the valorization of waste and biomass. *Waste and Biomass Valorization*, 2010,1(1), 3-7.

5. Wu, L.; Moteki, T.; Gokhale, A. A.; Flaherty, D. W.; & Toste, F. D. Production of fuels and chemicals from biomass: condensation reactions and beyond. *Chem*, 2016, 1(1), 32-58.

6. Block, P.; Calvo Barentin, C.; Ranaudo, F.; & Paulson, N. Imposing challenges, disruptive changes: rethinking the floor slab. *The Materials Book*, 2019, 67.

7. Pfab, E.; Filiciotto, L.; & Luque, R. The dark side of biomass valorization: a laboratory experiment to understand Humin formation, catalysis, and green chemistry. *Journal of Chemical Education*, 2019, 96(12), 3030-3037.

8. Lee, H. V., Hamid, S. B. A., & Zain, S. K. Conversion of lignocellulosic biomass to nanocellulose: structure and chemical process. *The Scientific World Journal*. 2014, 2014.

9. Berbel, J., & Posadillo, A. Review and analysis of alternatives for the valorisation of agro-industrial olive oil by-products. *Sustainability*, 2018, 10, 237.

10. Dahmen, N.; Lewandowski, I.; Zibek, S.; & Weidtmann, A. Integrated lignocellulosic value chains in a growing bioeconomy: Status quo and perspectives. *GCB Bioenergy*, 2019, 11, 107-117.

11. Yang, H.; Yan, R., Chen; H., Zheng; C., Lee; D. H.; & Liang, D. T. In-depth investigation of biomass pyrolysis based on three major components: hemicellulose, cellulose and lignin. *Energy & Fuels*, 2006, 20, 388-393.

12. Zhang, Y.; & Naebe, M. Lignin: A review on structure, properties, and applications as a light-colored UV absorber. *ACS Sustainable Chemistry & Engineering*, 2021, 9, 1427-1442.

13. Prieur, B.; Meub, M.; Wittemann, M.; Klein, R., Bellayer, S.; Fontaine, G.; & Bourbigot, S. Phosphorylation of lignin: characterization and investigation of the thermal decomposition. *Royal Society of Chemical Advances*, 2017, 7, 16866-16877.

14. Li, X.; Sun, C.; Zhou, B.; & He, Y. Determination of hemicellulose, cellulose and lignin in moso bamboo by near infrared spectroscopy. *Scientific Reports*, 2015, 5(1), 1-11.

15. Phanthong, P.; Reubroycharoen, P.; Hao, X.; Xu, G.; Abudula, A.; & Guan, G. Nanocellulose: Extraction and application. *Carbon Resources Conversion*, 2018, 1, 32-43.

16. Resasco, D. E.; Sitthisa, S.; Faria, J.; Prasomsri, T.; Ruiz, M. P.; & Albanese, J. A. F. Solid waste as a renewable resource: methodologies. *CRC Press*, 2015.

17. Liu, W. J.; Jiang, H.; & Yu, H. Q. Thermochemical conversion of lignin to functional materials: a review and future directions. *Green Chemistry*. 2015, 17, 4888-4907.

18. Asif, M. Sustainability of timber, wood and bamboo in construction. *In Sustainability of Construction Materials*, Woodhead Publishing, 2009, 31-54.

19. Zabed, H.; Sahu, J. N.; Boyce, A. N.; & Faruq, G. Fuel ethanol production from lignocellulosic biomass: an overview on feedstocks and technological approaches. *Renewable and Sustainable Energy Reviews*. 2016, 66, 751-774.

20. Stokke, D. D.; Wu, Q.; & Han, G. Introduction to wood and natural fiber composites. *John Wiley & Sons*, 2013.

21. Sella Kapu, N.; & Trajano, H. L. Review of hemicellulose hydrolysis in softwoods and bamboo. *Biofuels, Bioproducts and Biorefining*, 2014, 8(6), 857-870.

22. Gírio, F. M.; Fonseca, C., Carvalheiro, F.; Duarte, L. C., Marques, S.; & Bogel-Łukasik, R. Hemicelluloses for fuel ethanol: a review. *Bioresource Technology*, 2010, 101(13), 4775-4800.

23. Delbecq, F.; Wang, Y.; Muralidhara, A.; El Ouardi, K.; Marlair, G.; & Len, C. Hydrolysis of hemicellulose and derivatives—A review of recent advances in the production of furfural. *Frontiers in Chemistry*. 2018, 6, 146.

24. Xiao, C.; & Anderson, C. T. Roles of pectin in biomass yield and processing for biofuels. *Frontiers in Plant Science*, 2013, 4, 67.

25. Boanares, D.; Ferreira, B. G.; Kozovits, A. R.; Sousa, H. C.; Isaias, R. M. S.; & França, M. G. C. Pectin and cellulose cell wall composition enables different strategies to leaf water uptake in plants from tropical fog mountain. *Plant Physiology and Biochemistry*, 2018, 122, 57-64.

26. Hasani, M. Chemical modification of cellulose: New possibilities of some classical routes. *Chalmers Tekniska Hogskola* (Sweden), 2010.

27. Payen, A. Mémoire sur la composition du tissu propre des plantes et du ligneux. *Comptes Rendus*, 1838, 7,1052–1056.

28. Dumas, J. B.; Brogniart, A.; & Pelonze, T. J. Rapport sur un mémoire de M. Payen, relatif à là composition de la matière ligneuse. *Comptes Rendus*. 1839, 8, 51–53.

29. Staudinger, H. and Fritschi, J. Über isopren und kautschuk. 5. mitteilung. Über die hydrierung des kautschuks und über seine konstitution. *Helvetica Chimica Acta*, 1922, 5, 785– 806.

30. Irvine, J. C. and Hirst, E. L. The molecular structure of cotton cellulose. *Journal of the Chemical Society, Transactions*, 1923, 123, 518–532.

31. Haworth, W. N. and Machemer, H. Molecular structure of cellulose. *Journal of the Chemical Society*, 1932, 2270–2277.

32. Feldman, D. Wood—chemistry, ultrastructure, reactions. *Journal of Polymer Science: Polymer Letters Edition*, 1985, 23, 601-602.

33. Zhang, X.; Li, L.; & Xu, F. Chemical characteristics of wood cell wall with an emphasis on ultrastructure: A mini-review. *Forests*, 2022, 13, 439.

34. Shen, D.; Xiao, R., Gu, S.; & Luo, K. The pyrolytic behavior of cellulose in lignocellulosic biomass: a review. *Royal Society of Chemistry advances*, 2011, 1, 1641-1660.

35. Klemm, D.; Heublein, B.; Fink, H. P.; & Bohn, A. Cellulose: fascinating biopolymer and sustainable raw material. *Angewandte Chemie International Edition*, 2005, 44, 3358-3393.

36. Klemm, D.; Philpp, B.; Heinze, T.; Heinze, U.; & Wagenknecht, W. Comprehensive cellulose chemistry. Fundamentals and analytical methods. *Wiley-VCH Verlag GmbH*, 1998.

37. Medronho, B.; & Lindman, B. Brief overview on cellulose dissolution/regeneration interactions and mechanisms. *Advances in Colloids and Interface Science*, 2015, 222, 502-508.

38. Marsh, J. T.; & Wood, F. C. Introduction to the Chemistry of Cellulose. *Chapman and Hall*, 1942.

39. Lavoine, N.; Desloges, I.; Dufresne, A.; & Bras, J. Microfibrillated cellulose–Its barrier properties and applications in cellulosic materials: A review. *Carbohydrate Polymers*, 2012, 90, 735-764.

40. Siqueira, G.; Bras, J.; & Dufresne, A. Cellulosic bionanocomposites: a review of preparation, properties and applications. *Polymers*, 2010, 2, 728-765.

41. Saxena, I. M.; & Brown Jr, R. M. Cellulose biosynthesis: current views and evolving concepts. *Annals of Botany*, 2005, 96, 9-21.

42. Kaur, P.; Sharma, N.; Munagala, M.; Rajkhowa, R.; Aallardyce, B.; Shastri, Y.; & Agrawal, R. Nanocellulose: resources, physio-chemical properties, current uses and future applications. *Frontiers in Nanotechnology*, 2021, 3, 747329.

43. Gardner, K. H. and Blackwell, J. The structure of native cellulose. *Biopolymers*, 1974, 13, 1975–2001.

44. Huang, C.; Yu, H.; Abdalkarim, S. Y. H.; Li, Y.; Chen, X.; Yang, X.; ... & Zhang, L. A comprehensive investigation on cellulose nanocrystals with different crystal structures from cotton via an efficient route. *Carbohydrate Polymers*, 2022, 276, 118766.

45. Dufresne, A. Nanocellulose: potential reinforcement in composites. *National Polymer*, 2012, 2, 1–32.

46. Lagerwall, J. P.; Schütz, C.; Salajkova, M.; Noh, J.; Hyun Park, J.; Scalia, G.; & Bergström, L. Cellulose nanocrystal-based materials: from liquid crystal self-assembly and glass formation to multifunctional thin films. *NPG Asia Materials*. 2014, 6, 80.

47. Jonoobi, M.; Oladi, R.; Davoudpour, Y.; Oksman, K.; Dufresne, A.; Hamzeh, Y.; & Davoodi, R. Different preparation methods and properties of nanostructured cellulose from various natural resources and residues: a review. *Cellulose*. 2015, 22, 935-969.

48. Mariño, M.; Lopes da Silva, L.; Durán, N.; & Tasic, L. Enhanced materials from nature: nanocellulose from citrus waste. *Molecules*. 2015, 20, 5908-5923.

49. Ververis, C.; Georghiou, K.; Christodoulakis, N.; Santas, P.; & Santas, R. Fiber dimensions, lignin and cellulose content of various plant materials and their suitability for paper production. *Industrial Crops and Products*. 2004, 19, 245-254.

50. Gorgieva, S.; & Trček, J. Bacterial cellulose: Production, modification and perspectives in biomedical applications. *Nanomaterials*. 2019, 9, 1352.

51. Haldar, D.; & Purkait, M. K. Micro and nanocrystalline cellulose derivatives of lignocellulosic biomass: A review on synthesis, applications and advancements. *Carbohydrate Polymers*, 2020, 250, 116937.

52. Reshmy, R.; Philip, E.; Paul, S. A.; Madhavan, A.; Sindhu, R.; Binod, P.; ... & Sirohi, R. Nanocellulose-based products for sustainable applications-recent trends and

possibilities. *Reviews in Environmental Science and Bio/Technology*, 2020, *19*, 779-806.

53. Nicu, R.; Ciolacu, F.; & Ciolacu, D. E. Advanced functional materials based on nanocellulose for pharmaceutical/medical applications. *Pharmaceutics*, 2021, 13, 1125.

54. Gan, I.; & Chow, W. S. Antimicrobial poly (lactic acid)/cellulose bionanocomposite for food packaging application: A review. *Food Packaging and Shelf life*, 2018, 17, 150-161.

55. Khalid, M. Y.; Al Rashid, A.; Arif, Z. U.; Ahmed, W.; & Arshad, H. Recent advances in nanocellulose-based different biomaterials: types, properties, and emerging applications. *Journal of Materials Research and Technology*, 2021, 14, 2601-2623.

56. Nechyporchuk, O.; Belgacem, M. N.; & Bras, J. Production of cellulose nanofibrils: A review of recent advances. *Industrial Crops and Products*, 2016, 93, 2-25.

57. Czaikoski, A.; da Cunha, R. L.; & Menegalli, F. C. Rheological behavior of cellulose nanofibers from cassava peel obtained by combination of chemical and physical processes. *Carbohydrate Polymers*, 2020, 248, 116744.

58. Jonasson, S.; Bünder, A.; Niittylä, T.; & Oksman, K. Isolation and characterization of cellulose nanofibers from aspen wood using derivatizing and non-derivatizing pretreatments. *Cellulose*, 2020, 27, 185-203.

59. Trache, D.; Tarchoun, A. F.; Derradji, M.; Hamidon, T. S.; Masruchin, N.; Brosse, N.; & Hussin, M. H. Nanocellulose: from fundamentals to advanced applications. *Frontiers in Chemistry.* 2020, *8*, 392.

60. Van De Ven, T. G.; & Sheikhi, A. Hairy cellulose nanocrystalloids: a novel class of nanocellulose. *Nanoscale*, 2016, 8, 15101-15114.

61. Yang, H.; & van de Ven, T. G. Preparation of hairy cationic nanocrystalline cellulose. *Cellulose*, 2016, 23, 1791-1801.

62. Yang, H.; Chen, D.; & van de Ven, T. G. Preparation and characterization of sterically stabilized nanocrystalline cellulose obtained by periodate oxidation of cellulose fibers. *Cellulose*, 2015, 22, 1743-1752.

63. Gupta, G. K.; & Shukla, P. Lignocellulosic biomass for the synthesis of nanocellulose and its eco-friendly advanced applications. *Frontiers in Chemistry.* 2020, *8*, 601256.

64. Farooq, A.; Patoary, M. K.; Zhang, M.; Mussana, H.; Li, M.; Naeem, M. A.; ... & Liu, L. Cellulose from sources to nanocellulose and an overview of synthesis and properties of nanocellulose/zinc oxide nanocomposite materials. *International Journal of Biological Macromolecules*, 2020, *154*, 1050-1073.

65. Habibi, Y.; Lucia, L. A.; & Rojas, O. J. Cellulose nanocrystals: chemistry, self-assembly, and applications. *Chemical Reviews*, 2010, *110*, 3479-3500.

66. Mishra, R. K.; Sabu, A.; & Tiwari, S. K. Materials chemistry and the futurist eco-friendly applications of nanocellulose: Status and prospect. *Journal of Saudi Chemical Society*, 2018, *22*(8), 949-978.

67. Gorgieva, S.; & Trček, J. Bacterial cellulose: Production, modification and perspectives in biomedical applications. *Nanomaterials*, 2019, *9*(10), 1352.

68. Iwamoto, S.; Nakagaito, A. N.; & Yano, H. J. A. P. A. Nano-fibrillation of pulp fibers for the processing of transparent nanocomposites. *Applied Physics A*, 2007, *89*, 461-466.

69. Sofla, M. R. K.; Brown, R. J.; Tsuzuki, T.; & Rainey, T. J. A comparison of cellulose nanocrystals and cellulose nanofibres extracted from bagasse using acid and ball milling methods. *Advances in Natural Sciences: Nanoscience and Nanotechnology*, 2016, *7*, 035004.

70. Cao, X.; Habibi, Y.; Magalhães, W. L. E.; Rojas, O. J.; & Lucia, L. A. Cellulose nanocrystals-based nanocomposites: fruits of a novel biomass research and teaching platform. *Current Science*, 2011, 1172-1176.

71. Guhados, G.; Wan, W.; & Hutter, J. L. Measurement of the elastic modulus of single bacterial cellulose fibers using atomic force microscopy. *Langmuir*, 2005, *21*, 6642-6646.

72. Pradhan, D.; Jaiswal, A. K.; & Jaiswal, S. Emerging technologies for the production of nanocellulose from lignocellulosic biomass. *Carbohydrate Polymers*, 2022, 119258.

73. Mankar, A. R.; Pandey, A.; Modak, A.; & Pant, K. K. Pretreatment of lignocellulosic biomass: A review on recent advances. *Bioresource Technology*, 2021, 334, 125235.

74. Hubbell, C. A.; & Ragauskas, A. J. Effect of acid-chlorite delignification on cellulose degree of polymerization. *Bioresource technology*, 2010, 101, 7410-7415.

75. Johar, N.; Ahmad, I.; & Dufresne, A. Extraction, preparation and characterization of cellulose fibres and nanocrystals from rice husk. *Industrial Crops and Products*, 2012, 37, 93-99.

76. Charreau, H.; Cavallo, E.; & Foresti, M. L. Patents involving nanocellulose: Analysis of their evolution since 2010. *Carbohydrate Polymers*, 2020, 237, 116039.

77. Maciel, M. M. Á. D.; de Carvalho Benini, K. C. C.; Voorwald, H. J. C.; & Cioffi, M. O. H. Obtainment and characterization of nanocellulose from an unwoven industrial

textile cotton waste: Effect of acid hydrolysis conditions. *International Journal of Biological Macromolecules*, 2019, 126, 496-506.

78. Khalil, H. A.; Davoudpour, Y.; Islam, M. N.; Mustapha, A.; Sudesh, K.; Dungani, R.; & Jawaid, M. Production and modification of nanofibrillated cellulose using various mechanical processes: A review. *Carbohydrate Polymers*, 2014, 99, 649-665.

79. Omara, A. E. D.; Elsakhawy, T.; Alshaal, T.; El-Ramady, H.; Kovács, Z.; & Fári, M. Nanoparticles: A novel approach for sustainable agro-productivity. *Environment, Biodiversity and Soil Security*, 2019, 3, 29-62.

80. Gonçalves, S. M.; Dos Santos, D. C.; Motta, J. F. G.; Dos Santos, R. R.; Chávez, D. W. H.; & de Melo, N. R. Structure and functional properties of cellulose acetate films incorporated with glycerol. *Carbohydrate Polymers*, 2019, 209, 190-197.

81. Xu, Z.; Liang, B.; Tian, J.; & Wu, J. Anti-inflammation biomaterial platforms for chronic wound healing. *Biomaterials Science*, 9(12), 2021, 4388-4409.

82. Zhao, X.; Bhagia, S.; Gomez-Maldonado, D.; Tang, X.; Wasti, S.; Lu, S.; ... & Ozcan, S. Bioinspired design toward nanocellulose-based materials. *Materials Today*, 2023.

83. de Amorim, J. D. P.; de Souza, K. C.; Duarte, C. R.; da Silva Duarte, I.; de Assis Sales Ribeiro, F.; Silva, G. S.; ... & Sarubbo, L. A. Plant and bacterial nanocellulose: Production, properties and applications in medicine, food, cosmetics, electronics and engineering. A review. *Environmental Chemistry Letters*, 2020, 18, 851-869.

84. Shanmugam, K.; Nadeem, H.; Browne, C.; Garnier, G.; & Batchelor, W. Engineering surface roughness of nanocellulose film via spraying to produce smooth substrates. *Colloids and Surfaces A: Physicochemical and Engineering Aspects*, 2020, 589, 124396.

85. Jasmani, L.; Adnan, S.; Rusli, R.; Ibrahim, R.; & Mamat, M. H. NANOCELLULOSE USES IN ELECTRONICS. *Lignocellulosic Materials Towards a Sustainable Future*, 2023, 93.

86. Dias, O. A. T.; Konar, S.; Leão, A. L.; Yang, W.; Tjong, J.; & Sain, M. Current state of applications of nanocellulose in flexible energy and electronic devices. *Frontiers in Chemistry*, 2020, 8, 420.

87. Agarwal, J.; Sahoo, S.; Mohanty, S.; & Nayak, S. K. Progress of novel techniques for lightweight automobile applications through innovative eco-friendly composite materials: A review. *Journal of thermoplastic composite materials*, 2020, 33, 978-1013.

88. De France, K. J.; Hoare, T.; & Cranston, E. D. Review of hydrogels and aerogels containing nanocellulose. *Chemistry of Materials*, 2017, 29, 4609-4631.

89. Carosio, F.; Medina, L.; Kochumalayil, J.; & Berglund, L. A. Green and fire resistant nanocellulose/hemicellulose/clay foams. *Advanced Materials Interfaces*, 2021, 8, 2101111.

90. Spagnuolo, L.; D'Orsi, R.; & Operamolla, A. Nanocellulose for paper and textile coating: The Importance of surface chemistry. *ChemPlusChem*, 2022, 87, 202200204.

91. Li, A.; Xu, D.; Li, Y.; Wu, S.; Madyan, O. A.; Rao, J.; & Fan, M. Binary additives of polyamide epichlorohydrin-nanocellulose for effective valorization of used paper. *International Journal of Biological Macromolecules*, 2023, 226, 194-201.

92. Paul, J.; & Ahankari, S. S. Nanocellulose-based aerogels for water purification: A review. *Carbohydrate Polymers*, 2023, 120677.

93. Nehra, P.; & Chauhan, R. P. Antimicrobial activity of nanocellulose composite hydrogel isolated from an agricultural waste. *Archives of Microbiology*, 2023, *205*, 133.

94. Padhi, S.; Singh, A.; & Routray, W. Nanocellulose from agro-waste: a comprehensive review of extraction methods and applications. *Reviews in Environmental Science and Bio/Technology*, 2023, 9, 1-27.

95. Weng, R.; Chen, L.; Lin, S.; Zhang, H.; Wu, H.; Liu, K.; ... & Huang, L. Preparation and characterization of antibacterial cellulose/chitosan nanofiltration membranes. *Polymers*, 2017, *9*, 116.

96. Alvarado, D. R.; Argyropoulos, D. S.; Scholle, F.; Peddinti, B. S.; & Ghiladi, R. A. A facile strategy for photoactive nanocellulose-based antimicrobial materials. *Green Chemistry*, 2019, 21, 3424-3435.

97. Florio, W.; Becherini, S.; D'Andrea, F.; Lupetti, A.; Chiappe, C.; & Guazzelli, L. Comparative evaluation of antimicrobial activity of different types of ionic liquids. *Materials Science and Engineering: C*, 2019, 104, 109907.

98. Orelma, H.; Korpela, A.; Kunnari, V.; Harlin, A.; & Suurnäkki, A. Improving the mechanical properties of CNF films by NMMO partial dissolution with hot calender activation. *Cellulose*, 2017, 24, 1691-1704.

99. Uusi-Tarkka, E. K.; Levanič, J.; Heräjärvi, H.; Kadi, N.; Skrifvars, M.; & Haapala, A. All-Cellulose Composite Laminates Made from Wood-Based Textiles: Effects of Process Conditions and the Addition of TEMPO-Oxidized Nanocellulose. *Polymers*, 2022,14, 3959.

100. Zhang, S.; Zhang, N.; Qian, L.; Liu, Y.; Ren, H.; & Li, Y. Facile preparation of high strength aerogel based on polysulfonamide. *Materials Letters*, 2019, 250, 159-162.

101.   Qi, Y.; Guo, Y.; Liza, A. A.; Yang, G.; Sipponen, M. H.; Guo, J.; & Li, H. Nanocellulose: a review on preparation routes and applications in functional materials. *Cellulose*, 2023, 1-33.

102.   Khoo, K. S.; Tan, X.; Ooi, C. W.; Chew, K. W.; Leong, W. H.; Chai, Y. H. ... & Show, P. L. How does ionic liquid play a role in sustainability of biomass processing. *Journal of Cleaner Production*, 2021, *284*, 124772.

103.   Swatloski, R. P.; Spear, S. K.; Holbrey, J. D.; & Rogers, R. D. Dissolution of cellose with ionic liquids. *Journal of the American Chemical Society*, 2002, *124*, 4974-4975.

104.   Fukaya, Y.; Sugimoto, A.; & Ohno, H. Superior solubility of polysaccharides in low viscosity, polar, and halogen-free 1, 3-dialkylimidazolium formates. *Biomacromolecules*, 2006, *7*, 3295-3297.

105.   Sashina, E. S.; Kashirskii, D. A.; & Busygin, K. N. Dissolution of cellulose with pyridinium-based ionic liquids: effect of chemical structure and interaction mechanism. *Cellulose Chemistry and Technology*, 2016, *50*, 199-211.

106.   Ren, H. W.; Wang, Q. H.; Guo, S. H.; Zhao, D. S.; & Chen, C. M. The role and potential of morpholinium-based ionic liquids in dissolution of cellulose. *European Polymer Journal*, 2017, *92*, 204-212.

107.   Abe, M.; Kuroda, K.; & Ohno, H. Maintenance-free cellulose solvents based on onium hydroxides. *ACS Sustainable Chemistry & Engineering*, 2015, *3*, 1771-1776.

108.   Brehm, M.; Pulst, M.; Kressler, J.; & Sebastiani, D. Triazolium-based ionic liquids: A novel class of cellulose solvents. *The Journal of Physical Chemistry B*, 2019, *123*, 3994-4003.

109.   Li, D.; Sevastyanova, O.; & Ek, M. Pretreatment of softwood dissolving pulp with ionic liquids. *Holzforschung*, 2012, *66*, 935-943.

110.   Liu, Z.; Wang, H.; Li, Z.; Lu, X.; Zhang, X.; Zhang, S.; & Zhou, K. Characterization of the regenerated cellulose films in ionic liquids and rheological properties of the solutions. *Materials Chemistry and Physics*, 2011, *128*, 220-227.

111.   Aghmih, K.; Bouftou, A.; El Bouchti, M.; Boukhriss, A.; Gmouh, S.; & Majid, S. Synthesis and application of functionalized ionic liquids-based imidazolium as solvent for cotton fibre cellulose dissolution. *Cellulose*, 2023, *30*, 1467-1481.

112.   Wang, Y.; Wei, X.; Li, J.; Wang, F.; Wang, Q.; Zhang, Y.; & Kong, L. Homogeneous isolation of nanocellulose from eucalyptus pulp by high pressure homogenization. *Industrial Crops and Products*, 2017, 104, 237-241.

113. Ferreira, R. R.; Souza, A. G.; Nunes, L. L.; Shahi, N.; Rangari, V. K.; & dos Santos Rosa, D. Use of ball mill to prepare nanocellulose from eucalyptus biomass: challenges and process optimization by combined method. *Materials Today Communications*, 2020, 22, 100755.

114. de Souza, A. G.; Junqueira, M. T.; de Lima, G. F.; Rangari, V. K.; & Rosa, D. S. A new proposal of preparation of different polymorphs of nanocellulose from eucalyptus citriodora. *Journal of Polymers and the Environment*, 2020, 28, 1150-1159.

115. Isik, M.; Sardon, H.; & Mecerreyes, D. Ionic liquids and cellulose: dissolution, chemical modification and preparation of new cellulosic materials. *International Journal of Molecular Sciences*, 2014, 15, 11922-11940.

116. Sashina, E. S.; Kashirskii, D. A.; & Busygin, K. N. Dissolution of cellulose with pyridinium-based ionic liquids: Effect of chemical structure and interaction mechanism. *Cellulose Chemistry and Technology*, 2016, 50, 199-211.

117. Raju, V.; Revathiswaran, R.; Subramanian, K. S.; Parthiban, K. T.; Chandrakumar, K.; Anoop, E. V.; & Chirayil, C. J. Isolation and characterization of nanocellulose from selected hardwoods, viz., Eucalyptus tereticornis Sm. and Casuarina equisetifolia L., by steam explosion method. *Scientific Reports*, 2023, 13, 1-15.

118. Tozluoglu, A.; Poyraz, B.; Mcdonald, A. G.; & Candan, Z. Developing nanocellulose-based biofilms from kraft and $NaBH_4$-modified kraft pulp. *Cellulose Chemistry and Technology*, 2018, 52, 223-237.

119. Hassan, R.; Nazir, F.; Roosh, M.; Qaisar, A.; Habib, U.; Sajini, A. A.; & Iqbal, M. Synthesis, characterization, biological evaluation, and in silico studies of imidazolium-, pyridinium-, and ammonium-based ionic liquids Containing n-butyl side chains. *Molecules*, 2022, 27, 6650.

120. Ashokan, D.; & Rajathi, K. A green Approach for synthesis of pyridinium sulfonamide Ionic Liquids: Characterization and their biological activities. *Chemistry Africa*, 2023, 1-13.

121. Ben, H.; Chen, X.; Han, G.; Shao, Y.; Jiang, W.; Pu, Y.; & Ragauskas, A. J. Characterization of whole biomasses in pyridine based ionic liquid at low temperature by 31P NMR: an approach to quantitatively measure hydroxyl groups in biomass as their original structures. *Frontiers in Energy Research*, 2018, 6, 13.

122. Taheri, N.; Abdolmaleki, A.; & Fashandi, H. Pyridinium-based ionic liquid/water mixture intended for efficient dissolution of cellulose, chitosan and chitin: The pivotal contribution of water. *Carbohydrate Polymers*, 2018, 195, 413-419.

123. Saher, S.; Saleem, H.; Asim, A. M.; Uroos, M.; & Muhammad, N. Pyridinium based ionic liquid: A pretreatment solvent and reaction medium for catalytic conversion of cellulose to total reducing sugars (TRS). *Journal of Molecular Liquids*, 2018, 272, 330-336.

124. Alrefaee, S. H. Effect of alkyl chain length and halide ions on the corrosion inhibition potential of imidazolium and pyridinium based ionic liquids: computational studies. *Journal of Molecular Liquids*, 2021, 344, 117848.

125. Pradhan, D.; Jaiswal, A. K.; & Jaiswal, S. Emerging technologies for the production of nanocellulose from lignocellulosic biomass. *Carbohydrate Polymers*, 2022, 119258.

126. El Miri, N.; Abdelouahdi, K.; Zahouily, M.; Fihri, A.; Barakat, A.; Solhy, A.; & El Achaby, M. Bio-nanocomposite films based on cellulose nanocrystals filled polyvinyl alcohol/chitosan polymer blend. *Journal of Applied Polymer Science*, 2015, 132.

127. Khalili, H.; Salim, M. H.; Tlemcani, S. E. J.; Makhlouf, R.; Hassani, F. Z. S. A.; Ablouh, H.; ... & El Achaby, M. Bio-Nanocomposite Films Based on Cellulose Nanocrystals Filled Polyvinyl Alcohol/Alginate Polymer Blend. *Journal of Fibers and Polymer Composites*. 2022, 1, 77-96.

128. Hernández-Varela, J.; Chanona-Pérez, J. J.; Hernández, P. R.; Altamirano, S. V.; Calderon, H.; Franco, K. M.; & Santiago, E. A. Biodegradable polymers: New alternatives using nanocellulose and agroindustrial residues. *Microscopy and Microanalysis*, **2020**, 26, 356-359.

129. Yunus, N. M.; Mutalib, M. A.; Man, Z.; Bustam, M. A.; & Murugesan, T. Solubility of CO2 in pyridinium based ionic liquids. *Chemical Engineering Journal*. 2012, 189, 94-100.

130. Verma, C.; Mishra, A.; Chauhan, S.; Verma, P.; Srivastava, V.; Quraishi, M. A.; & Ebenso, E. E. Dissolution of cellulose in ionic liquids and their mixed cosolvents: A review. *Sustainable Chemistry and Pharmacy*. 2019, 13, 100162.

131. Shill, K.; Padmanabhan, S.; Xin, Q.; Prausnitz, J. M.; Clark, D. S.; & Blanch, H. W. Ionic liquid pretreatment of cellulosic biomass: enzymatic hydrolysis and ionic liquid recycle. *Biotechnology and Bioengineering*. 2011, 108, 511-520.

132. Abraham, R. J.; Fisher, J.; Loftus, P.; & Abraham, R. J. Introduction to NMR spectroscopy. New York: *Wiley*, 1988, 2.

133. Tan, W. L.; McNeill, C. R. X-ray diffraction of photovoltaic perovskites: Principles and applications. *Applied Physics Reviews* 2022, *9*, 021310.

134. Pavia, D. L.; Lampman, G. M.; Kriz, G. S.; & Vyvyan, J. A. Introduction to spectroscopy. *Cengage Learning*, 2014.

135. Smith, B. C. Fundamentals of Fourier transform infrared spectroscopy. CRC press. 2011.

136. Kazarian, S. G.; & Chan, K. A. ATR-FTIR spectroscopic imaging: recent advances and applications to biological systems. *Analyst*. 2013, 138(7), 1940-1951.

137. Banwell, C. N., & McCash, E. M. Fundamentals of molecular spectroscopy. Indian Edition, 2017.

138. Mihkel, K. O. E. L. Physical and chemical properties of ionic liquids based on the dialkkylimidazo-lium cation. *Estonian Procedure Academy of Sciences, Chem*istry. 2000, *49*(3), 145-155.

139. Mohammed, A., & Abdullah, A. Scanning electron microscopy (SEM): A review. *In Proceedings of the 2018 International Conference on Hydraulics and Pneumatics—HERVEX*, Băile Govora, Romania ,2018, 2018, 7-9.

140. Hunter, R. J. Zeta potential in colloid science: principles and applications. *Academic Press*. 2013, 2.

141. Prakash, S.; Mishra, R.; Malviya, R.; & Sharma, P. K. Measurement techniques and pharmaceutical applications of zeta potential: a review. *Journal of Chronotherapy and Drug Delivery*, 2014, 5(2), 33-40.

142. Brand-Williams, W.; Cuvelier, M. E.; & Berset, C. L. W. T. Use of a free radical method to evaluate antioxidant activity. *LWT-Food science and Technology*, 1995, 28, 25-30.

143. Oyaizu, M. Studies on products of browning reaction antioxidative activities of products of browning reaction prepared from glucosamine. *The Japanese Journal of Nutrition and Dietetics*. 1986, 44, 307-315.

144. Nie, K.; Song, Y.; Liu, S.; Han, G.; Ben, H.; Ragauskas, A. J.; & Jiang, W. Preparation and characterization of microcellulose and nanocellulose fibers from artemisia vulgaris bast. *Polymers*. 2019, 11(5), 907.

145. H. Yu.; C. Yan.; X. Lei.; Z. Qin.; & J. Yao. Novel approach to extract thermally stable cellulose nanospheres with high yield. *Materials Letters*, 2014, 131, pp. 12-15

146.   U. Ikhuoria, E.; O. Omorogbe, S.; G. Agbonlahor, O.; & A. Etiuma, R. Nanocellulose Crystals from Coir Fibre for Template Application. *Chemical Science International Journal*. 2015, 9, 1–11.

147.   Rahimi, M. K. S.; Brown, R. J.; Tsuzuki, T.; and Rainey, T. J. A comparison of cellulose nanocrystals and cellulose nanofibres extracted from bagasse using acid and ball milling methods. *Advances in Natural Sciences: Nanoscience and Nanotechnology*. 2016, 7, 1-9

148.   Thakur, M.; Sharma, A.; Ahlawat, V.; Bhattacharya, M.; & Goswami, S. Process optimization for the production of cellulose nanocrystals from rice straw derived α-cellulose. *Materials Science for Energy Technologies*. 2020, 3, 328-334.

149.   Zielińska, D.; Skrzypczak, A.; Peplińska, B.; & Borysiak, S. Nanocellulose-based polymer composites functionalized with new gemini ionic liquids. *International Journal of Molecular Sciences*. 2022, 23, 15807.

150.   Vekariya, R. L.; & Kumar, N. S. Micellization behavior of surface-active N-alkyl pyridinium dodecylsulphate task-specific ionic liquids in aqueous solutions. *Colloids and Surfaces A: Physicochemical and Engineering Aspects*. 2017, 529, 203-209.

151.   Wulandari, W. T.; Rochliadi, A.; & Arcana, I. M. Nanocellulose prepared by acid hydrolysis of isolated cellulose from sugarcane bagasse. *In IOP Conference Series: Materials Science and Engineering*, 2016, 107, 012045.

152.   Sultana, T.; Sultana, S.; Nur, H. P.; & Khan, M. W. Studies on mechanical, thermal and morphological properties of betel nut husk nano cellulose reinforced biodegradable polymer composites. *Journal of Composites Science*, 2020, 4, 83.

153.   Rezende, M. C.; & Aracena, A. A general framework for the solvatochromism of pyridinium phenolate betaine dyes. *Chemical Physics Letters*, 2013, 558, 77-81.

154.   Anandhan, K.; Cerón, M.; Perumal, V.; Ceballos, P.; Gordillo-Guerra, P.; Pérez-Gutiérrez, E., & Percino, M. J. Solvatochromism and pH effect on the emission of a triphenylimidazole-phenylacrylonitrile derivative: experimental and DFT studies. *Royal Society of Chemistry Advances*, 2019, 9, 12085-12096.

155.   Mai, S., Ashwood, B., Marquetand, P., Crespo-Hernández, C. E., & González, L. Solvatochromic effects on the absorption spectrum of 2-thiocytosine. *The Journal of Physical Chemistry B*, 2017, 121(20), 5187-5196.

156.   Sone, K.; & Fukuda, Y. Solvatochromism of transition metal complexes with organic ligands in donor and acceptor solvents. *Reviews in Inorganic Chemistry*, 1990, 11, 123-154.

157.   Akgün, D.; Özcan, D. O.; & Bikem, Ö. V. E. Z. Optimization and characterization of cellulose nanocrystal production from aseptic tetra pak food packaging waste. *Journal of the Turkish Chemical Society Section A: Chemistry*, 2022, 9, 131-148.

158.   Ilyas, R. A.; Sapuan, S. M.; Ishak, M. R. Isolation and characterization of nanocrystalline cellulose from sugar palm fibres (Arenga Pinnata). *Carbohydrate Polymers*, 2018, 181, 1038-1051.

159.   Vivian Abiaziem, C.; Bassey Williams, A.; Ibijoke Inegbenebor, A.; Theresa Onwordi, C.; Osereme Ehi-Eromosele, C.; & Felicia Petrik, L. Preparation and characterisation of cellulose nanocrystal from sugarcane peels by XRD, SEM and CP/MAS 13C NMR. *In Journal of Physics: Conference Series*, 2019, 1299, 012123.

160.   Paredes, X.; Fandino, O.; Comunas, M. J.; Pensado, A. S.; & Fernández, J. Study of the effects of pressure on the viscosity and density of diisodecyl phthalate. *The Journal of Chemical Thermodynamics*, 2009, 41, 1007-1015.

161.   Kurnia, K. A.; Wilfred, C. D.; & Murugesan, T. Thermophysical properties of hydroxyl ammonium ionic liquids. *The Journal of Chemical Thermodynamics*, 2009, 41, 517-521.

162.   Yunus, N. M.; Mutalib, M. A.; Man, Z.; Bustam, M. A.; & Murugesan, T. Thermophysical properties of 1-alkylpyridinum bis (trifluoromethylsulfonyl) imide ionic liquids. *The Journal of Chemical Thermodynamics*, 2010, 42, 491-495.

163.   Mehanny, S.; Abu-El Magd, E. E.; Ibrahim, M., Farag, M.; Gil-San-Millan, R.; Navarro, J.; & El-Kashif, E. Extraction and characterization of nanocellulose from three types of palm residues. *Journal of Materials Research and Technology*, 2021, 10, 526-537.

164.   AbouSamra, M. M.; El Hoffy, N. M.; El-Wakil, N. A.; Awad, G. E.; & Kamel, R. Computational investigation to design ofloxacin-loaded hybridized nanocellulose/lipid nanogels for accelerated skin repair. *Gels*, 2022, 8, 593.

165.   Yang, X.; Han, F.; Xu, C.; Jiang, S.; Huang, L.; Liu, L.; & Xia, Z. Effects of preparation methods on the morphology and properties of nanocellulose (NC) extracted from corn husk. *Industrial Crops and Products*, 2017, 109, 241-247.

166. Morais, J. P. S.; de Freitas Rosa, M.; Nascimento, L. D.; Do Nascimento, D. M.; & Cassales, A. R. Extraction and characterization of nanocellulose structures from raw cotton linter. *Carbohydrate Polymers*, 2013, 91, 229-235.

167. Siddiquee, M.A.; Saraswat, J.; Imtiyaz, K.; Bhat, A.R.; Wani, F.A.; Alanazi, A.M.; Khan, A.A.; Rizvi, M.M.A.; Patel, R. In-vitro cytotoxicity, synergistic antibacterial activity and interaction studies of imidazolium-based ionic liquids with levofloxacin. *The Journal of Molecular Liquids*, 2021, 325, 115125.

168. Shahidi, F.; & Zhong, Y. Measurement of antioxidant activity. *Journal of Functional Foods*, 2015, 18, 757-781.

169. Valencia, L.; Arumughan, V.; Jalvo, B.; Maria, H. J.; Thomas, S.; & Mathew, A. P. Nanolignocellulose extracted from environmentally undesired Prosopis juliflora. *American Chemical Society Omega*, 2019, 4, 4330-4338.

170. Matavos-Aramyan, S.; Matavos-Aramyan, H.; & Soukhakian, S. Synthesis of two novel alanine-based antibacterial and antioxidant chiral ionic liquids. *SN Applied Sciences*, 2019, 1(8), 908.

171. Ferreira, I. C.; Baptista, P.; Vilas-Boas, M.; & Barros, L. Free-radical scavenging capacity and reducing power of wild edible mushrooms from northeast Portugal: Individual cap and stipe activity. *Food Chemistry*, 2007, 100, 1511-1516.

172. Bickelhaupt, F. M., & Baerends, E. J. Kohn-Sham density functional theory: predicting and understanding chemistry. *Reviews in Computational Chemistry*, 2000, 1-86.

173. Zhang, I. Y.; Wu, J.; & Xu, X. Extending the reliability and applicability of B3LYP. *Chemical Communications*, 2010, 46, 3057-3070.

174. Jensen, F. Introduction to computational chemistry. *John Wiley & Sons*, New York, **2017.**

175. Alrefaee, S. H. Effect of alkyl chain length and halide ions on the corrosion inhibition potential of imidazolium and pyridinium based ionic liquids: computational studies. *Journal of Molecular Liquids*, **2021**, 344, 117848.

176. Chaudhary, M. K.; Srivastava, A.; Singh, K. K.; Tandon, P.; & Joshi, B. D. Computational evaluation on molecular stability, reactivity, and drug potential of frovatriptan from DFT and molecular docking approach. *Computational and Theoretical Chemistry*, **2020**, 1191, 113031.

177. Ernzerhof, M. Validity of the extended Koopmans' theorem. *Journal of Chemical Theory and Computation*, **2009**, 5(4), 793-797.

178.   Murray, J. S.; & Sen, K. Molecular electrostatic potentials: concepts and applications. **1996.**

179.   Bayoumy, A. M.,;Ibrahim, M.; & Omar, A. Mapping molecular electrostatic potential (MESP) for fulleropyrrolidine and its derivatives. *Optical and Quantum Electronics*, **2020**, 52, 1-13.

180.   Lukasheva, N. V.; Tolmachev, D. A.; & Karttunen, M. Mineralization of phosphorylated cellulose: Crucial role of surface structure and monovalent ions for optimizing calcium content. *Physical Chemistry Chemical Physics*, **2019**, 21, 1067-1077.